

Control of Salinity Intrusion Caused by Sea Level Rise

by

Kristinn Gudmundsson

Thesis submitted to the Faculty of the

Virginia Polytechnic Institute and State University

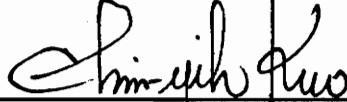
in partial fulfillment of the requirements for the degree of

Master of Science

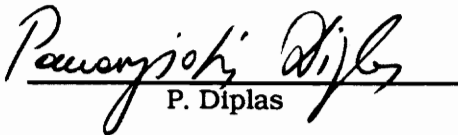
in

Civil Engineering

APPROVED:



Chin Y. Kuo, Chairman



P. Diplas



G. V. Loganathan

May 24, 1991

Blacksburg, Virginia

LD

5655

V 855

1991

6846

C.2

Control of Salinity Intrusion Caused by Sea Level Rise

by

Kristinn Gudmundsson

Chin Y. Kuo, Chairman

Civil Engineering

(ABSTRACT)

The objectives of this research are to take advance steps to assess the potential impacts of sea level rise on our nation's estuarine environments and water resources management. Specific engineering solutions to control salinity intrusion are studied. Structure measures such as construction of tidal barriers, tidal locks, and through long term stream flow augmentation are investigated for their suitability.

Quantification of the extent of the impacts is accomplished by means of computer model simulations. A laterally integrated two-dimensional, time dependent, finite difference numerical model is used to study time-varying tidal height, current and salinity. Through a selected estuary, parametric studies on scenarios of projected sea level rise, stream flow, channel roughness, change in cross-section profile, etc. are performed in order to have an in-depth understanding of estuarine processes for cases such as present condition versus future sea level rise, with or without control measures. The results of the parametric studies are summarized and engineering applications of individual control methods are discussed.

Acknowledgments

I wish to thank Dr. Chin Y. Kuo for his guidance in the completion of this thesis. I would also like to thank Dr. P. Diplas and Dr. G.V. Loganathan for their time in reviewing the manuscript and their willingness to serve on the committee.

My fellow graduate students in the Hydrosystems Division get special thanks for being great company and for the assistance they provided me during the course of this study. Other faculty members and staff of the Hydrosystems Division deserve acknowledgments for making these two years at Virginia Tech so enjoyable.

I would like to thank the National Science Foundation for funding this project.

Finally I would like to thank my parents for their support and understanding during the course of my study.

Table of Contents

Abstract	ii
Acknowledgments	iii
Table of Contents	iv
List of Illustrations	vii
List of Symbols	xiv
1. Introduction	1
1.1 Study of Sea Level Rise	1
1.2 Background Information and Related On-Going Research	2
1.3 Research Objectives	5
2. Numerical Model	6
2.1 Basic Equations	6
2.2 Boundary Conditions	10
2.3 Upstream Boundary Conditions	11
2.4 Downstream Boundary Conditions	12

Table of Contents

2.5 The Estuary Under Study	12
3. Results	14
3.1 Freshwater Augmentation	14
3.1.1 Upstream Boundary	15
3.1.2 Downstream Boundary	16
3.1.3 Discussion of Results for Freshwater Augmentation	18
3.1.4 Engineering Applications of Freshwater Augmentation	21
3.2 Tidal Barriers	23
3.2.1 Upstream Boundary Conditions	23
3.2.2 Downstream Boundary Conditions	23
3.2.3 Discussion of Results for Tidal Barriers	25
3.2.4 Engineering Applications of Tidal Barriers	29
3.3 Tidal Locks	31
3.3.1 Upstream and Downstream Boundary Conditions	31
3.3.2 Discussion of Results for Tidal Locks	33
3.3.4 Engineering Applications of a Tidal Lock	34

Table of Contents

3.4 Effect of Bottom Friction	37
3.4.1 Discussion of Results	38
4. Conclusions	39
References	42
Figures	46
Appendix A: Derivation of Governing Equations	112
Appendix B: Sample Input for the Numerical Model	118
Appendix C: Sample Output from the Numerical Model	124
Vita	145

List of Illustrations

Figure 1.1	Change in sea level with respect to adjacent land for stations from the District of Columbia to South Carolina.	47
Figure 2.1	Coordinate system used in the numerical model.	48
Figure 2.2	Grid pattern, location and indexing of variables.	49
Figure 2.3	Location of the Rappahannock River-lower inset and longitudinal segmentation scheme.	50
Figure 2.4	Model interpretation of the Rappahannock River estuary.	51
Figure 3.1	Stage-discharge curve for the Rappahannock River.	52
Figure 3.2	Depth-averaged salinity at transect 25 for different conditions of freshwater inflow and sea level rise.	53
Figure 3.3	Depth-averaged salinity at transect 26 for different conditions of freshwater inflow and sea level rise.	54
Figure 3.4	Depth-averaged salinity at transect 27 for different conditions of freshwater inflow and sea level rise.	55
Figure 3.5	Depth-averaged salinity at transect 28 for different conditions of freshwater inflow and sea level rise.	56

List of Illustrations

Figure 3.6	Depth-averaged salinity at transect 29 for different conditions of freshwater inflow and sea level rise.	57
Figure 3.7	Depth-averaged salinity at transect 30 for different conditions of freshwater inflow and sea level rise.	58
Figure 3.8	Depth-averaged salinity at transect 31 for different conditions of freshwater inflow and sea level rise.	59
Figure 3.9	Depth-averaged salinity at transect 32 for different conditions of freshwater inflow and sea level rise.	60
Figure 3.10	Depth-averaged salinity at transect 33 for different conditions of freshwater inflow and sea level rise.	61
Figure 3.11	Depth-averaged salinity at transect 34 for different conditions of freshwater inflow and sea level rise.	62
Figure 3.12	Depth-averaged salinity at transect 35 for different conditions of freshwater inflow and sea level rise.	63
Figure 3.13	Depth-averaged salinity at transect 36 for different conditions of freshwater inflow and sea level rise.	64
Figure 3.14	Average salinity in bottom layer of transect 25 for different conditions of freshwater inflow and sea level rise.	65
Figure 3.15	Average salinity in bottom layer of transect 26 for different conditions of freshwater inflow and sea level	

List of Illustrations

	rise.	66
Figure 3.16	Average salinity in bottom layer of transect 27 for different conditions of freshwater inflow and sea level rise.	67
Figure 3.17	Average salinity in bottom layer of transect 28 for different conditions of freshwater inflow and sea level rise.	68
Figure 3.18	Average salinity in top layer of transect 25 for different conditions of freshwater inflow and sea level rise.	69
Figure 3.19	Average salinity in top layer of transect 26 for different conditions of freshwater inflow and sea level rise.	70
Figure 3.20	Average salinity in top layer of transect 27 for different conditions of freshwater inflow and sea level rise.	71
Figure 3.21	Average salinity in top layer of transect 28 for different conditions of freshwater inflow and sea level rise.	72
Figure 3.22	Average salinity in top layer of transect 29 for different conditions of freshwater inflow and sea level rise.	73
Figure 3.23	Average salinity in top layer of transect 30 for different conditions of freshwater inflow and sea level rise.	74
Figure 3.24	Average salinity in top layer of transect 31 for different conditions of freshwater inflow and sea level rise.	75

List of Illustrations

Figure 3.25	Average salinity in top layer of transect 32 for different conditions of freshwater inflow and sea level rise.	76
Figure 3.26	Average salinity in top layer of transect 33 for different conditions of freshwater inflow and sea level rise.	77
Figure 3.27	Average salinity in top layer of transect 34 for different conditions of freshwater inflow and sea level rise.	78
Figure 3.28	Average salinity in top layer of transect 35 for different conditions of freshwater inflow and sea level rise.	79
Figure 3.29	Average salinity in top layer of transect 36 for different conditions of freshwater inflow and sea level rise.	80
Figure 3.30	5 ppt isohalines for 55 cm vs. no SLR, for normal flow condition.	81
Figure 3.31	10 ppt isohalines for 55 cm vs. no SLR, for normal flow condition.	82
Figure 3.32	Cases 1, 2, and 3, of estuary constriction.	83
Figure 3.33	Cases 4, 5, and 6, of estuary constriction.	84
Figure 3.34	Depth-averaged salinities at transects 25 to 30, for different cases of estuary constriction.	85
Figure 3.35	Depth-averaged salinities at transects 30 to 36, for different cases of estuary constriction.	86

List of Illustrations

Figure 3.36	Water surface elevations at transects 2 to 36, for different cases of estuary constriction.	87
Figure 3.37	Average bottom layer salinities in transects 25 to 36, for different cases of estuary constriction.	88
Figure 3.38	Average top layer salinities in transects 25 to 36, for different cases of estuary constriction.	89
Figure 3.39	Average salinities in the bottom layer of transect 25 to 36, in a flat-bottom channel, for different cases of estuary constriction.	90
Figure 3.40	Average salinities in the top layer of transect 25 to 36, in a flat-bottom channel, for different cases of estuary constriction.	91
Figure 3.41	Average salinities in the bottom layer of transect 25 to 36, in a flat-bottom channel box shape, for different cases of estuary constriction.	92
Figure 3.42	Average salinities in the top layer of transect 25 to 36, in a flat-bottom channel box shape, for different cases of estuary constriction.	93
Figure 3.43	Depth-averaged salinity in an unchanged channel, for no SLR vs. 55 cm SLR.	94
Figure 3.44	Depth-averaged salinity for cases 3, 5, and 6 for normal flow and 55 cm SLR.	95

List of Illustrations

Figure 3.45	Depth-averaged salinity for cases 3, 5, and 6 for drought flow and 55 cm SLR.	96
Figure 3.46	A schematic view of a tidal lock, with submerged gates, and a navigational channel.	97
Figure 3.47	A schematic view of a tidal lock, with radial gates, and a navigational channel.	98
Figure 3.48	Tidal amplitudes prescribed at the downstream boundary for a tidal lock system.	99
Figure 3.49	Depth-averaged salinities at transects 25 to 36 for different tidal amplitudes.	100
Figure 3.50	Average salinities in the bottom layer of transects 25 to 36 for different tidal amplitudes.	101
Figure 3.51	Average salinities in the top layer of transects 25 to 36 for different tidal amplitudes.	102
Figure 3.52	Water surface elevations at transects 2 to 36 for different tidal amplitudes.	103
Figure 3.53	Average net flux at transects 25 to 36 for different tidal amplitudes.	104
Figure 3.54	Depth-averaged salinity for no SLR vs. 55 cm SLR.	105
Figure 3.55	Average salinities at transects 25 to 36 for different tidal amplitudes.	106

List of Illustrations

Figure 3.56	Average salinities at transects 25 to 36 for different tidal amplitudes.	107
Figure 3.57	Potential change of Manning's n values in the Rappahannock River due to sea level rise.	108
Figure 3.58	Depth-averaged salinities at transects 25 to 36 for different values of Manning's n, and 55 cm SLR.	109
Figure 3.59	Water surface elevations at transects 2 to 36 for different values of Manning's n, and 55 cm SLR.	110
Figure 3.60	Maximum water surface elevations at transects 2 to 36 for different values of Manning's n, and 55 cm SLR.	111

List of Symbols

A	=	Cross-sectional area of the uppermost transect (cm^2).
A_n	=	Tidal amplitude (cm).
B	=	Width of estuary (cm).
B_b	=	Estuary width at the bottom of a layer (cm).
B_k	=	Width of layer k (cm).
B_T	=	Estuary width at the top of a layer (cm).
C	=	Drag coefficient.
e_x	=	Turbulent eddy viscosity in the X direction.
e_y	=	Turbulent eddy viscosity in the Y direction.
e_z	=	Turbulent eddy viscosity in the Z direction.
F	=	Tide conversion factor.
g	=	Gravitational acceleration (cm/sec^2).
H	=	Wave height (cm).
HHW	=	Highest high water within a period of simulated tidal cycles (cm).
h'	=	Total depth of water (cm).
h_k	=	Height of layer k (cm).
L	=	Wave length (cm).

List of Symbols

P	= Pressure (N/cm^2).
P_o	= Empirical function of temperature and salinity.
$Q(t)$	= Freshwater inflow (cm^3/sec).
q	= Tributary inflow through unit area of X-Y plane (cm^3/sec).
q_k	= Tributary inflow for layer k (cm^3/sec).
SLR	= Sea level rise (cm).
SS	= Storm surge (cm).
s	= Salinity in parts per thousand (ppt).
s_t	= Salinity concentration of tributary flow (ppt).
T	= Wave period.
t	= Time (sec).
u	= Velocity in the X direction (cm/sec).
u_b	= Longitudinal velocity at the bottom of a layer (cm/sec).
u_k	= Longitudinal velocity in layer k (cm/sec).
u_T	= Longitudinal velocity at the top of a layer (cm/sec).
u_t	= Longitudinal velocity of tributary flow (cm/sec).
v	= Velocity in Y the direction (cm/sec).
W	= Wind speed (cm/sec).
w	= Velocity in Z the direction (cm/sec).
w_b	= Vertical velocity at the bottom of a layer (cm/sec).
w_T	= Vertical velocity at the top of a layer (cm/sec).

List of Symbols

- Z = Depth (cm).
- ε_X = Turbulent mass diffusion coefficient in the X direction.
- ε_Y = Turbulent mass diffusion coefficient in the Y direction.
- ε_Z = Turbulent mass diffusion coefficient in the Z direction.
- η = Water surface elevation with respect to mean sea level (cm).
- Θ_n = Phase angle (degrees).
- λ = Function of temperature, in empirically derived equation of state.
- ρ = Density of water (gm/cm³).
- ρ_a = Density of air (gm/cm³).
- ρ_0 = Constant in empirically derived equation of state (1.4326).
- σ_n = Tidal frequency (degrees/sec).
- τ_b = Interfacial shear stress at the bottom of a layer.
- τ_T = Interfacial shear stress at the top of a layer.

1. Introduction

1.1 Study of Sea Level Rise

The effects of sea level rise caused by the greenhouse effect include coastal flooding and drainage problems, salinity change in estuaries, saltwater intrusion in coastal aquifers, shoreline retreat, inundation of marshes and wetlands, social, economic and legal impacts in terms of land use change (Barth and Titus, 1984). The most significant changes are flood inundation and salinity intrusion in estuaries. These changes are long lasting conditions whereas the changes due to extreme events such as storm surge and drought which are only for a limited duration under the present climate regime. It is necessary to improve the understanding of the hydrologic and hydraulic response to the projected sea level rise and explore possible measures in order to manage our nation's estuarine resources.

The objectives of this research are to take advance steps to assess the potential impacts of sea level rise on our nation's estuarine environments and water resources management. Specific engineering solutions are recommended to control inundation and salinity intrusion. Structure measures such as tidal barriers and tidal locks, and through long term constant stream flow augmentation are investigated for their suitability.

Quantification of the extent of the impacts is accomplished by means of computer model simulations. A laterally integrated two-dimensional, time-dependent, finite-difference numerical model is used to study time-varying tidal height, current and salinity. Through a selected estuary, parametric studies on scenarios of projected sea level rise, streamflow, change in channel cross-section profile, etc. is performed in order to have

1. Introduction

an in-depth understanding of estuarine processes for cases such as present condition versus future sea level rise, with or without control measures.

1.2 Background Information and Related On-Going Research

Earth's surface temperature is governed by the principle of heat balance among sun radiation received, reflected and heat retained. Carbon dioxide, water vapor and other gases in the atmosphere absorb some of the heat energy and therefore increase the temperature due to this heat energy trapped in the atmosphere. This phenomenon is referred to as the greenhouse warming or greenhouse effect. Hoffman (1984) has reported that CO₂ concentration in the atmosphere has increased 20% since the industrial revolution, and an 8% increase during the periods of 1958-82 has been observed at NOAA's Mauna Loa Observatory in Hawaii (Keeling, Bacastow and Whorf, 1982). The concentration of all greenhouse gases and vapor is expected to double by the year 2050 or sooner. In spite of the forecast uncertainties for global climate conditions, the national Academy of Sciences has issued two reports which conclude that the Earth's average surface temperature would increase 1.5 ° - 4.5 ° C (3-8° F) due to the doubling of greenhouse gases (Charney, 1979; Smagorinsky, 1982).

The global warming causes the global sea level to rise due to thermal expansion of seawater itself, snow and ice melt from mountains and polar glaciers, and ice discharges from the ice sheets in Greenland, West Antarctica and East Antarctica. In the past century, studies based upon tidal gauge measurements to determine trends have concluded that the worldwide sea level has risen 10-15 cm (4-6 inches) (Gornitz, *et al.* 1982). Changes in the past half century for the Mid-Atlantic region are shown in

1. Introduction

Figure 1.1. The projected changes of the accelerated sea-level rises for 2025 and 2075 (low, medium, and high scenarios) are shown for comparison with baseline (Barth and Titus, 1984). In a recent National Academy of Sciences' report, Revelle (1983) estimated that the global sea level could rise 50-150 cm (5/3 to 5 feet) by 2080. This does not take into consideration the deglaciation of the antarctic ice sheet. In a separate report by the Environmental Protection Agency (Hoffman, Keyes and Titus, 1983), scenarios of future sea level rise have been projected. The estimates for low scenarios are 13 cm by 2025 and 38 cm by 2075. High estimates are 55 cm by 2025 and 211 cm by 2075. Mid-range highs and lows are 39 cm by 2025, 137 cm by 2075; 26 cm by 2025, 91 cm by 2075. Local trends could add 1 to 2 cm per decade to the global rise along much of the Atlantic Coast and as much as 10 cm per decade in the Gulf Coast. The global warming is likely to be accomplished by significant changes in the evaporation and precipitation patterns. An atmospheric doubling of greenhouse gases would cause rainfall and evaporation to increase 11% worldwide (Environmental Protection Agency, 1984). Prediction model for a specific region or a specific frequency of rainfall recurrence is not currently available.

Sea level rise associated with the greenhouse effect is a national and international emerging problem. Its impacts remain to be open areas of research.

Taking coastal drainage problems as an example, implications in terms of design of a drainage system now against the risk of a rise in sea level or retrofitting the system in the future should be evaluated by planners and designers (Titus *et al.*, 1987). The uniqueness of storm water drainage in coastal areas has been presented by Kuo (1980, 1984, 1989). During an

1. Introduction

extraordinary storm such as a hurricane, the tide elevation associated with the storm surge is high. As a result, the flood protection measures such as a flood wall, levee, pumping station and a flap gate are necessary. If the sea level rises and/or land subsides, the head which the pump is against will increase (Kuo, 1986a, 1986b) and the height of the flood wall has to be also increased.

It is known that as the sea level rises saltwater will move further into the estuary. Spawning migrations by many fish species could be changed since the increased salinity would alter the physio-chemical signals which lead the fish into the estuary (de Sylva, 1986). Experiments have shown that many species of fish can detect a salinity difference of 0.5 ppt, and that the first reaction of fish to an unsuitable salinity is to escape (McLusky, 1989). Most freshwater animals cannot tolerate higher salinity than 5 ppt (McLusky, 1989). Furthermore, nuisance environment would move into the estuary and damage the breeding grounds of the native organisms and shell fish beds. Salinity of 15 ppt, and over, favors the development of MSX, *Minchinia Nelsoni*, which is a parasite of oysters in the Chesapeake Bay. MSX can have serious effects on oyster populations in higher salinity range of estuaries (Lippson, 1973). Besides changing conditions in the estuary, the intrusion of saltwater in estuaries and coastal aquifers will affect the water supply in many communities. The implications were demonstrated during a severe drought which struck the Delaware River Basin in the 1960's. During the worst period of the drought, the salt front advanced 33 miles up the river and forced some industries near Philadelphia to seek water from a municipal system that imports water from the Susquehanna River Basin (Hull and Titus, 1986).

1.3 Research Objectives

A rise in the sea level would affect the tides, currents, and sediment and salinity distributions within estuaries. Quantification of the extent of these effects has been accomplished by means of computer model simulations (Kuo, *et al.*, 1987; Yannaccone, 1987). A laterally integrated two-dimensional, time-dependent numerical model was used to study time-varying tidal height, current speed, salinity and suspended sediment concentration (turbidity) throughout the estuary. The Rappahannock River estuary in Virginia was selected as a case study. The objective of this research is to investigate the effectiveness of different engineering solutions to control salinity intrusion, by model simulations. The model is a systematic sequence of mathematical procedures derived from the conservation of mass equation, the equation of motion, the mass balance equation for salt and suspended sediment, and the equation of state. Finite difference equations then were written for each layer and solved numerically using prescribed boundary conditions. This numerical model was developed and verified by Kuo, *et al.* (1978) and has been adapted and modified to take the sea level rise into consideration via a change in the seaward boundary condition. The astronomic tide and the increased height of the sea level due to the greenhouse effect form the boundary condition at the mouth of the river. The response of the estuary to the sea level rise has been analyzed based on EPA's projection for the rise in terms of the high and low sea level scenarios.

2. Numerical Model

2.1 Basic Equations

"In 1978, Kuo, Nichols and Lewis developed a two-dimensional, time-dependent numerical model which would simulate the movement of water and suspended sediment in an estuary. Within the estuary, the model computes values for four main parameters: tidal height, current, salinity, and suspended sediment concentration. Three basic external forces are entered into the model as boundary conditions: tidal wave propagation, river inflow, and river-borne sediment inflow. The model is time dependent because these parameters and forces interact with one another and are continually changing with time.

In their classification of tidal models, Hinwood and Wallis (1975) state that a two-dimensional model is quite satisfactory for narrow estuaries which have no abrupt changes in cross section. Since Virginia's estuaries fit this description generally, a two-dimensional approach is taken. This means that the model will simulate the transport processes longitudinally and vertically throughout the estuary. All of the parameters computed by the model will be uniformly distributed laterally across the estuary at their respective transects.

To describe the time-varying tidal height, current and salinity distribution in an estuary, five equations are used in the computer model" (Kuo *et al.*, 1978; Yannaccone, 1987). They are: the equation of motion for an incompressible but non-homogeneous fluid, the hydrostatic equation, the continuity equation for an incompressible fluid, the mass-balance

2. Numerical Model

equation for salts, and an empirically derived equation of state. It is assumed that the fluid is laterally homogeneous and that there is no flux of mass and momentum through the lateral boundary of the estuary except at those points where tributaries enter. The equation of motion, the continuity equation, and the mass-balance equation are integrated laterally and the resultant equations are then integrated vertically over a horizontal layer, say k^{th} layer. To do this the estuary will be cut into horizontal slices through which mass and momentum may be exchanged. The results of both the vertical and horizontal integration give the following equations. The details of the derivations can be found in Appendix A.

a) the longitudinal equation of motion for an incompressible but non-homogeneous fluid

$$\begin{aligned} \frac{\partial}{\partial t}(u_k B_k h_k) + \frac{\partial}{\partial X}(u_k B_k h_k u_k) + w_T u_T B_T - w_b u_b B_b = \\ - \frac{B_k h_k}{\rho_k} \left(\frac{\partial P}{\partial X} \right)_k + \frac{\partial}{\partial X} \left(e_{X_k} B_k h_k \left(\frac{\partial u}{\partial X} \right)_k \right) + \tau_T - \tau_b + q_k u_l h_k \end{aligned} \quad (2.1)$$

b) the continuity equation for the top layer

$$\frac{\partial \eta}{\partial t} = \frac{1}{B_1} (w_b B_b - \frac{\partial}{\partial X}(u_1 B_1 h_1) + q_1 h_1) \quad (2.2)$$

b) the continuity equation for all other layers

$$w_T = \frac{1}{B_T} (w_b B_b - \frac{\partial}{\partial X}(u_k B_k h_k) + q_k h_k) \quad (2.3)$$

d) the mass-balance equation for salts

$$\frac{\partial}{\partial t}(s_k B_k h_k) + \frac{\partial}{\partial X}(u_k B_k h_k s_k) + w_T s_T B_T - w_b s_b B_b =$$

2. Numerical Model

$$\frac{\partial}{\partial X}(\epsilon_x h \frac{\partial s}{\partial X})_k + (\epsilon_z B \frac{\partial s}{\partial Z})_T - (\epsilon_z B \frac{\partial s}{\partial Z})_b + q_k s_t h_k \quad (2.4)$$

where

B_k, u_k, h_k, q_k = width, longitudinal velocity, height, and tributary inflow for the k^{th} layer, respectively

u_b, w_b, B_b = longitudinal velocity, vertical velocity, and estuary width, respectively, at the bottom of a layer

u_T, w_T, B_T = longitudinal velocity, vertical velocity, and estuary width, respectively, at the top of a layer

e_x = turbulent eddy viscosity in the X direction

P = pressure

s = salinity in parts per thousand

t = time

ϵ_x, ϵ_z = turbulent mass diffusion coefficients in the X and Z directions, respectively

η = water surface elevation with respect to mean sea level

ρ = density of water

$\tau_T = (\epsilon_z B \frac{\partial u}{\partial Z})_T$ and $\tau_b = (\epsilon_z B \frac{\partial u}{\partial Z})_{Tb}$ = interfacial shear stresses.

The fifth governing equation is an empirically derived equation of state

$$(P + P_o) \left[\frac{1}{\rho} - \frac{1}{\rho_o} \right] = \lambda \quad (2.5)$$

2. Numerical Model

where

P_o, ρ_o, λ = empirical functions of temperature and salinity

Equation (2.5) relates the water density with the salinity, temperature, and pressure. Since the effect of pressure on density is negligible for water depths discussed here, equation (2.5) may be simplified:

$$\rho = \frac{P_o}{\lambda + \frac{P_o}{\rho_o}} \quad (2.6)$$

where

$$\lambda = 1779.5 + 11.25T - 0.0745T^2 - (3.80 + 0.01T)s$$

$$\rho_o = 1.4326$$

$$P_o = 5890 + 38T - 0.375T^2 + 3s$$

Here, ρ is the density in grams per cubic centimeter, T is the temperature in degrees Celsius, and s is the salinity in parts per thousand.

Figures 2.1 and 2.2 show the coordinate system used by the model and the layer configuration, respectively. It is assumed that all of the variables are nearly constant throughout the height of each layer and the momentum and mass fluxes normal to the bottom of the channel and to the free surface are zero. The pressure term in the equation of motion is approximated by:

$$\left[\frac{\partial P}{\partial X} \right]_k = \left[\frac{\partial P}{\partial X} \right]_{k-1} + \frac{gh_{k-1}}{2} \frac{\partial \rho_{k-1}}{\partial X} + \frac{gh_k}{2} \frac{\partial \rho_k}{\partial X} \quad (2.7)$$

2. Numerical Model

Taking the top layer, for example, it is written as

$$\left[\frac{\partial P}{\partial X} \right]_1 = \frac{g}{2} (h_1 + \eta) \frac{\partial \rho_1}{\partial X} + g \rho_1 \frac{\partial \eta}{\partial X} \quad (2.8)$$

where η represents the surface elevation with respect to mean sea level and h_1 is the thickness of the top layer.

The relationships between the vertical mass and momentum exchange coefficients and the density stratification of the water column take the following form in the model developed by Kuo *et al.* (1978) who used an empirical formula for the mass exchange coefficient suggested by Pritchard (1960):

$$e_z = \epsilon_z = (v_o + v_w) (1 + 0.276 Ri)^{-2} \quad (2.9)$$

where

$$Ri = -\frac{g}{\rho} \frac{\frac{\partial \rho}{\partial Z}}{\left[\frac{\partial u}{\partial Z} \right]^2} = \text{Richardson number} \quad (2.9a)$$

$$v_o = \frac{8.59 \cdot 10^{-3} \cdot |u| \cdot [Z(h' - Z)]^2}{h'^3} \quad (2.9b)$$

$$v_w = 9.57 \cdot 10^{-3} \cdot \frac{Z(h' - Z)H}{h'T} \cdot \exp\left[\frac{-2\pi Z}{L}\right] \quad (2.9c)$$

and where

Z = depth at which ϵ_z or e_z is being calculated

h' = total depth of water

H = wave height

2. Numerical Model

T = wave period

L = wave length

For the horizontal exchange coefficients, the relationship $e_x = 10^5 \cdot e_z$ and $\varepsilon_x = 10^5 \cdot \varepsilon_z$ given by Dyer (1973) were used.

2.2 Boundary Conditions

At the bottom of the channel and at the free surface, the vertical velocity is zero. In addition, there is no mass flux of salt across the top or bottom boundaries. Therefore for the top layer

$$\varepsilon_z \cdot \left[\frac{\partial s}{\partial Z} \right]_T = 0 \quad (2.10)$$

and for the bottom layer

$$\varepsilon_z \cdot \left[\frac{\partial s}{\partial Z} \right]_b = 0 \quad (2.11)$$

Within the estuary, energy may be introduced by wind stresses or dissipated by the frictional forces created by bottom stresses. Mathematically, the wind stresses and bottom stresses result from depth integration of the longitudinal equation of motion. For the model, these stresses are formulated in the following manner:

$$\text{Wind stress} = C \rho_a W^2 \quad (2.12)$$

In Eq. (2.12), the drag coefficient C is equal to 1.3×10^{-3} , and the air density ρ_a equals $1.2 \times 10^{-3} \text{ gm/cm}^3$. The variable W represents the wind speed in m/s at a height of ten meters. As for the bottom stresses

2. Numerical Model

$$\text{Bottom stress} = \rho u_b \cdot |u_b| \cdot gn^2 (h_b)^{-1/3} \quad (2.13)$$

In Eq. (2.13), the density, longitudinal velocity component in the bottom layer, thickness of the bottom layer, and the Manning friction coefficient are represented by ρ , u_b , h_b , and n respectively.

2.3 Upstream Boundary Conditions

The upstream boundary of the model is located at the landward limit of tidal influence. It is at this point where the velocity u is specified:

$$U = Q(t)/A \quad (2.14)$$

$Q(t)$ represents the freshwater flow, and A is the cross-sectional area. The salinity at this boundary is set equal to zero at all times.

2.4 Downstream Boundary Conditions

The downstream boundary is at the mouth of the river where the ocean salinity is specified and the tidal height η as a function of time is calculated with a harmonic function:

$$\eta(t) = F \left[\sum_{n=1}^5 A_n \cos(\Theta_n + \sigma_n t) + \text{SLR} \right] + (\text{SS} - \text{HHW}) \quad (2.15)$$

In the first term, F is the tide conversion factor. The sum within the bracket represents five major tidal constituents and the magnitude of the sea level rise SLR. The last term is the difference between the storm surge SS and the highest high water HHW. A_n , Θ_n and σ_n are tidal amplitude, phase angle and frequency respectively. The tide conversion factor (F) for the Rappahannock River estuary was determined to be 0.44 by Yannaccone (1987). A sea level rise of 100 cm, at the Atlantic Coast,

therefore corresponds to a sea level rise of 44 cm at the mouth of the Rappahannock River estuary.

2.5 The Estuary Under Study

This study is a parametric study of the Rappahannock River estuary, but the model can be applied to any estuary, provided that geometric properties are given. "The Rappahannock River estuary offers several advantages for modeling. Its configuration is relatively straight and its bottom geometry is simple. There is a single axial channel which deepens irregularly with distance seaward from 5 m at Tappahannock to 14 m at the mouth. Shoals, averaging 2 m to 3 m deep, border the main channel. The estuary is largely free of extensive pollution, and sedimentation is unaffected by major dams and extensive channel dredging. Because the estuary is 175 km long (including the tidal portion of the river) and narrow (less than 8 km), lateral variations of flow and sediment concentration are small relative to the longitudinal variations. This feature allows a two-dimensional (vertical and longitudinal) analysis" (Kuo, *et al.*, 1987). In Figure 2.3 the location of the Rappahannock River is shown.

Geometrical data is provided with the model. The estuary is divided into 35 segments that are 5000 meters in length, each. Cross-sectional data is specified at the end of each segment (transect). The most upstream transect is labeled 2 and the last one, at the seaward boundary, is labeled 36. Figure 2.4 shows the model interpretation of the Rappahannock River estuary.

3. Results

3.1 Freshwater Augmentation

Freshwater augmentation is an operation of releasing water from upstream reservoirs to augment the streamflow such that the salinity level in the estuary may be brought down to a desired level.

Freshwater discharge is the primary factor controlling salinity in estuaries (Dyer, 1973) and since beginning of time has nature been balancing the delicate mixture of fresh and salt water required for the ecosystem of estuaries. But some of man's activities in the last century, such as diversion of rivers or, as in this case, greenhouse effect causing sea level rise, tend to alter that balance and thus causing increase or decrease in salinity in estuaries. An example is the changes in salinity regimes in the Charleston Harbor, South Carolina where mean surface salinity dropped from 30.1 ppt to 16.8 ppt as a result of the diversion of the Santee River in 1942 into the Cooper River, which flows into the harbor (Kjerfve and Magill, 1990). But man is not always responsible for salinity intrusion as was demonstrated during a severe drought which struck the Delaware River basin in the 1960's as mentioned earlier in this text.

As has been stated above and demonstrated in examples, salinity intrusion is directly related to the amount of freshwater discharge into the estuary. The parametric study of freshwater augmentation and its effects on salinity changes in the Rappahannock estuary will therefore be presented first in this chapter.

3. Results

3.1.1 Upstream Boundary

The model input for the upstream boundary is horizontal velocity, which is determined by a given discharge and a corresponding river stage, and salinity. The stage is determined by a stage-discharge curve for the Rappahannock River as shown in Figure 3.1. Salinity at the upstream boundary is always prescribed as 0 ppt.

Freshwater discharges used, in the study, ranged from drought flow to normal flow. Constant-flow values were used for various flows between drought and normal flow. "Normal flow is taken as the mean flow recorded at a USGS stream gauging station over the period of record. For the Rappahannock River, the gauging station closest to the upstream boundary is located near Fredericksburg. Over a period extending back to September, 1907, the average discharge has been approximately $47.0 \text{ m}^3/\text{s}$ (1660 cfs)" (Yannaccone, 1987). A study by Loganathan, Kuo, and McCormic (1985) determines the 10-year, 7-day average low flow for the Rappahannock River to be $1.52 \text{ m}^3/\text{s}$. In the study, 7-day flows of varying return periods were calculated for 115 Virginia stream gauging stations using the log-Boughton distribution.

Freshwater inflows are converted into horizontal velocities by dividing the discharges by the channel cross-sectional area, at the most landward transect. The cross-sectional data for the Rappahannock River estuary, provided with the model, is assumed to be under normal flow conditions. Therefore, the river stage at normal flow will be used as a point of reference. For model simulations of normal flow, the river cross-sections are used as given. During flows between normal and drought, the river stage falls, but never more than 0.70 m. Since this is less than the two meter thickness of the top computational layer, no changes are made in

3. Results

layer thickness. Not making these changes maintains the constant layer thickness which exists throughout the estuary. The difference in river stages at normal flow and flows below that, is subtracted from the depth which exists at normal conditions, and corresponding cross-sectional area is determined. This area is then used to determine the horizontal velocity for the discharge in question (Yannaccone, 1987).

Study of the effects of flood-flows paired with sea level rise, on salinity intrusion, was performed by Yannaccone (1987). In his study, Yannaccone added two subroutines to the model to allow for time-dependent hydrograph as input. In this study, more emphasis was placed on studying the effects on low flows since it is more critical in terms of salinity intrusion. A complete list of freshwater inflows studied is shown in Table 3.1.

3.1.2 Downstream Boundary

The downstream boundary conditions include astronomic tidal height, salinity and, of course, sea level rise. The astronomic tide is computed with the harmonic function presented in Eq. (2.15). Values of sea level rise were chosen as 13 cm, 38 cm, 55 cm, and 211 cm (Hoffman, Keyes and Titus, 1983). The sea level rise is added to the astronomic tide and the sum is multiplied by a tide conversion factor (0.44) that adjusts the tidal height at lower Chesapeake Bay, computed by Eq. (2.15), to the actual tidal height at the mouth of the Rappahannock River. The salinity at the downstream boundary is assumed to be 16 ppt and does not vary with depth. It is also assumed that this value is constant for all sea level rise scenarios, although the salinity in the Chesapeake Bay may increase some due to sea level rise. Another model for the Bay is required to predict this increase.

3. Results

Table 3.1 Freshwater discharges simulated.

<u>River Stage</u>	<u>Discharge</u>	<u>Horizontal Velocity</u>
0.05 m	1.52 m ³ /s	0.83 cm/s
0.32 m	10.0 m ³ /s	4.94 cm/s
0.49 m	20.0 m ³ /s	9.39 cm/s
0.63 m	30.0 m ³ /s	13.52 cm/s
0.70 m	40.0 m ³ /s	17.64 cm/s
0.75 m	47.0 m ³ /s	20.40 cm/s

3. Results

3.1.3 Discussion of Results for Freshwater Augmentation

The model output gives salinity data in two ways. First is as a single value of salinity at a fixed time, being the last time step in each tidal cycle simulated, for as many tidal cycles as specified. Second is an average value of salinity for the last tidal cycle simulated. In that case the salinity values for each time step (46 seconds), during a tidal cycle of 12.42 hours, are added up and averaged. For both cases, salinities are given as a single value for each layer and at every transect in the estuary.

Figures 3.2 to 3.13 show the results for flows ranging from normal (47 m³/s) to drought flow (1.52 m³/s). The values plotted represent vertically averaged salinities for a particular transect in the estuary, under different flow conditions. Transect 29, for example, has 7 layers and the model calculates salinity for each layer. These seven salinity values were added up and averaged to obtain a single value that would represent salinity at transect 29. This depth-averaged value serves only as a measure of the total change in salinity at a transect in the estuary, but does not fully reflect the changes in bottom or surface layers.

Results are not presented for transects that are upstream of transect 25. The reason being that model results fluctuated and salinities were low (less than 1 ppt) for that part of the estuary, whereas that was not the case for the lower estuary, i.e. transects 25 to 36.

Figures 3.2 to 3.13 show that in the lower estuary (transects 31-36) the salinity is less affected by either sea level rise or streamflow augmentation as the middle estuary (transects 25-30). This is illustrated on the graphs by how close the lines of different scenarios lie together, and their slope. In the lower estuary the lines lie closer together than in the middle

3. Results

estuary indicating a lesser change in salinity for a given flow condition and various sea level rise scenarios. Also, in the lower estuary, the lines have smaller gradient, than in the middle estuary, indicating that the salinity there is not significantly affected by the amount of freshwater augmented. This was expected because the lower estuary is a much larger body of water than the middle estuary, and is being fed by salt water in greater amount than fresh water. For flows between low flow and normal flow, Figures 3.2 to 3.13 indicate a general trend of salinity change in the lower and the middle estuary and can be used to estimate the amount of freshwater inflow needed to maintain current salinity level in a given transect, under different conditions of sea level rise. This is discussed in section 3.1.4.

Figures 3.14 to 3.17 depict the effects of sea level rise and flow on bottom salinities. The estuary bottom is home to oysters, clams and other species, and any significant changes in bottom salinity could damage or destroy the grounds that provide the right environment for these organisms. At transect 25 (Figure 3.14), the average bottom salinity increases approximately 1 ppt if the SLR is 38 cm and 1.4 ppt if the SLR is 55 cm. A sea level rise of 211 cm would bring the salinity level at the bottom at transect 25 to almost 16 ppt, which is the same salinity that is assumed to exist at the mouth of the Rappahannock River. Such an increase in salinity would clearly have devastating effects on all organisms that depend on moderately brackish environment. At transects 26 and 27 (Figures 3.15 and 3.16), the changes in salinity are of similar magnitude as at transect 25, but are less effected by freshwater inflow, at least for the flows depicted. From transect 28 to the river mouth the changes in bottom salinity were not greater than 0.2 ppt regardless of sea level rise and freshwater inflow, except for sea level rise of 211 cm in

3. Results

which case the bottom salinities reached that of the seaward boundary (16 ppt).

In Figures 3.18 to 3.29, surface salinities are plotted for transects 25 to 36. The surface layer is not less important than the bottom layer in the estuary ecosystem. The distribution of algae at the water surface, which are consumed by animals, is affected by salinity (Lippson, 1979) and severe changes in surface salinity would affect most estuary life-forms. Analyzing Figures 3.18 to 3.29 concludes that the same trend takes place in the surface layer as for the depth averaged case. The salinity is less affected by freshwater flow in the lower estuary than the middle estuary. It should be emphasized that these results are for discharges of relatively low magnitude and although same trend would be expected the variations in salinity from one transect to another could be different for higher flows.

In Figures 3.30 and 3.31, the 5 ppt and 10 ppt isohalines are shown under normal flow condition and sea level rise of 55 cm. The location of the isohalines represents the location where the salinity is 5 or 10 ppt on the average over the 20th tidal cycle. The extreme situation within that tidal cycle, such as at ebb tide, is therefore not shown in those graphs. The advancement of the 5 ppt isohaline is approximately 2 km, in the bottom layer. The 10 ppt isohaline advances 6 km, in the bottom layer, showing that a sea level rise of 55 cm (which corresponds to 24.2 cm at the mouth of the Rappahannock) can effect bottom organism in the estuary.

3.1.4 Engineering Applications of Freshwater Augmentation

Operation of upstream dams in a river basin is affected by legal, environmental, and engineering constraints, to name a few. If streamflow released from the upstream reservoirs is required to lower the salinity level in an estuary due to sea level rise, planners and engineers need to know the effects of such an operation. Careful consideration must be made to understand the degree of salinity decrease due to flow augmentation and how this release affect other water uses in the basin. A numerical model such as this one can be used to provide some information of such a basinwide study.

As illustrated in Figure 3.5 (transect 28), for example, it can be seen that in order to maintain the same salinity (8.6 ppt) that exists at current sea level under drought conditions, a flow augmentation of $47.0 \text{ m}^3/\text{s} - 1.52 \text{ m}^3/\text{s} = 45.5 \text{ m}^3/\text{s}$ is needed if the sea level would rise by 38 cm. That amounts to approximately 3.9 million cubic meters per day. Going upstream of transect 28 it can be seen that less freshwater needs to be augmented to lower the salinity level, caused by a 38 cm sea level rise. The opposite holds true for downstream of transect 28. As mentioned earlier the average bottom salinity increases approximately 1 ppt, at transect 25 (see Figure 3.14), if the SLR is 38 cm and 1.4 ppt if the SLR is 55 cm. Assuming a linear relationship between the salinity and the discharge for flows greater than $47.0 \text{ m}^3/\text{s}$, a flow augmentation of $48.0 \text{ m}^3/\text{s}$ would be needed to bring the salinity level to that of no SLR and drought conditions if the sea level would rise 38 cm. If the salinity level of no SLR and normal flow conditions is to be maintained, then much more flow augmentation is required.

3. Results

Salinity levels could therefore be controlled by augmenting freshwater from upstream reservoirs. The minimum capacity of those reservoirs would have to be such that it would be sufficient to meet the demands set by the amount of sea level rise and how far the salt front needed to be controlled.

3.2 Tidal Barriers

Constriction of the estuary cross-section is to limit flow of saltwater into the estuary and thus reduce the salinity level.

3.2.1 Upstream Boundary Conditions

Since the objectives of this part of the study is parametric study of the effects of cross-sectional changes on salinity intrusion, the upstream boundary conditions was kept constant for all scenarios simulated. Freshwater discharge is set at normal flow, $47 \text{ m}^3/\text{s}$, and does not change.

3.2.2 Downstream Boundary Conditions

The most significant change in downstream, or seaward, boundary is the constriction of the two most seaward transects. As mentioned in chapter 2, the model provides cross-sections of the estuary which are spaced 5000 m apart. This imposes some restrictions on how tidal barriers can be simulated with this model because any changes that are made to the cross-sections have to extend over the entire 5000 meters. Blocking of this magnitude would hardly be done in real life, but despite these shortcomings in the model the results of this parametric study could prove useful. Changes were made to the width and depth of the cross-sections. Figure 3.32 shows those cases where changes were only made to the most seaward transect (#36). In Case 1, constriction was placed in the third and fourth layer, making them the same width as the fifth layer. In Case 2, the first and second layer were narrowed to the same width as that of the third layer but other layers were unchanged. In Case 3, the top three layers were all set to have the same width as the fourth layer and

3. Results

the bottom four layers were unchanged. The reduction in cross-sectional area for cases 1, 2, and 3 is 14.4%, 35.8%, and 41.4% respectively. Figure 3.33 shows those cases where changes were made to the two most seaward transects. In Case 4, layer two through four were narrowed to the width of layer five, in transect 36, and in transect 35 layers two through eight were set to have the same width as layer five in transect 36. The reduction in cross-sectional area in Case 4 is 32.8% for transect 36 and 44.8% for transect 35. In Case 5, the width of the top layer of both transects was set the same, 2000 meters, and that width was then extended to the bottom of each transect. The reduction in area is 28.3% for transect 36 and 27.0% for transect 35. Most constriction was made in Case 6, where the top width of each transect was narrowed to 1000 meters and the remaining layers, except for the last two, were constricted further. The reduction in cross-sectional area is 62.8% for transect 36 and 63.6% for transect 35.

Salinity at the seaward boundary is 16 ppt, as before, and does not vary with depth. The tidal heights were calculated in the same manner as was done in the study of freshwater augmentation, with the exception that no sea level rise was added to the tidal height for the time being. The reason for that was to exclude other factors that could contribute to salinity intrusion and concentrate on the effects of cross-sectional changes on salinity distribution.

Each simulation was run for 50 tidal cycles (621 hours) and average salinities for the 50th tidal cycle were then calculated. 50 tidal cycles were chosen as run time to allow the estuary to adjust to the new configuration and reach equilibrium in the numerical scheme.

3.2.3 Discussion of Results for Tidal Barriers

As before, depth-averaged salinity will be used to compare the effects of the imposed constrictions on salinity distribution in the estuary. Figures 3.34 and 3.35 depict the salinity at every transect from 25 to 36 for each case of constriction plus salinity distribution in an unconstricted estuary. All cases are subject to the same boundary conditions: normal flow and no sea level rise.

Analyzing Figures 3.34 and 3.35, case by case, it can be seen that Case 1 constriction results in practically no significant change in salinity for the greater part of the estuary shown. Cases 2 and 3 result in a slight decrease in salinity. This decrease is approximately 0.3 ppt in the middle part of the estuary, but becomes less in the lower part. Cases 2 and 3 give no significant difference in results. For case 4 the average salinity levels increases in the middle part of the estuary. Between transects 30 and 31 the salinity, in case 4, reaches the same level as that of the unconstricted case. From transect 31 and seaward the salinity for case 4 is less than for the unconstricted case. The only scenarios that resulted in significant decrease in salinity were Case 5 and Case 6. For the greater part of the estuary shown, the depth-averaged salinity is 0.8 -1.2 ppt lower than it would be under the same flow conditions in an unconstricted estuary. The main difference between cases 1 through 4 and cases 5 and 6 is that for the latter the top layer is also constricted. Constriction of the top layer appears to be necessary to achieve any significant reduction in salinity, for the conditions given. That is not surprising, since the top layer is about 40% and 24% of the cross-sectional area of transects 36 and 35, respectively, thus contributing a large portion of the incoming salt-water. Constriction of both transect 36 and 35 also appears to be needed for achieving salinity reduction.

3. Results

Comparing cases 5 and 6, it can be seen that both cases give similar results, in terms of salinity reduction, and that no significant difference can be noted. Thus blocking greater than case 5 does not appear to decrease the salinity significantly, for these conditions of inflow and sea level under consideration. The effects of further blocking is depicted in Figure 3.36, where water-surface elevations are plotted for each case studied. For Case 6 (the case where constriction is greatest) the water surface elevation (WSE) is considerably higher than the other cases. The main reason is backwater effects upstream of the blocking. The graph is distorted some, because at transect 36 the WSE is fixed, by the downstream boundary condition prescribed for the model as can be seen where all the lines come together in a single point.

An important point to be made is that the model uses average widths of adjacent reaches and layers in calculating salinity concentrations. This means that narrowing transect 35 affects the width of transect 34 and further upstream. Also, the model creates a transect seaward of transect 36 (the last transect where salinity is calculated for) and assigns it the same geometry as transect 36. So in effect, constricting two transects in the model means a significant narrowing of the channel width that would be greatest at the estuary mouth, and widen gradually upstream.

In Figure 3.37, salinities in the bottom layer are plotted for each transect from 25 to 36. As can be seen, the salinities differ greatly from transect to transect. The trend in salinity changes is the same as for depth averaged salinities. As with depth-averaged salinities, cases 5 and 6 result in lowest salinities in the bottom layer. Values for transects upstream of transect 25 are not plotted because they are low (approach zero) and that the numerical model did not give stable results for that part of the

3. Results

estuary.

A possible explanation for the high fluctuation in salinity from one transect to another is the irregularities in bottom geometry and how the numerical model handles such irregularities. When a transect has more number of layers than the adjoining transect upstream, the model does not calculate horizontal velocities (i.e. $\text{horizontal velocity}=0.0$) in the layers of the downstream transect that are below the bottom layer of the upstream section. For example, transect 28 has 5 layers and transect 29 7 layers and horizontal velocities are calculated for 5 layers for both transects, but salinities are calculated for all 5 and 7 layers for transects 28 and 29, respectively. Vertical velocities do not exist for the bottom layer at any transect. This might distort the salinity distribution because even though an abrupt rise or fall in bottom does change the horizontal velocities, the stagnation point would not extend over a 5 km stretch as the model assumes.

In Figure 3.38, salinities in the top layer are plotted for the same part of the estuary as before. Same trend, in terms of salinity increase or decrease, takes place as for the bottom layer.

To study the possible effects of channel bottom geometry on salinity distribution, three trial runs were made for a channel that for the greater part had no changes in bottom elevation. This hypothetical channel had ten layer from transect 17 to the mouth, but from the upstream boundary to transect 16 the bottom configuration was the same as for the original channel. Channel width for each transect remains the same as the original channel. Runs were made for a channel with no constriction (unconstricted case) and cases 4 and 6. 20 tidal cycles were simulated for

3. Results

this configuration. Strictly speaking, these two simulations (original channel vs. channel with a flat bottom) can not be compared directly since the results shown in Figures 3.34, 3.35, 3.37, and 3.38 are for the 50th tidal cycle. But the salinity distribution, shown in Figures 3.39, 3.40, 3.41, and 3.42 should not differ that much from the 20th tidal cycle to the 50th that a completely different trend would take place.

Figure 3.39 shows salinity levels in the bottom layer of a flat-bottom channel, that has 10 layers and the same longitudinal and transverse dimensions as the Rappahannock River estuary, under normal flow conditions and no sea level rise. Case 4 and 6 refer to the same type of constriction as before. The difference in salinity from an unconstricted case to Case 6 is quite large and mostly uniform over the stretch. Case 4 shows a decrease in salinity in the bottom layer. In Figure 3.40, salinities in the top layer are plotted for the same part of the channel. There the salinities do not change significantly from an unconstricted case to the case of greatest constriction.

To study the effects of the combined change in both the channel depth and transverse dimensions on the salinity distribution in an unconstricted vs. blocked channel, a hypothetical box-shaped channel was created and the model was applied to it. This channel was 10 layers (20 meters) deep, from transect 20 to the mouth, and had constant width (2000 meters). Two types of constriction schemes were tested: 1) all but top layer of the last two transects were narrowed to width of 1000 meters (Case A). 2) same as in 1) except that the top layer was narrowed to 1500 meters (Case B). Same flow conditions were used as for previous trials ($47.0 \text{ m}^3/\text{s}$) and no sea level rise. Twenty tidal cycles were simulated and average salinities for the 20th tidal cycle are presented in Figures 3.41

3. Results

and 3.42. Figure 3.41 shows the salinity in the bottom layer for the three cases mentioned above. It is clear that salinity decreases significantly when constriction is applied to the channel and the difference in salinity, between an unconstricted channel and a constricted channel, is constant upstream of the constriction. It is also apparent that not constricting the top layer (case A) does not have much effect on the salinity distribution as compared to case B where the top layer is constricted. In Figure 3.42 the salinity in the top layer are plotted for the same stretch as before. There the trend is the same as in the bottom layer. The salinity decrease is constant and difference in salinity for case A and B is not significant.

When Figures 3.37 (Rappahannock River estuary), 3.39 (flat-bottom channel), and 3.41 (flat-bottom, box-shape channel) are compared, it is most apparent how the salinity fluctuations diminish from the real Rappahannock River to ideal estuaries. It thus can be concluded that irregularities in bottom elevation and channel width do contribute to uneven salinity distribution.

3.2.4 Engineering Applications of Tidal Barriers

Knowing that certain types of constrictions effectively reduces salinity in the estuary, it would be useful to know how much blocking is needed to lower the salinity in the event of a sea level rise.

Cases 3, 5, and 6 (Figures 3.32 and 3.33) were run with a sea level rise of 55 cm and flow conditions of drought and normal. Simulation time was 40 tidal cycles.

Figure 3.43 shows the effects of 55 cm sea level rise on the unconstricted estuary, for drought and normal flow conditions. Taking transect 27 as an

3. Results

example, it can be seen that a sea level rise of 55 cm causes an increase of 0.4 ppt and 1.2 ppt, for normal flow and drought flow respectively, as compared to normal flow condition and no sea level rise. In Figure 3.44, the salinity is plotted for cases 3, 5, and 6 for normal flow condition and 55 cm sea level rise. In order to maintain the salinity at the level of no sea level rise (7.2 ppt), a constriction greater than case 3, but less than 5 or 6 is required.

Salinity intrusion is greatest during low flows. Figure 3.45 shows that 7.2 ppt at transect 27 falls below all three curves which represent constriction cases 3, 5, and 6. It indicates that constriction more than case 6 is required. But droughts are usually a short term condition and the differences in salinity, between that of no SLR and that of cases 5 and 6 in Figure 3.45, are not critical. Therefore, judgement has to be exercised or risk analysis has to be performed in order to determine the degree of the constriction required. It should be noted that the results of this type of analysis may differ from case to case depending upon the estuary and the degree of constriction.

The difference between case 3 and cases 5 and 6, in terms of fill material needed, is quite great. To avoid excessive cost, a combination of freshwater augmentation and tidal barrier could be an alternative to prevent salinity intrusion. In that case an optimal combination of river discharge and barrier size would have to be analyzed.

3.3 Tidal Locks

"A navigation lock can act as an effective barrier to preclude almost all salinity intrusion. However, a small amount of salt water will move upstream through the lock during each lockage. Saltwater intrusion through locks can be further reduced by measures such as submerged flap gates in the lock floor and lock water intakes in an upstream sump where denser water will collect" (EM 1110-2-1613, U. S. Army Corps of Engineers).

3.3.1 Upstream and Downstream Boundary Conditions

Figure 3.46 shows schematic diagram of a tidal lock. A physical barrier is placed across the channel. This barrier consists of a number of gates which allow for flow to pass through and a navigational channel. The barrier across the channel causes the tidal amplitude upstream of the lock to be less than the actual tide downstream. The salinity level upstream of the lock is less than downstream since fresh water is collected upstream and less salt water is mixing with the freshwater inflow. Horizontal velocities just upstream of the lock are close to zero, except for localized areas close to the gates.

Figure 3.47 shows a different type of a lock and gate system. In this case, no salt water moves upstream, except for a small amount during the operation of the navigational system. The water level upstream of the barrier is higher than downstream and the amplitude is zero. This configuration would practically cause the salinity in the estuary to lower to zero.

As the existing model stands it is quite difficult, if not impossible, to make

3. Results

a realistic simulation of a tidal lock because the number of unknown factors involved in the physical process is too great. Also, the model does not allow for some of the adjustments that are required, such as making the seaward boundary velocities to be zero. The unknown factors include: the tidal range upstream of the lock, change in tidal phase angle and frequency of the lockage, actual salinity profile immediately upstream of the lock, and number and size of gates required to ensure upstream discharge to pass through. Determination of these factors and others would require an extensive and detailed hydraulic analysis on lock system, and is beyond the scope of this research.

Instead a parametric study was performed to investigate the effects of different tidal amplitudes at the upstream of the lock on salinity distribution and compare the results to the current tidal amplitude for a given flow condition. The idea is that a tidal lock would decrease the tidal amplitude upstream of the lock. Applying a factor other than 1 to the tidal amplitude downstream of the lock to obtain the amplitude upstream of the lock, the change in salinity could be simulated. No changes were made to tidal phase angle or frequency. Tidal heights for simulations are shown in Figure 3.48. Factor of 0.25, 0.50, 0.75, and 1.25 was applied to the tidal height formula (Equation 2.15). No changes were made to the estuary cross-section and a flow of $47.0 \text{ m}^3/\text{s}$ (normal flow condition) was used for all cases. Salinity at the downstream boundary (at the lock) was maintained at 16 ppt. The same salinity had to be kept at the downstream boundary, for all amplitudes simulated, in order to study the effects of tidal amplitude only.

As previously stated this is mainly a parametric study of the effects of different tidal heights at the seaward boundary on salinity distribution

and is not a detail simulation of a tidal lock itself. This simple way of prescribing the downstream boundary condition does provide some insights to the problem.

3.3.2 Discussion of Results for Tidal Locks

Figures 3.49, 3.50, and 3.51 illustrate the effects of different tidal amplitudes on salinity distribution in the estuary, from transect 25 to transect 36. The salinity values shown are average values for the 20th tidal cycle. In Figure 3.49, the depth average salinities are shown for the aforementioned amplitudes. It is apparent that a decrease in amplitude causes an increase in the average salinity in every transect in the estuary, whereas an increase in amplitude results in decreased average salinity. The difference in salinity, from an unchanged amplitude to a decreased amplitude, is small at the mouth of the estuary but becomes greater when moved upstream and reaches a very significant difference (6.6 ppt between unchanged tidal amplitude and amplitude reduction of 75%) at transect 25. The same trend can be observed from figures 3.50 and 3.51, where bottom layer and top layer salinities are plotted respectively. In the bottom layer salinities fluctuate from one transect to another but the trend is the same and the differences in salinity for various amplitudes are much greater than that experienced in the top layer.

Water surface elevations, for the 20th tidal cycle, are shown in Figure 3.52. From transect 25 to transect 36 the difference in water surface elevation is small (less than 2 cm) and it increases to 9 cm, at transect 2 (near Fredericksburg), from an unchanged tidal amplitude and a tide suppressed 75%.

The increase in salinity, due to decreased tidal amplitude, may be caused

3. Results

by less mixing in the deeper portion of the estuary. When the amplitude at the seaward boundary is decreased, smaller head exists and thus the magnitude of tidal inflow and outflow is less, causing less mixing. Taking average horizontal velocities (horizontal velocities are calculated at every time step, for every layer, within a tidal cycle and can have a negative or positive direction where positive means going towards the mouth. The average horizontal velocities are therefore the average value of all velocities calculated within the 20th tidal cycle.) for the 20th tidal cycle and multiplying them by the channel cross-sectional area at a given transect, the net flux can be obtained. In Figure 3.53 a comparison is made of the net flux at each transect, from 25 to 36, for tidal amplitudes ranging from 0.25 to 1.25 times the current amplitude. As can be seen, there is a positive (in the direction out of the estuary) net flux at every transect depicted but that flux is considerably less for cases with decreased tidal amplitude. Lower flows in and out of the estuary could mean that less “flushing” takes place and saltier water collects in the estuary. It should be emphasized that the results presented are for the Rappahannock River estuary specifically, and may not be applicable to other estuaries.

3.3.3 Engineering Applications of a Tidal Lock

It has been demonstrated that reduced tidal amplitude causes higher salinities in the estuary, given the same initial salinity of 16 ppt at the downstream boundary. It is also true that the salinity just upstream of the lock must be lower than that below the lock since only limited amount of salt water would migrate upstream through the gates (see Figure 3.46).

It is expected that the salinity in the estuary would increase when sea level rises and construction of a tidal lock might be a feasible solution for

3. Results

reducing salinity by cutting off the seawater intrusion. The lock system provides lower tidal amplitudes at the upstream of the lock and causes salinity increase in the estuary. On the other hand, the salinity level reduces significantly at the downstream boundary due to the lock system. It is possible to study the inter-relationship between salinity decrease and amplitude decrease for a given sea level rise.

Several scenarios involving normal and low flow, a representative sea level rise of 55 cm, and different tidal amplitudes were simulated. A linear relationship between downstream salinity and tidal amplitude was assumed. In other words, if the amplitude at the most seaward transect is unchanged the salinity is 16 ppt and if the amplitude is zero the salinity is 0 ppt. Scenarios simulated were: (1) Unchanged amplitude and 16 ppt salinity at the downstream boundary, (2) 75% amplitude and 12 ppt salinity, (3) 50% amplitude and 8 ppt salinity, (4) 25% amplitude and 4 ppt salinity, (5) zero amplitude and zero salinity. The scenarios were run for both normal flow ($47.0 \text{ m}^3/\text{s}$) and drought flow ($1.52 \text{ m}^3/\text{s}$).

Figure 3.54 shows the increase in salinity due to a sea level rise of 55 cm, for normal and drought flow. Taking transect 27 as an example, it can be seen that under normal flow conditions the depth average salinity would increase from 6.4 ppt to 7.2 ppt due to 55 cm sea level rise. In Figure 3.55, depth averaged salinities are plotted at every transect from 25 to 36, for amplitudes simulated under normal flow condition and 55 cm sea level rise. Salinity of 6.4 ppt at transect 27 corresponds to a point on the graph that is approximately midway between 100% amplitude and 75% amplitude, and 16 and 12 ppt respectively. In terms of engineering applications, this information provides the guideline for the lock and gate operation if the salinity level during a sea level rise is to be maintained at

3. Results

the level of no sea level rise.

Same principle would apply to other flow scenarios, such as long term drought condition. In case of a drought and a 55 cm sea level rise, the depth averaged salinity level at transect 27 would become 7.6 ppt (see Figure 3.54). If the objective were to lower that to that of normal flow condition and no sea level rise, approximately 80% reduction in amplitude has to be achieved through the lock and gate system in order to maintain 6.4 ppt salinity level (based on Figure 3.56).

Different sea level rise scenarios and flow conditions would yield different set of curves for engineering applications but the method of analysis would be the same as the one just described above.

3.4 Effect of Bottom Friction

One of the physical consequences of sea level rise is the inundation of low-lying areas, such as tidal wetlands. The flooding of wetlands has many adverse effects in terms of environmental effects and land use change. In this study, the hydrologic and hydraulic aspects of the sea level rise are of interest. In particular, the focus will be the effect of bottom friction on salinity distribution and the change in water level in the estuary.

The numerical model accepts only a single value of Manning's friction coefficient for each transect in the estuary. The Manning's n has been assumed to be the same everywhere on the wetted perimeter of the channel. If the low-lying areas, which are subjected to flooding have different frictional characteristics than the channel bottom, the laterally-averaged Manning's roughness coefficient could change. This depends, of course, on the extend of flooding and the magnitude of the change in Manning's n , due to different degree of change in wetland characteristics.

To study the effects of change in bottom friction, the Manning's n was altered at every transect from 28 (located 40 km from the mouth of the estuary) to the seaward boundary. The value of the frictional coefficient for this part of the estuary is 0.015 in the calibrated model. Values of 0.012, 0.015, and 0.018 were paired with the same flow conditions ($47.0 \text{ m}^3/\text{s}$) and sea level rise (55 cm). A change of more than 0.003 in Manning's n would hardly take place since the flooded area along the banks is relatively small compared to the main channel area. Also the difference in n for existing channel bottom and banks to be flooded might not be that great. The values chosen (0.012 and 0.018) were not

3. Results

determined by any specific criteria, but rather chosen as references for a parametric study. In Figure 3.57, Manning's n is shown along the length of the estuary. These simulations were run for twenty tidal cycles.

3.4.1 Discussion of Results

The effects of change in bottom friction on salinity distribution and water surface elevations are illustrated in Figures 3.58, 3.59, and 3.60. Values presented are average values for the 20th tidal cycle, except the maximum water surface elevation which is taken over the 20th tidal cycle.

As was expected, the change in bottom friction had almost no effect on salinity distribution in the estuary. This can be seen in Figure 3.58 where depth-averaged salinities for the three cases of Manning's n are plotted. It is apparent that the change in bottom friction does not cause any significant change in salinity.

Figure 3.59 depicts the water surface elevation at each transect in the estuary for the 20th tidal cycle. The Mean Sea Level is now at 24.2 cm, relative to current MSL, which corresponds to a 55 cm sea level rise (55 cm multiplied by a tide conversion factor of 0.44 gives 24.2 cm). Water surface elevations are not affected by change in bottom friction over the entire length of the estuary.

The maximum water surface elevations over the 20th tidal cycle are shown in Figure 3.60. The variations in elevation are not more than 3 cm, between the original value of Manning's n (0.015) and the two perturbed values. The reach of the estuary, where frictional values were changed, is relatively deep. Therefore any velocity changes in the bottom layer due to change in friction have less impact on the velocity profile than they would have in a shallower channel.

4. Conclusions

One of the problems associated with sea level rise is the intrusion of salinity into bays and estuaries, affecting groundwater sources and marine life. Different engineering solutions exist to control salinity intrusion. The feasibility of those solutions is usually determined by cost, efficiency, environmental, and institutional factors. A two-dimensional, time-dependent numerical model was used to simulate specific engineering solutions to control salinity intrusion into the Rappahannock River estuary. Parametric studies of three different control schemes were performed. They were: (1) augmentation of freshwater from upstream reservoirs, (2) constriction of the estuary cross-section near the mouth of the estuary by means of tidal barriers, and (3) a tidal lock and gate system. Emphasis was placed on studying critical cases such as drought over an extended period of time in combination with various sea level rise scenarios.

Augmentation of freshwater from upstream reservoirs was simulated by altering the freshwater inflow at the upstream boundary. Different low streamflows were paired with the projected sea level rise, at the downstream boundary. Model results showed that freshwater augmentation is effective in lowering salinity levels in the middle estuary. Salinity levels in the lower estuary were less affected than the middle estuary and therefore less controllable by augmentation. In the upper estuary where the channel cross-sections become smaller, constant

4. Conclusions

freshwater discharges would effectively maintain salinity levels that exist before any sea level rise.

Tidal barriers were simulated by narrowing the width of the channel at the seaward boundary in order to decrease the flux of salt water into the estuary. Six different simulations were made with constrictions varying in width, length, and height. All scenarios were run under the normal streamflow condition and no sea level rise so that clear comparison could be made of the effectiveness of each constriction. Results showed that the effectiveness of a tidal barrier to control salinity levels is dependent on the degree of constriction. Submerged barriers resulted in less decrease in salinity, and in some cases caused increase in salinity in parts of the estuary. A constriction extending from the bottom to the surface gave a uniform decrease of approximately 1 ppt for a great part of the estuary. The estuary geometry affects the salinity distribution in general. To study these effects, two ideal channels that had different geometrical features than the Rappahannock River were constructed. The channels include a flat bottom with variable width and a flat bottom with constant width. They had the same length as the Rappahannock River and all other model input parameters were identical. The results of these simulations indicated that almost any constrictions at the seaward boundary would contribute to lowering salinity levels at any transect upstream of the constriction.

Engineering control on salinity through tidal locks could not be realistically simulated without detail information on lock hydraulics and reconstructing a major part of the numerical model. Instead, a parametric study was performed on the effects of lower tidal amplitude on salinity distribution. One of the characteristics of tidal locks is that upstream of

4. Conclusions

the lock the tidal amplitude is less than downstream because the gates regulate the discharge through the lock. Regulating the flow of salt water into the estuary results in lower salinities upstream of the lock and thus lower salinity in the entire estuary. Results for current amplitude was compared to results for three lower amplitudes: 75%, 50%, and 25%. Parametric study on the effects of varying tidal amplitude showed that lower amplitude causes the salinity to increase. By comparing the net flux of water at each station it is apparent that lower tidal amplitude results in less flux in and out of the estuary than under current conditions and thus causing less mixing in the estuary. However, the salinity level in the estuary reduces due to the cutoff of seawater intrusion by the tidal lock system.

The final investigation carried out in the study was the effects of change in bottom friction on water surface elevations and salinity. Sea level rise causes inundation of low-lying areas. These areas then become part of the channel and thus contributing to the resistance created by bottom roughness. Frictional values were changed for a portion of the estuary, extending 40 km from the mouth, and the model was run for same flow conditions and sea level rise for all cases. Results indicate that no significant changes take place within the estuary due to the change in bottom friction.

When these results are interpreted, it should be kept in mind that they represent only the order of magnitude and that they may not be applicable to estuaries other than the Rappahannock River estuary. Several site-specific factors that exist in the field may not be incorporated in these simulations. But the general methodology can be used to investigate any estuary. This parametric study is useful in estimating the effectiveness of different engineering solutions to control salinity intrusion in estuaries.

References

- Barth, M.C., and Titus, J.G., Eds., *Greenhouse Effect and Sea Level Rise: A Challenge for This Generation*. Van Nostrand Reinhold, New York, N. Y., 1984.
- Charney, J., *Carbon Dioxide and Climate: A Scientific Assessment*. National Academy of Science Press, Washington, D.C., 1979.
- de Sylva, D.P., "Increased Storms and Estuarine Salinity and other Ecological Impacts of the 'Greenhouse Effect'." *Proceedings of the International Conference on Health and Environmental Effects of Ozone Modification and Climate Change*, Vol. 4, June, 1986.
- Dyer, K.R., *Estuaries: A Physical Introduction*. John Wiley and Sons, New York, 1973.
- Gornitz, V., Lebedeff, S., and Hansen, J., "Global Sea Level Trend in the Past Century." *Science*, Vol. 217, 1982.
- Hinwood, J.B., and Wallis, I.G., "Classification of Models of Tidal Waters." *Journal of the Hydraulics Division*, ASCE, Vol. 101, No. HY10, Proc. Paper 11643, October, 1975, pp. 1315-1327.
- Hoffman, J.S., Keyes, D., and Titus, J.G., *Projecting Future Sea Level Rise*. U.S. GPO#055-000-0236-3. Washington, D.C.: Government Printing Office, 1983.

References

- Hoffman, J.S., "Estimates of Future Sea Level Rise." In: *Greenhouse Effect and Sea Level Rise: A Challenge for This Generation*, eds., Barth, M.C., Titus, J.G., Van Nostrand Reinhold, New York, N.Y., 1984.
- Hull, C.H.J., and Titus, J.G., eds., *Greenhouse Effect, Sea Level Rise, and Salinity in the Delaware Estuary*. Washington, D.C., U.S. Environmental Protection Agency, EPA, 230-05-86-010, 1983.
- Keeling, C.D., Bacastow, R.B., and Whorf, T.P., "Measurements of the Concentration of Carbon Dioxide at Mauna Loa, Hawaii." *Carbon Dioxide Review: 1982*, W. Clark, Ed., Oxford University Press, New York, N.Y., 1982.
- Kjerfve, B., and Magill, K.E., "Salinity Changes in Charleston Harbor 1922-1987." *Journal of Waterway, Port, Coastal, and Ocean Engineering*, ASCE, Vol. 116, No. 2, March/April, 1990.
- Kuo, A.Y., Nichols, M., and Lewis, J., *Modeling Sediment Movement in the Turbidity Maximum of an Estuary*, Virginia Water Resources Research Center Bulletin #111, June, 1978.
- Kuo, C.Y., Ed., *Urban Storm Water Management in Coastal Areas*, American Society of Civil Engineers, 1980.
- Kuo, C.Y., "Some Hydraulic Problems Related to Storm Water Drainage Design in Coastal Areas." *Proceedings of the Southeastern Conference on Theoretical and Applied Mechanics XII*. Gallaway Gardens, Ga., Invited Paper, Vol. II, May, 1984.
- Kuo, C.Y., "Flooding in Tapei, Taiwan and Coastal Drainage." *Proceedings of the International Conference on Health and Environmental*

References

- Effects of Ozone Modification and Climate Change*, Arlington, Virginia, Vol. 4, June, 1986.
- Kuo, C.Y., "Sea Level Rise and Coastal Storm Water Drainage." In *Proceedings of the Water Forum '86*, American Society of Civil Engineers, Invited Paper, August, 1986.
- Kuo, C.Y., Yannaccone, J.A., and Kuo, A.Y., "Sea Level Rise and Estuarine Processes." In *Proceedings of the National Conference on Hydraulic Engineering*, August, 1987.
- Kuo, C.Y., and Campell, R.A., "An Overview of Coastal Storm Water Drainage Problems." *Proceedings of the 1989 National Conference on Hydraulic Engineering*, August, 1989.
- Lippson, A.J., et.al., *Environmental Atlas of the Potomac Estuary*, Maryland Department of Natural Resources, William & Heintz Map Corporation, Washington, D.C., 1979.
- Lippson, A.J., *The Chesapeake Bay in Maryland, an Atlas of Natural Resources*, John Hopkins University Press, 1973.
- Loganathan, G.V., Kuo, C.Y., and Yannaccone, J.A., "Joint Probability Distribution of Tides and Streamflow in Estuaries." *International Journal of Nordic Hydrology*, Vol. 18, No. 4/5, 1987.
- McLusky, D.S., *The Estuarine Ecosystem*, Blackie and Son Ltd, Glaskow, 1989.
- Pritchard, D.W., "The Movement and Mixing of Contaminants in Tidal Estuaries." In *Waste Disposal in the Marine Environment*,

References

- Pergamon Press, New York, N.Y., 1960.
- Titus, J.G., Kuo, C.Y., Gibbs, M.J., LaRoche, T.B., Webb, M.K., and Waddell, J.O., "Sea Level Rise and Coastal Drainage Systems." *Journal of Water Resources Planning and Management*, American Society of Civil Engineers, March, 1987.
- U.S. Army Corps of Engineers, "Tidal Hydraulics, Engineering and Design." *Engineering Manual, EM 1110-2-1607*, August, 1965.
- U.S. Army Corps of Engineers, "Hydraulic Design of Deep Draft Navigation Projects, Engineering and Design." *Engineering Manual, EM 1110-2-1613*, April, 1983.
- U.S. Army Corps of Engineers, "Hydraulic Design of Deep Draft Navigation Projects, Engineering and Design." *Engineering Manual, EM 1110-2-1202*, May, 1983.
- U.S. Environmental Protection Agency, Potential Climatic Impacts of Increasing Atmospheric CO₂ with Emphasis on Water Availability and Hydrology in the United States, Government Printing Office, Washington, D.C., 1984.
- Yannaccone, J.A., "Numerical Simulation of the Effects of Sea Level Rise on Estuarine Processes." M.S. Thesis, Department of Civil Engineering, Virginia Polytechnic Institute and State University, May, 1987.

Figures

Figures

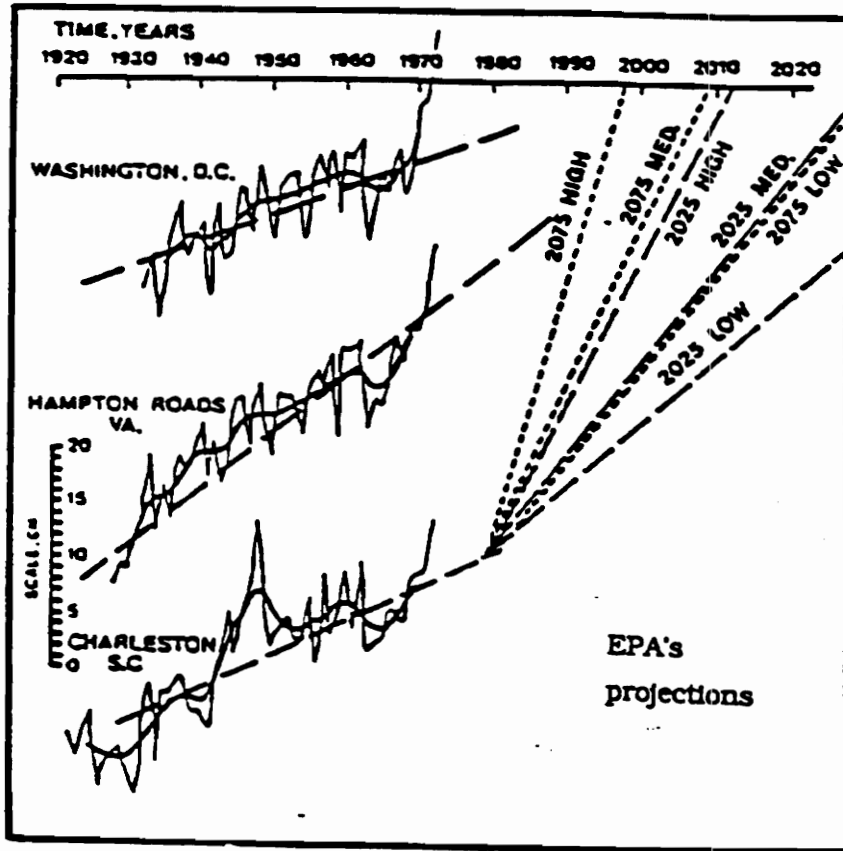


Figure 1.1 Change in sea level with respect to adjacent land for stations from the District of Columbia to South Carolina.

Figures

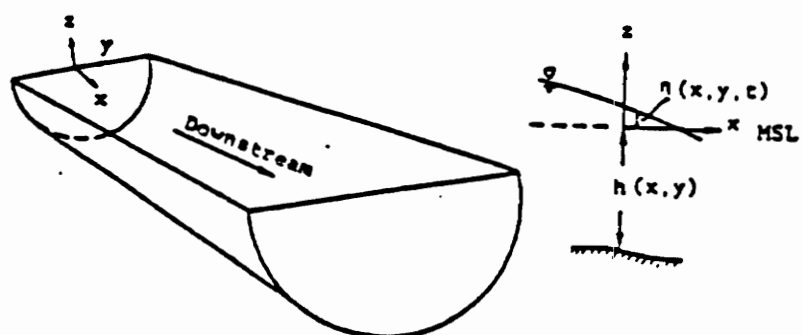


Figure 2.1 Coordinate system used in the numerical model (from Kuo, Nichols and Lewis, 1978).

Figures

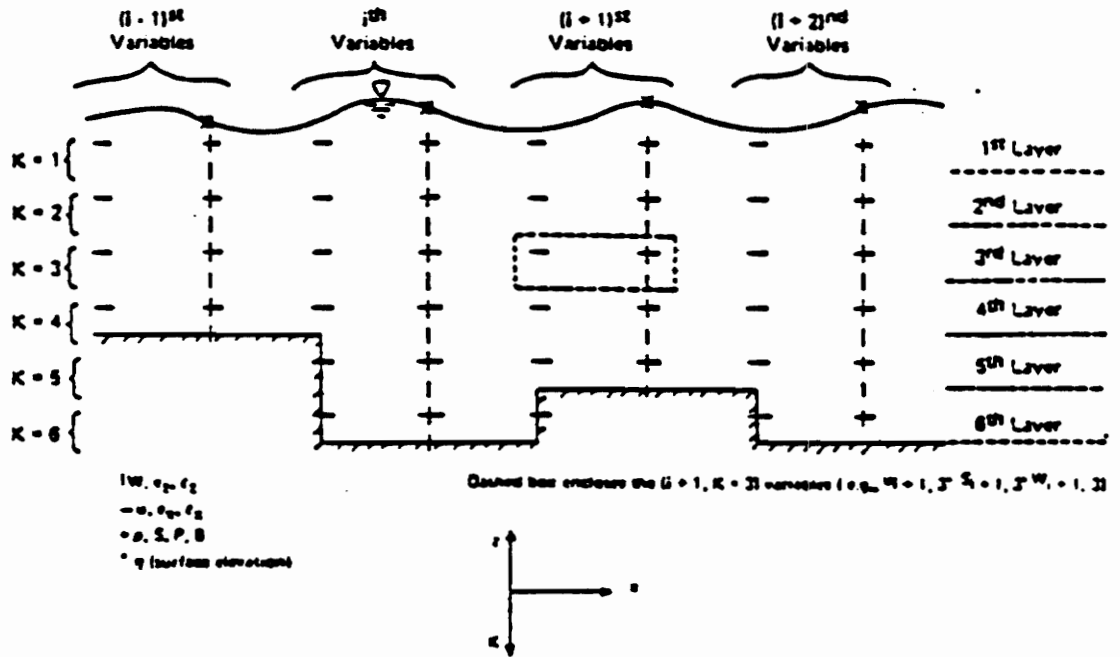


Figure 2.2 Grid pattern, location and indexing of variables (from Kuo, Nichols and Lewis, 1978).

Figures

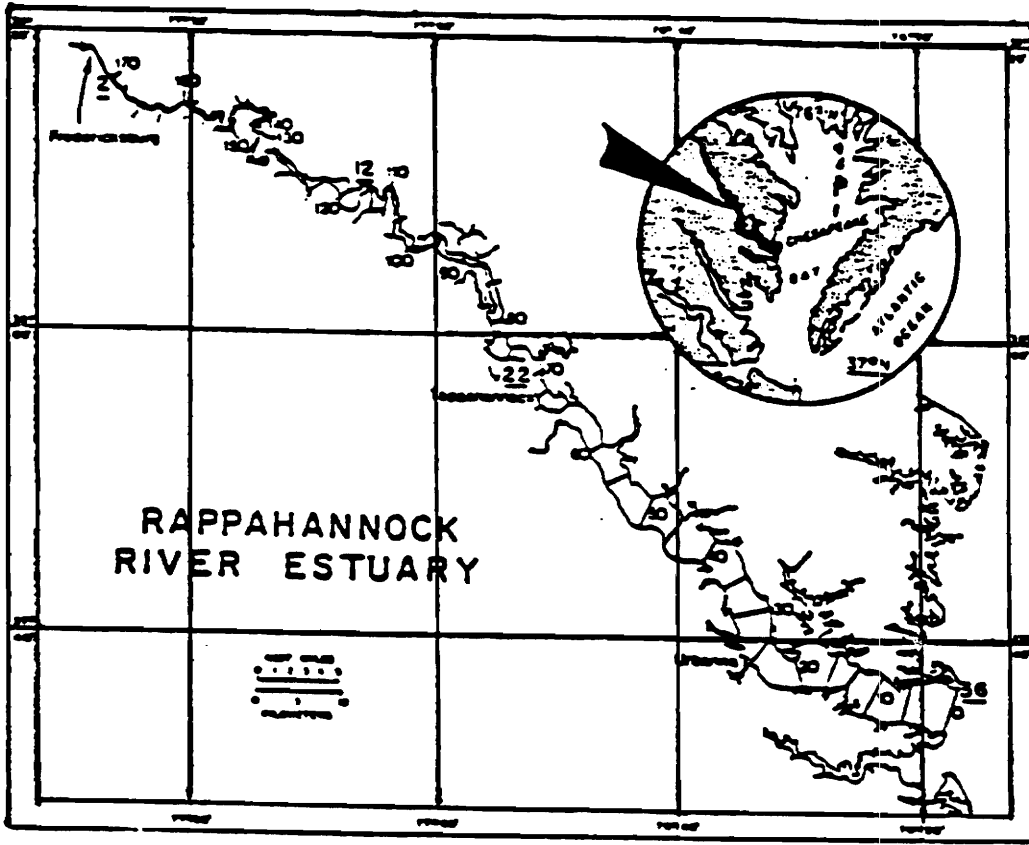


Figure 2.3 Location of the Rappahannock River-lower inset and longitudinal segmentation scheme (from Kuo, Nichols and Lewis, 1978).

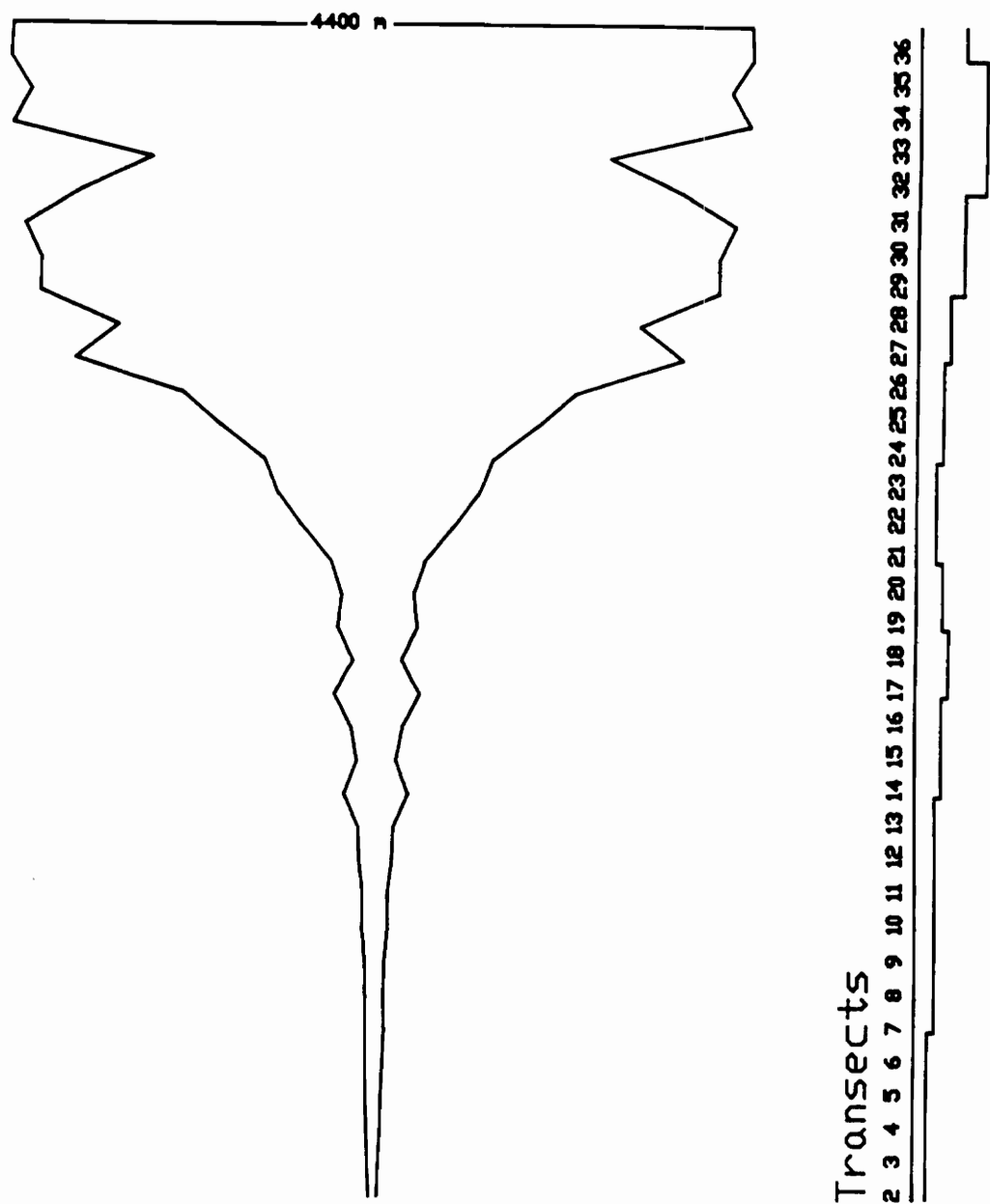


Figure 2.4 Model interpretation of the Rappahannock River estuary.

Figures

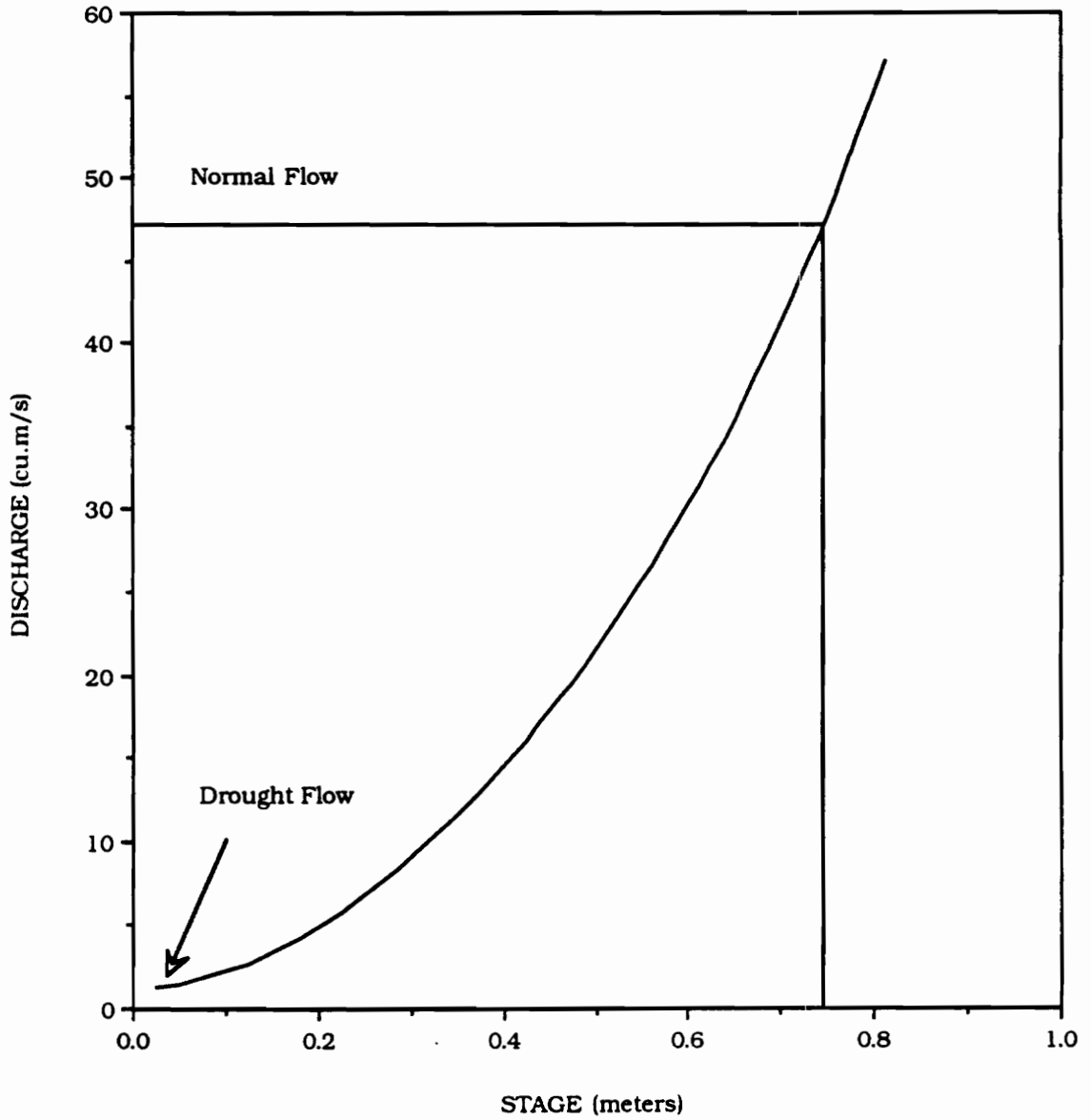


Figure 3.1 Stage-discharge curve for the Rappahannock River (from Yannaccone, 1987).

Figures

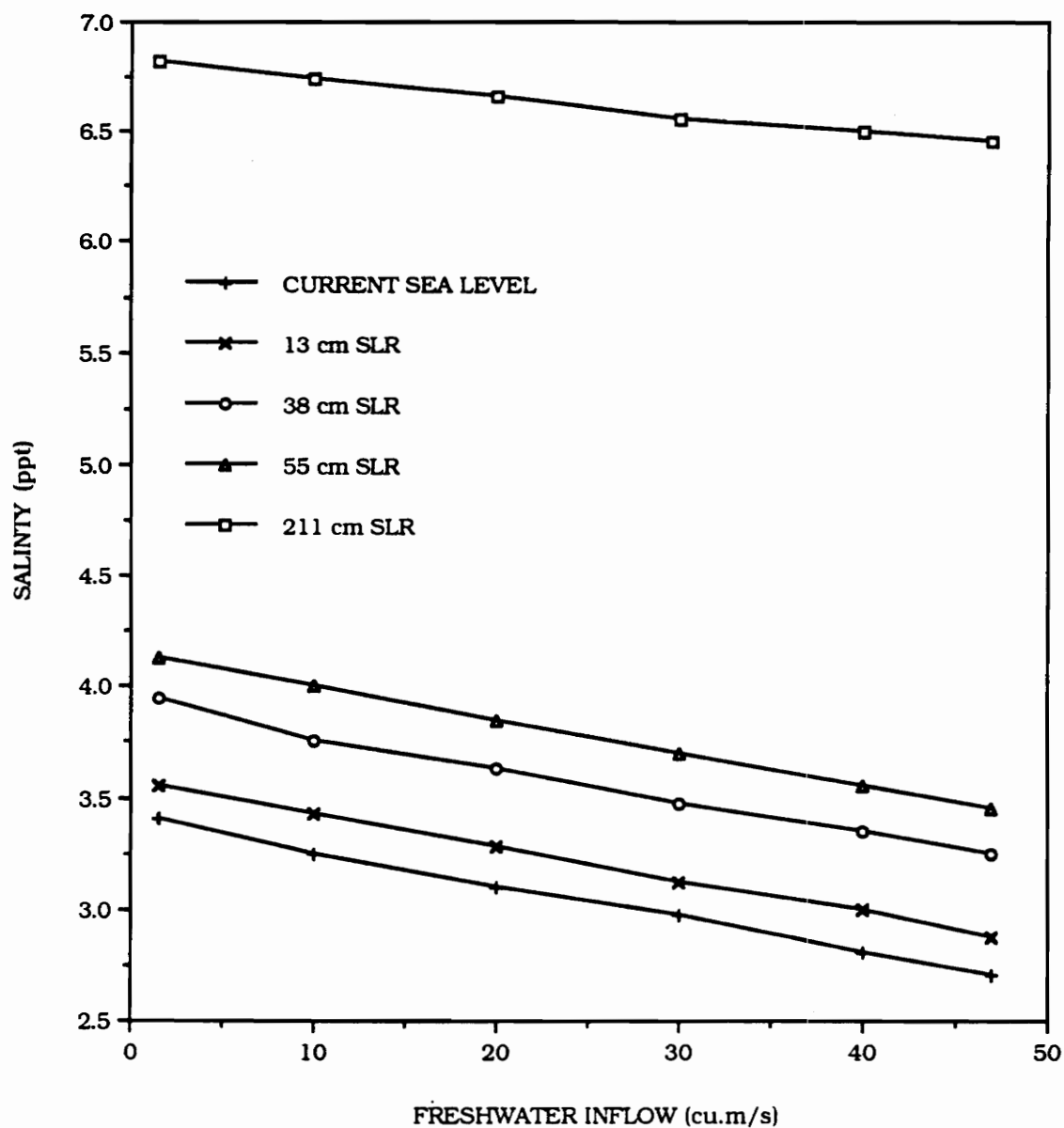


Figure 3.2 Depth-averaged salinity at transect 25 for different conditions of freshwater inflow and sea level rise.

Figures

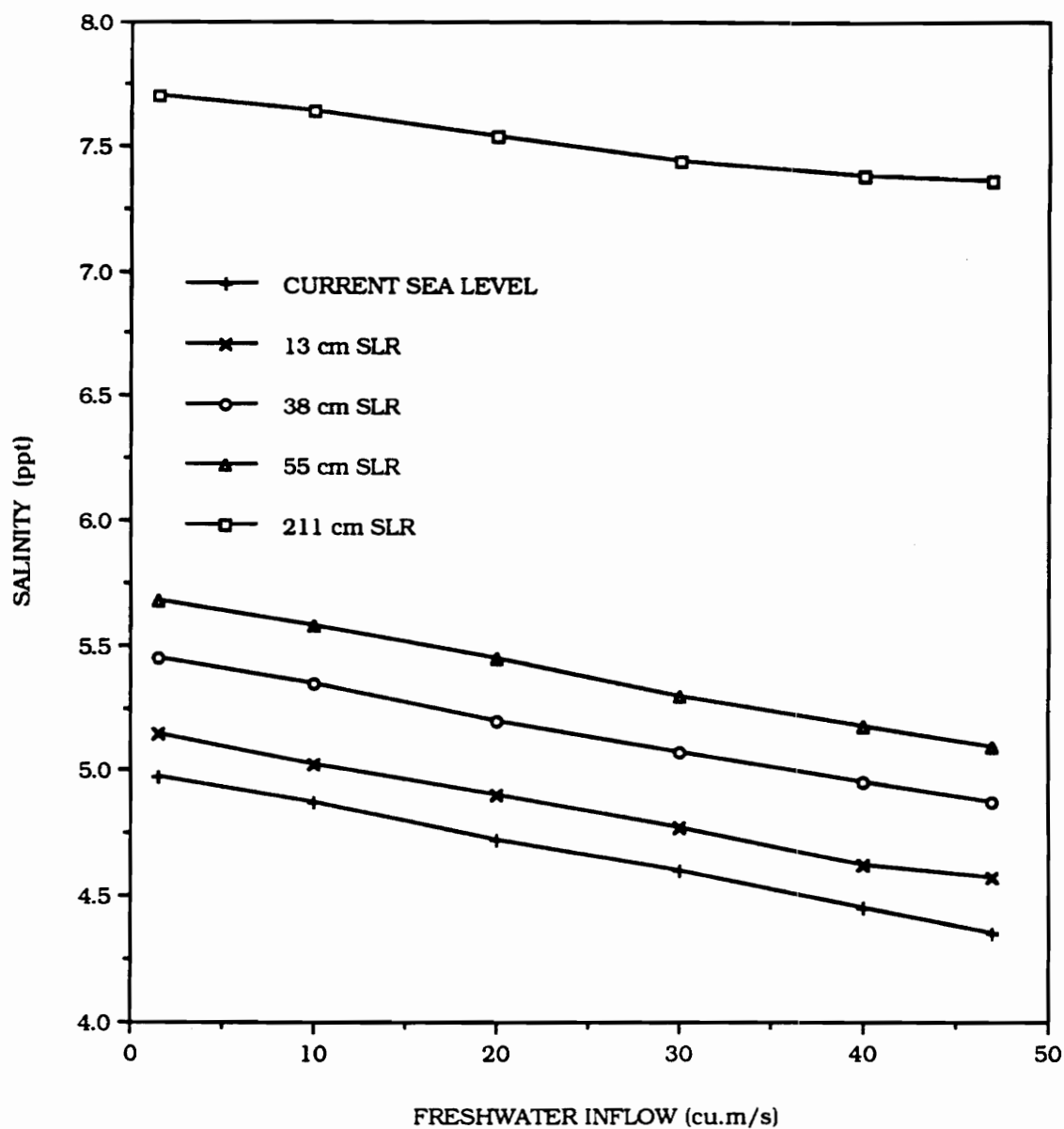


Figure 3.3 Depth-averaged salinity at transect 26 for different conditions of freshwater inflow and sea level rise.

Figures

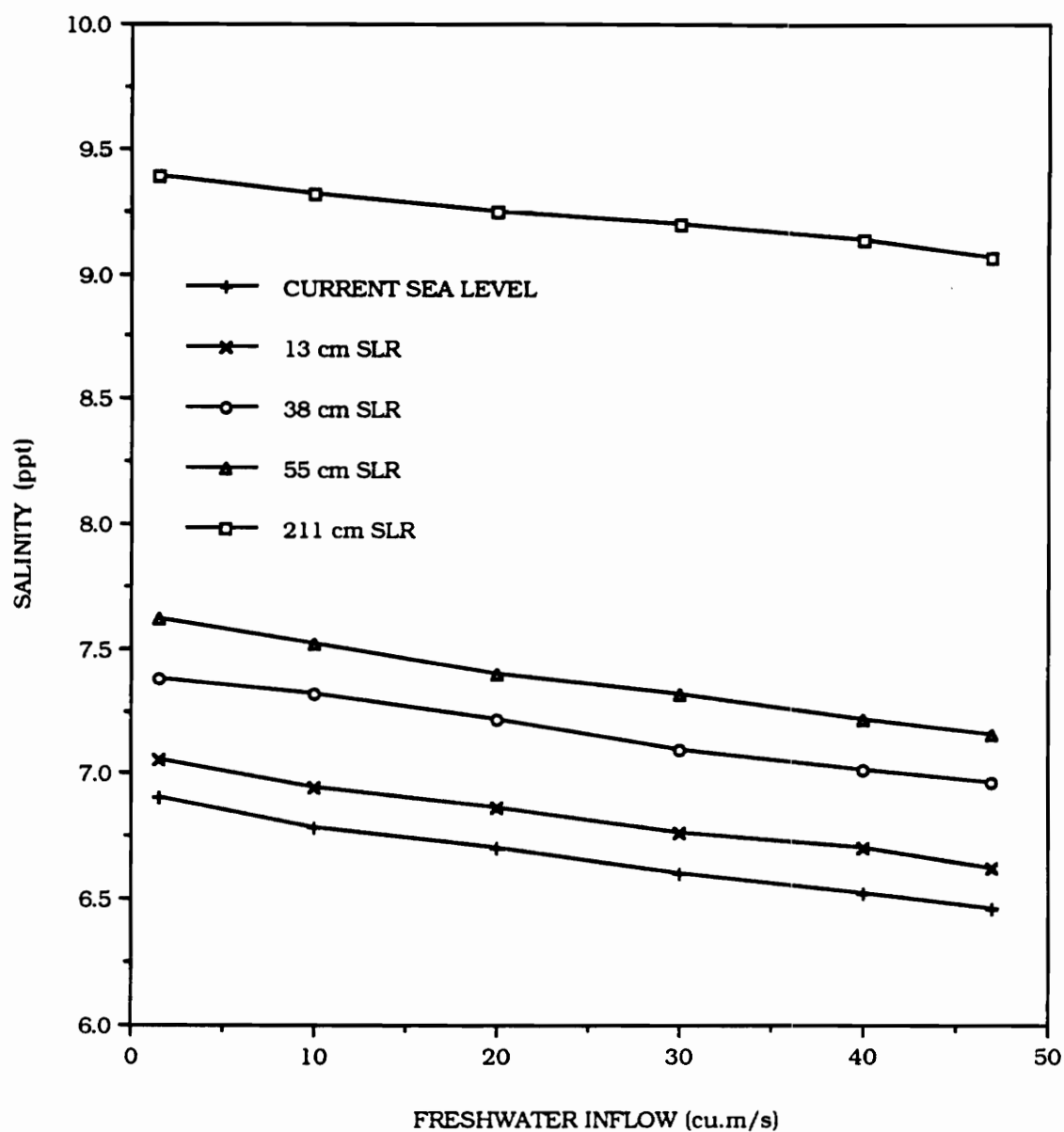


Figure 3.4 Depth-averaged salinity at transect 27 for different conditions of freshwater inflow and sea level rise.

Figures

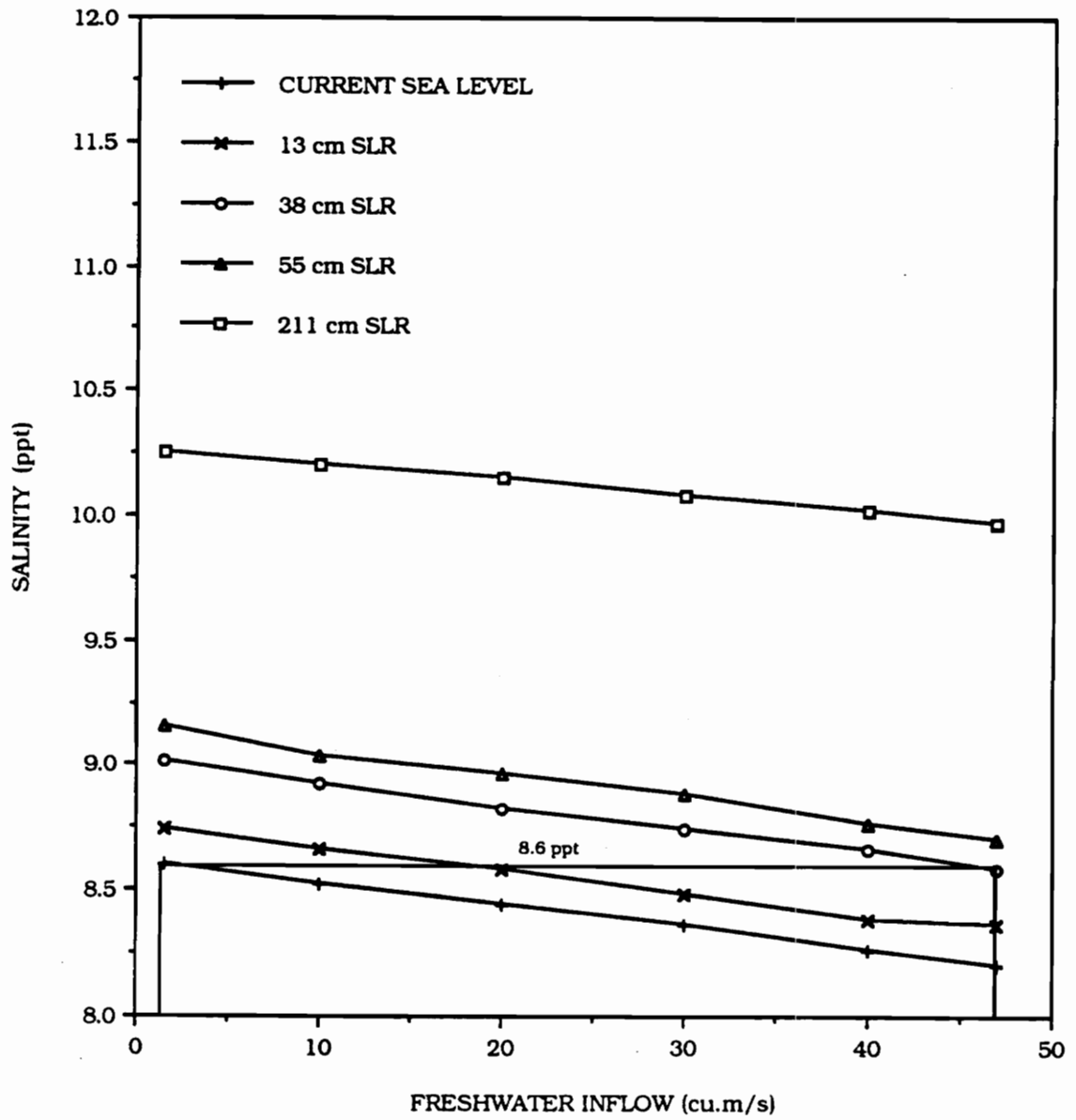


Figure 3.5 Depth-averaged salinity at transect 28 for different conditions of freshwater inflow and sea level rise.

Figures

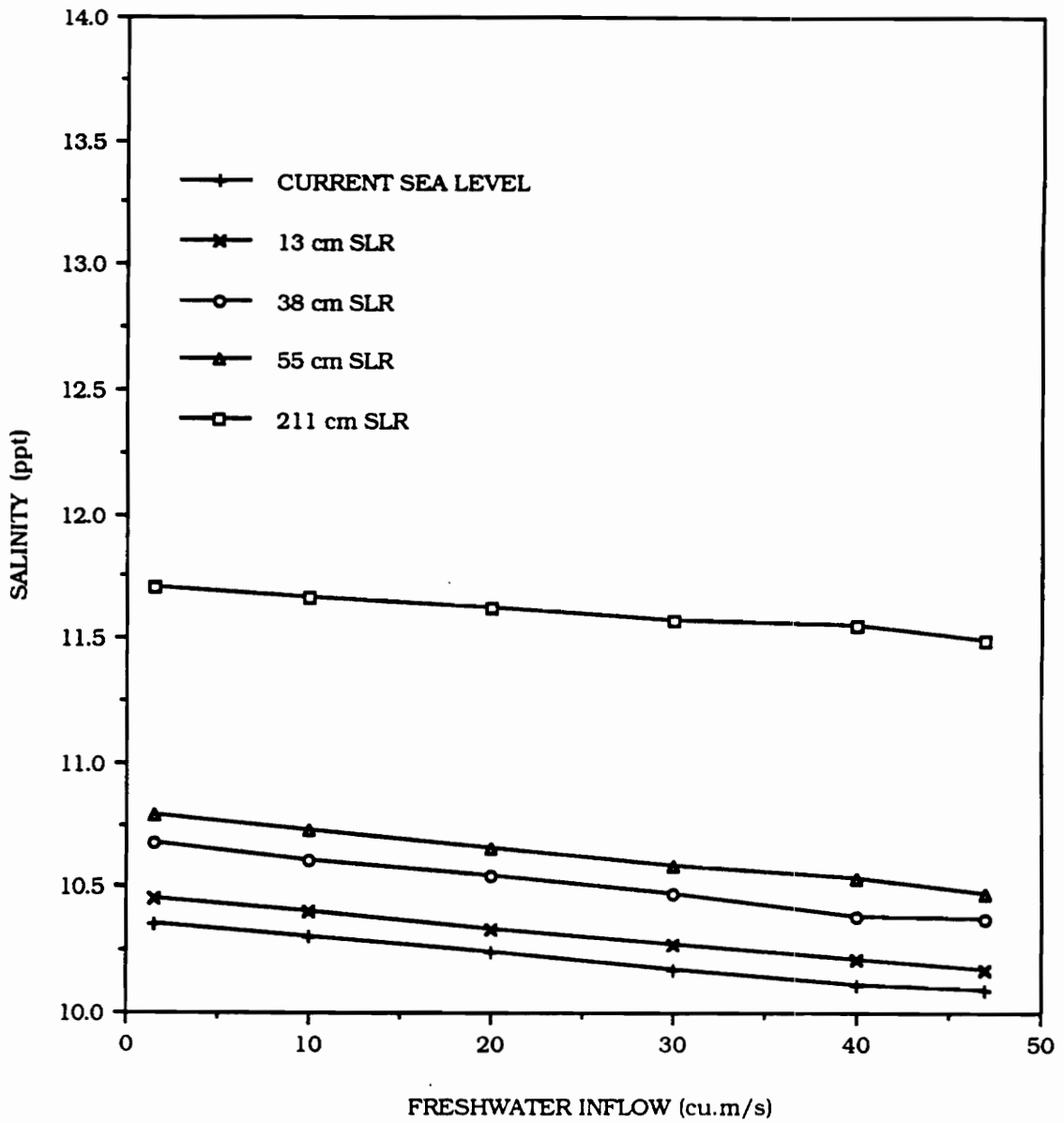


Figure 3.6 Depth-averaged salinity at transect 29 for different conditions of freshwater inflow and sea level rise.

Figures

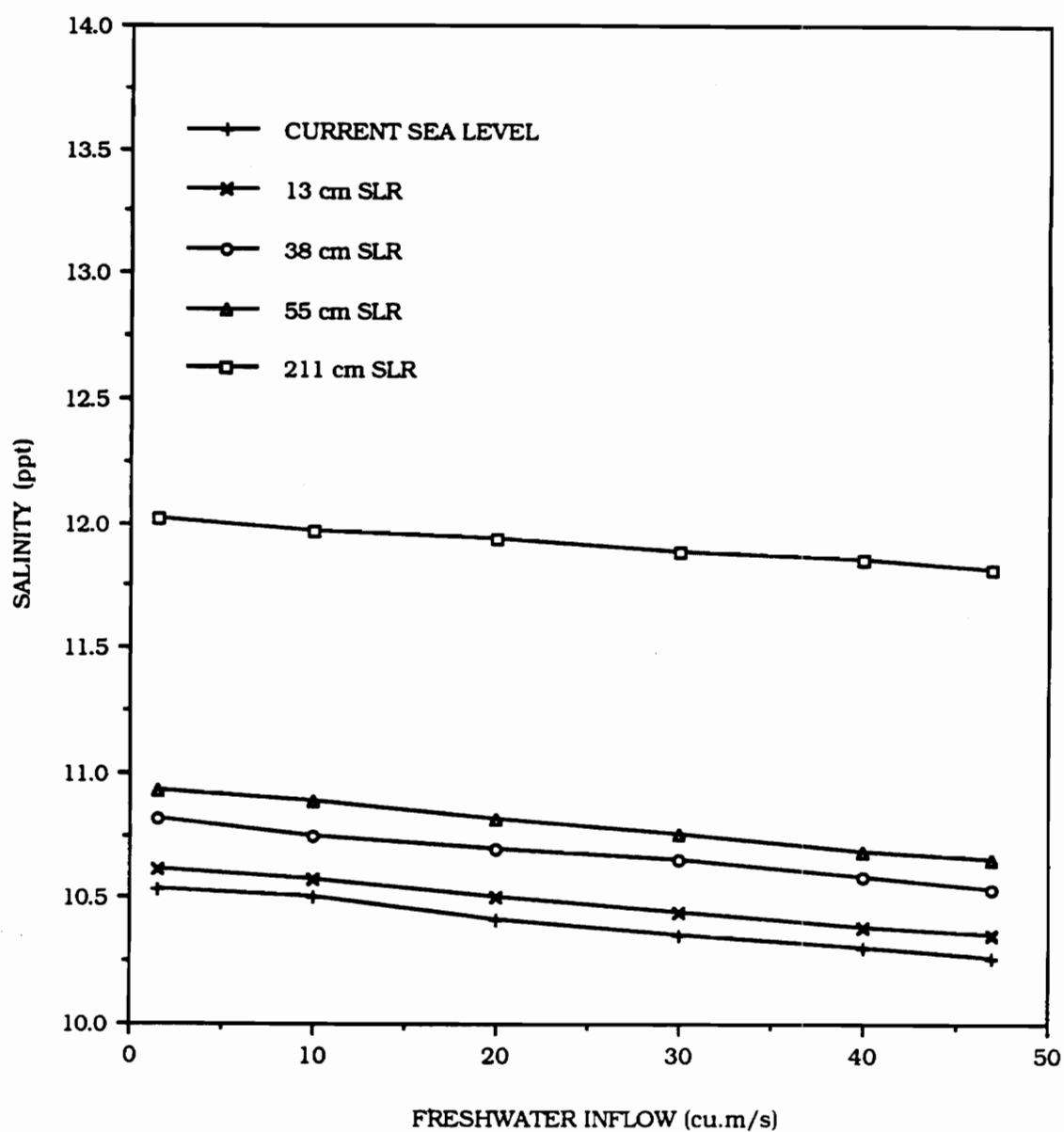


Figure 3.7 Depth-averaged salinity at transect 30 for different conditions of freshwater inflow and sea level rise.

Figures

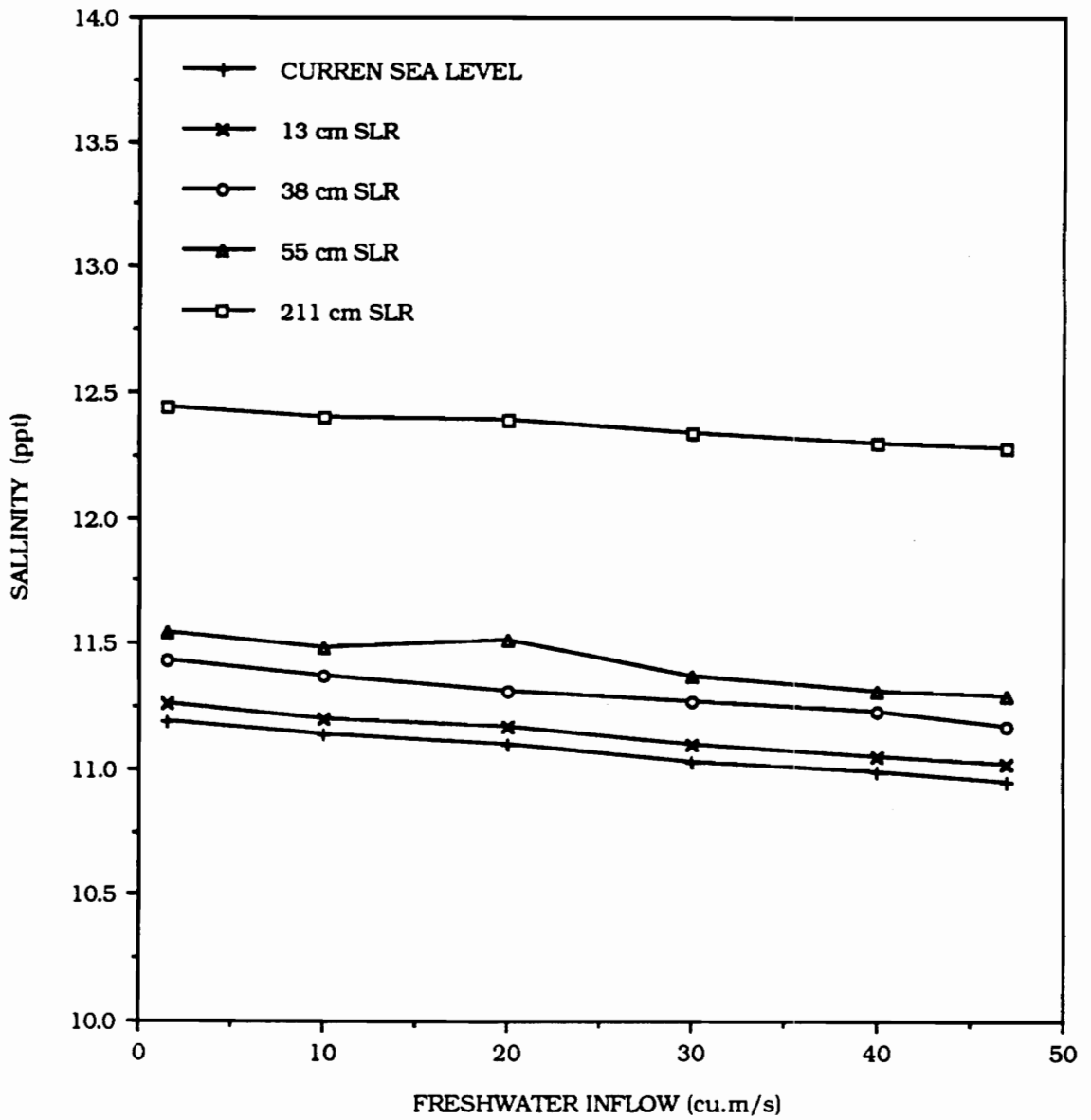


Figure 3.8 Depth-averaged salinity at transect 31 for different conditions of freshwater inflow and sea level rise.

Figures

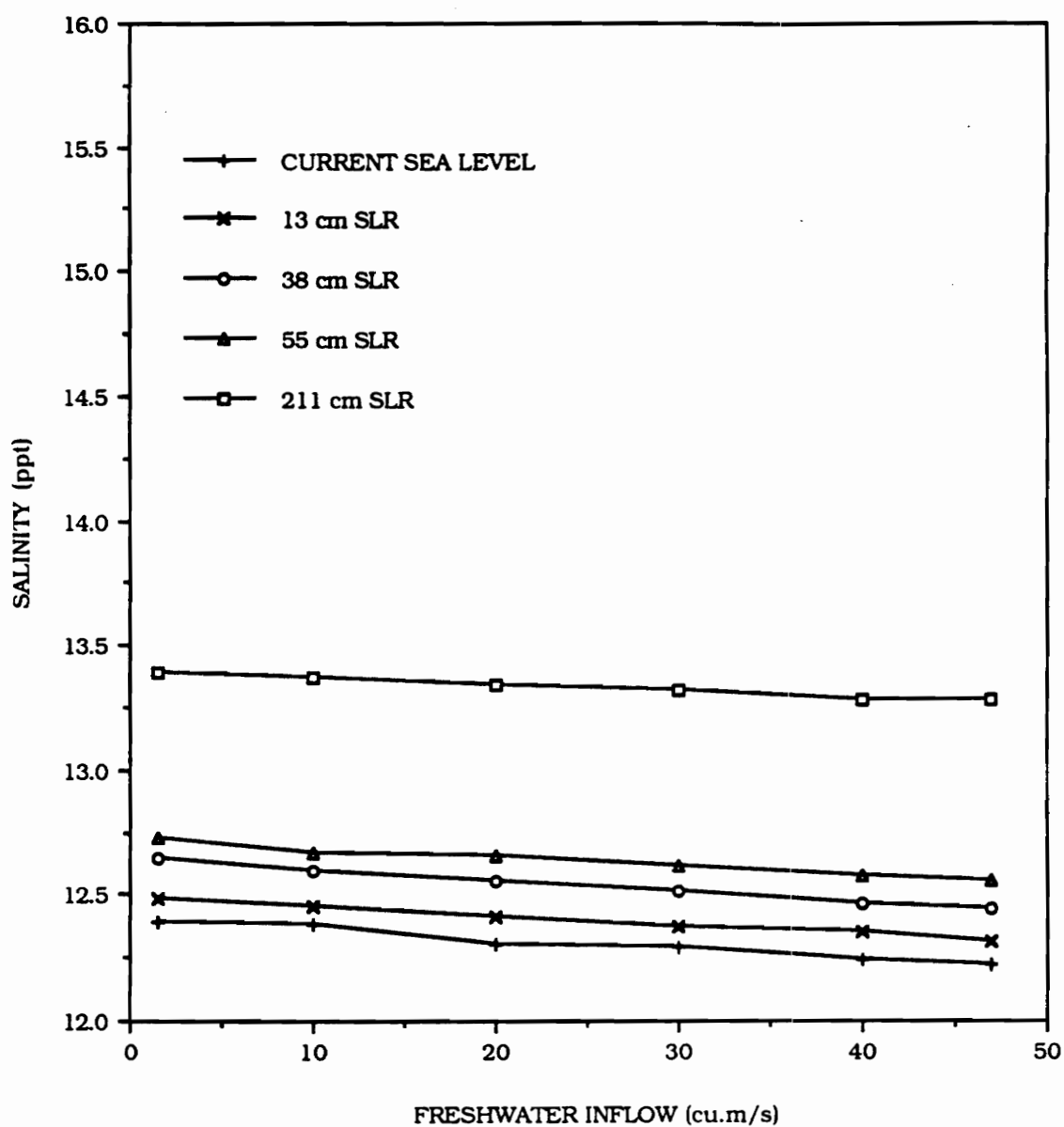


Figure 3.9 Depth-averaged salinity at transect 32 for different conditions of freshwater inflow and sea level rise.

Figures

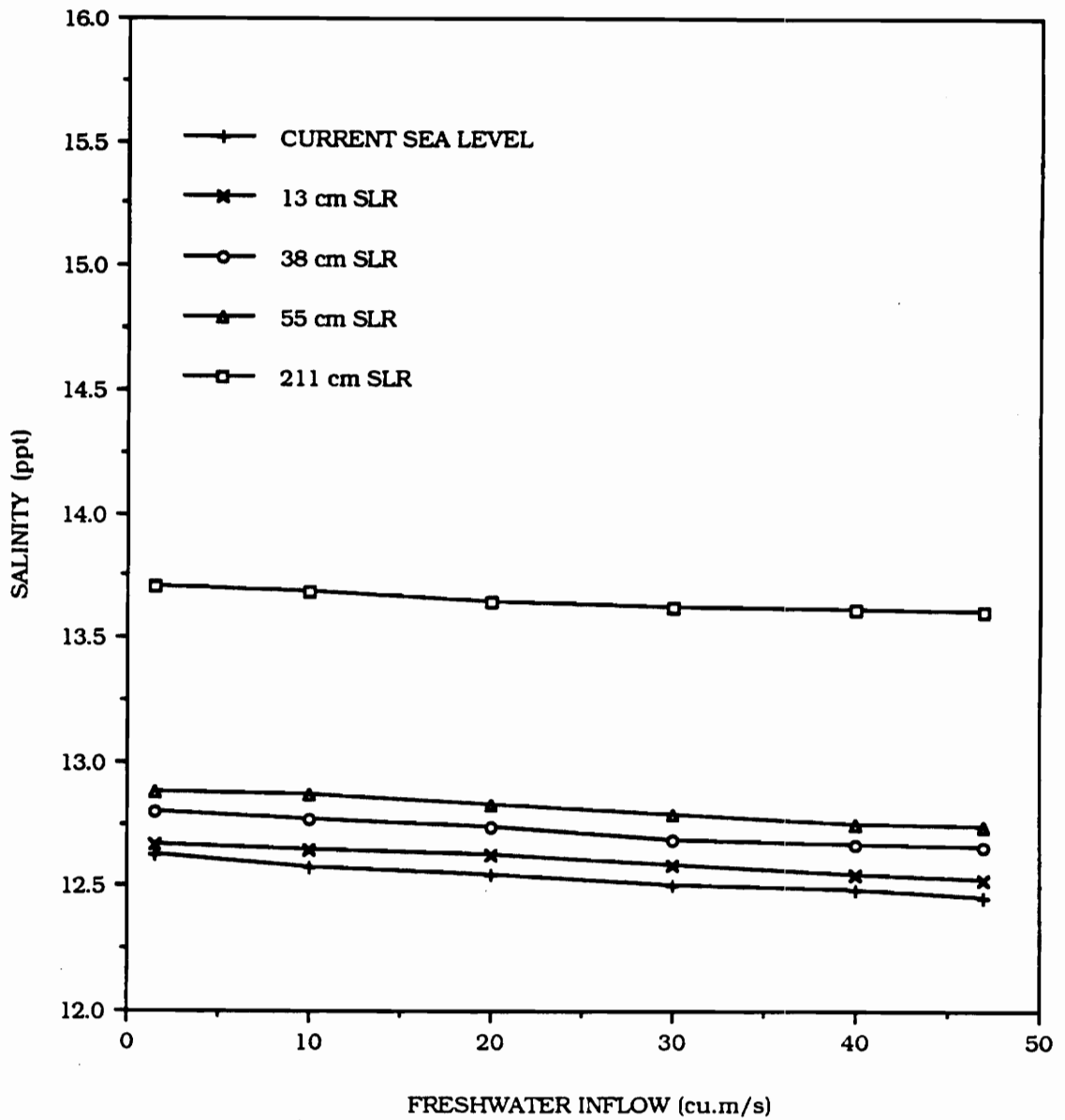


Figure 3.10 Depth-averaged salinity at transect 33 for different conditions of freshwater inflow and sea level rise.

Figures

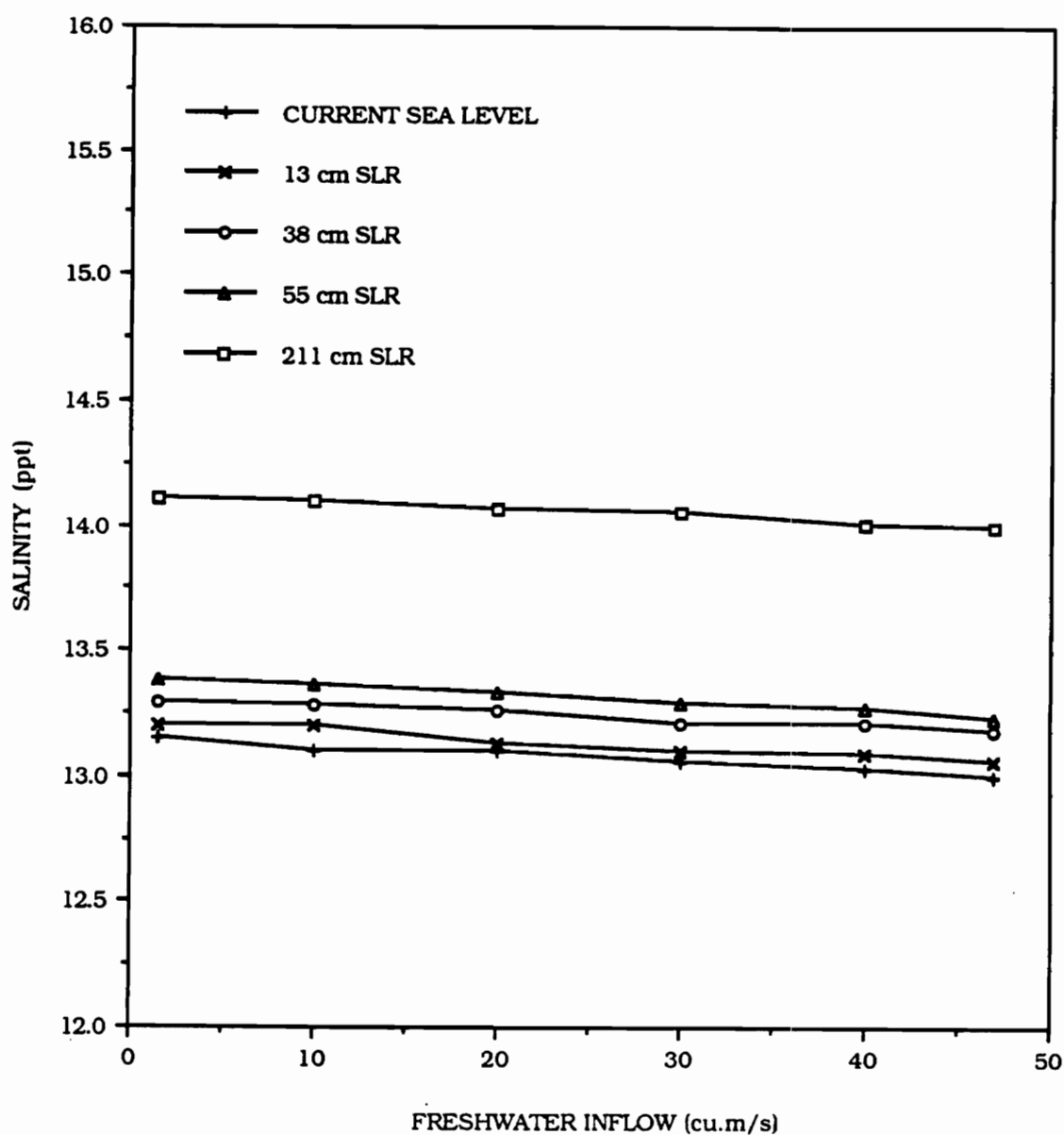


Figure 3.11 Depth-averaged salinity at transect 34 for different conditions of freshwater inflow and sea level rise.

Figures

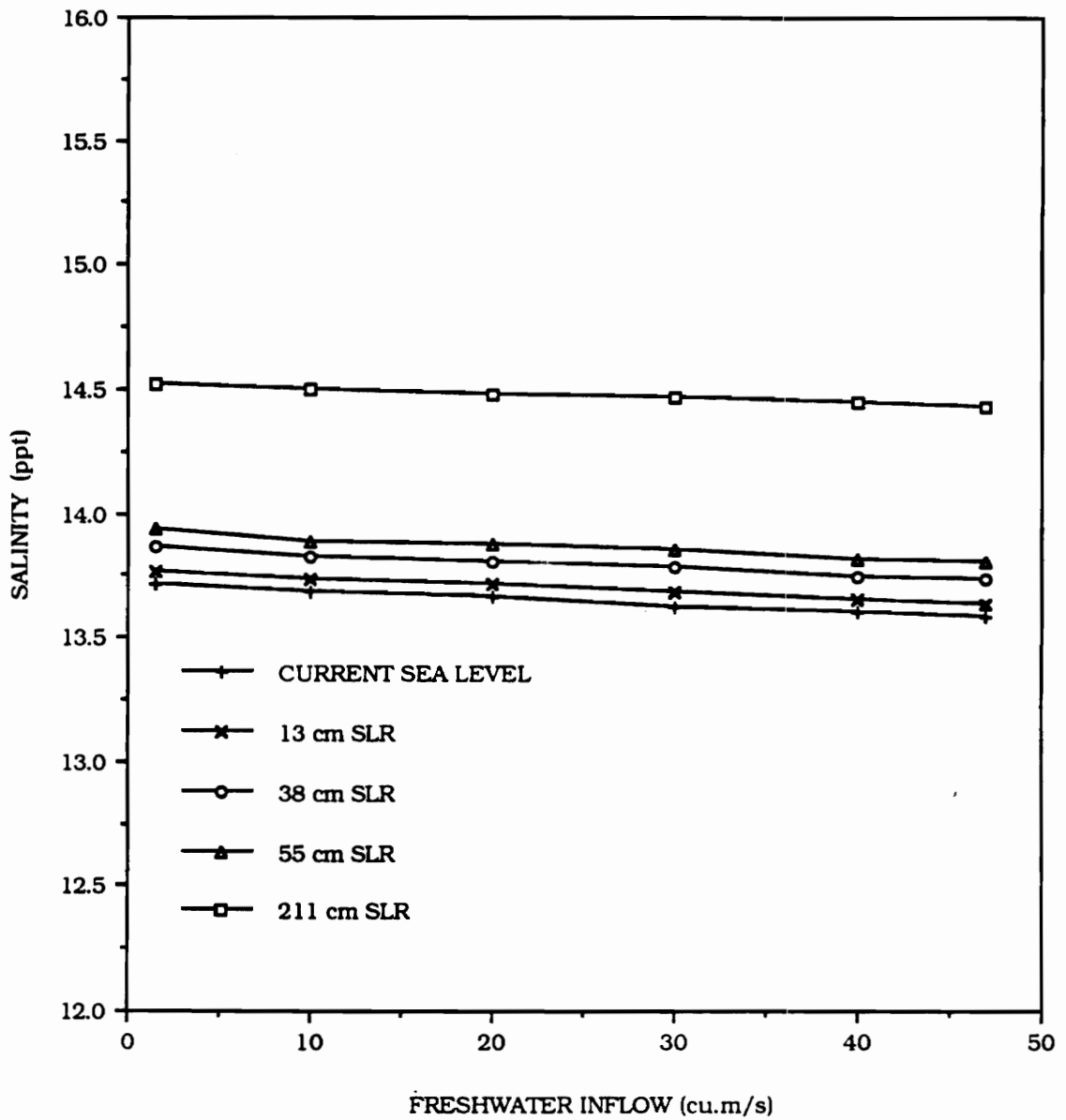


Figure 3.12 Depth-averaged salinity at transect 35 for different conditions of freshwater inflow and sea level rise.

Figures

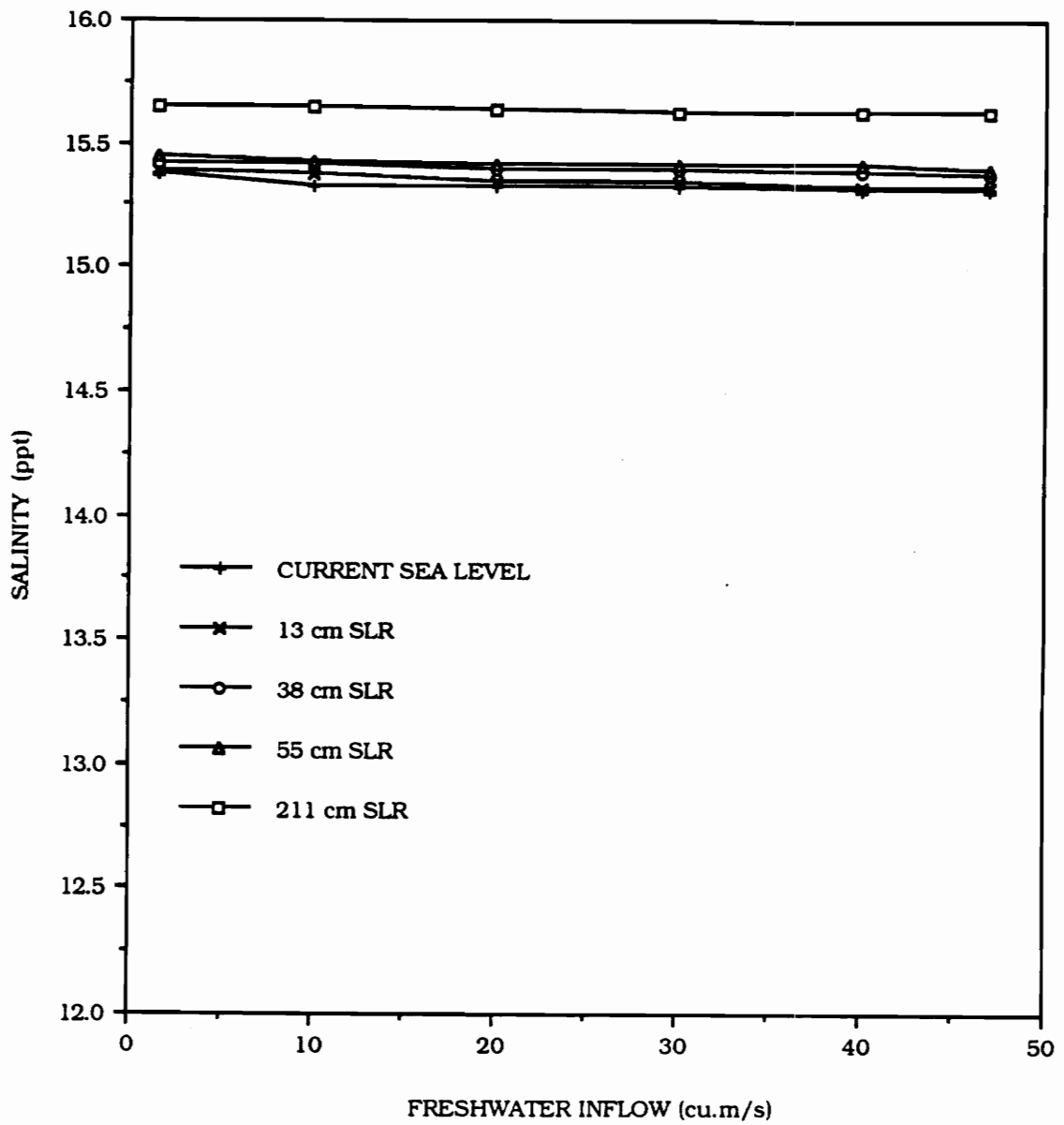


Figure 3.13 Depth-averaged salinity at transect 36 for different conditions of freshwater inflow and sea level rise.

Figures

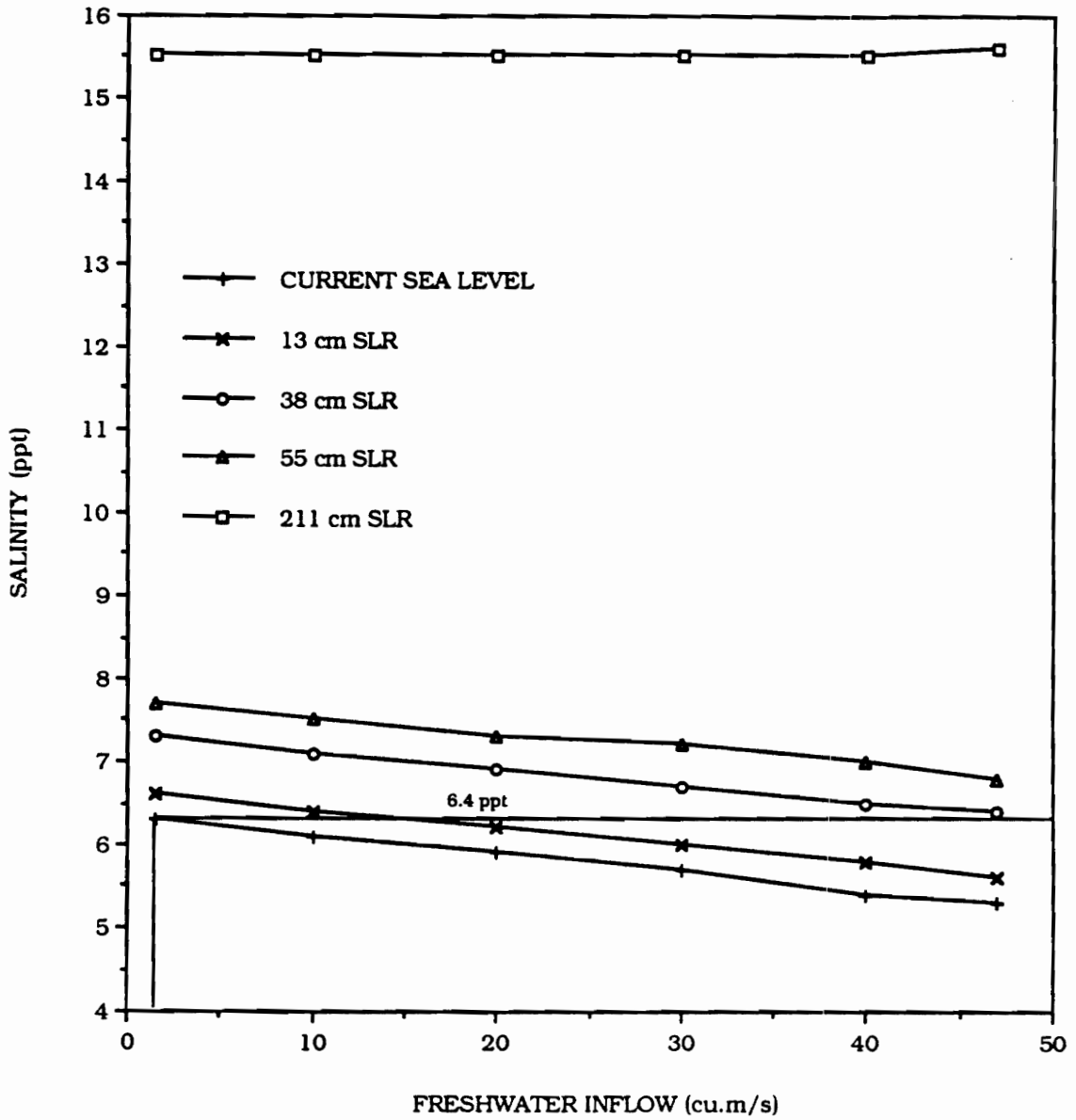


Figure 3.14 Average salinity in bottom layer of transect 25 for different conditions of freshwater inflow and sea level rise.

Figures

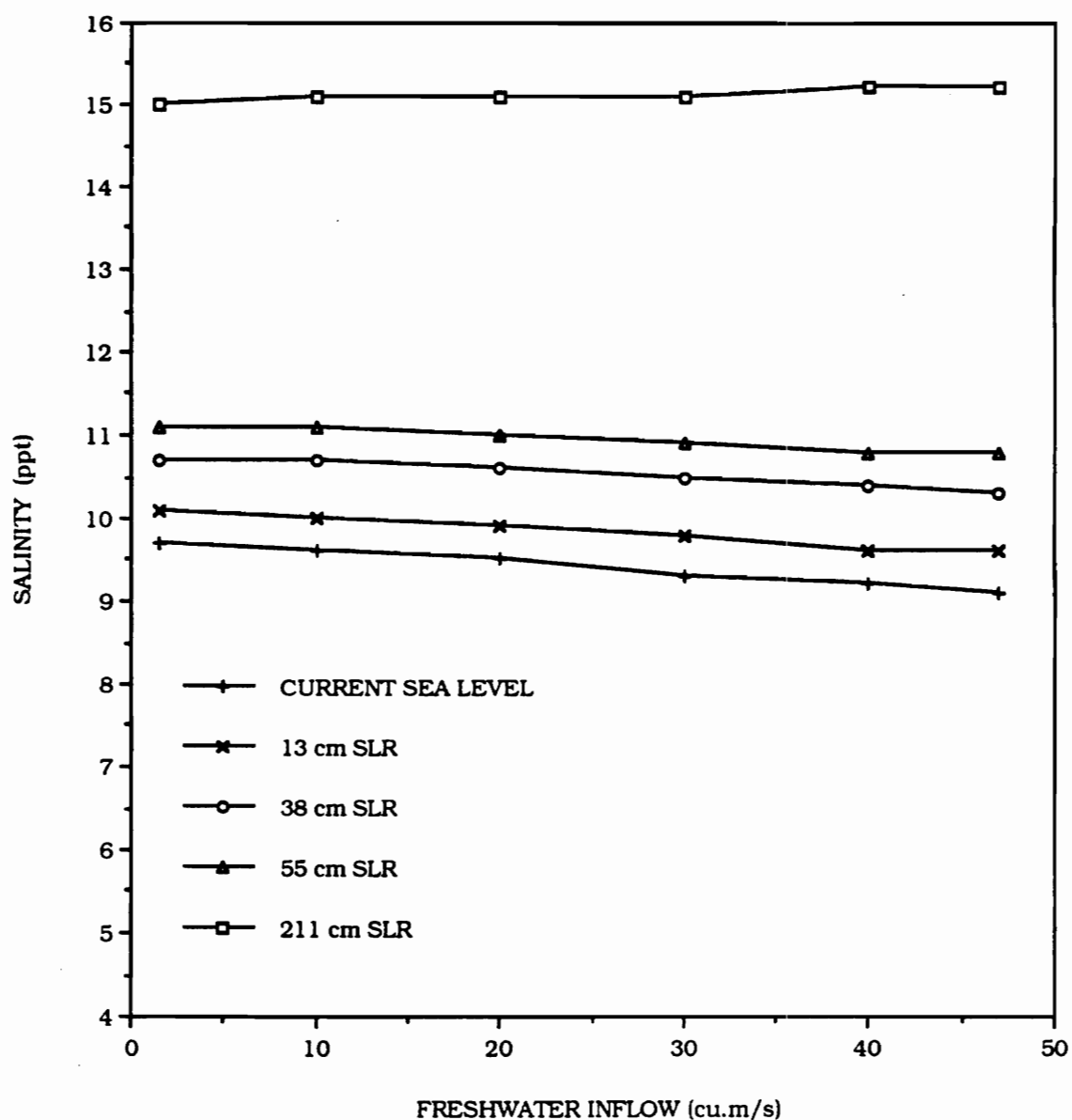


Figure 3.15 Average salinity in bottom layer of transect 26 for different conditions of freshwater inflow and sea level rise.

Figures

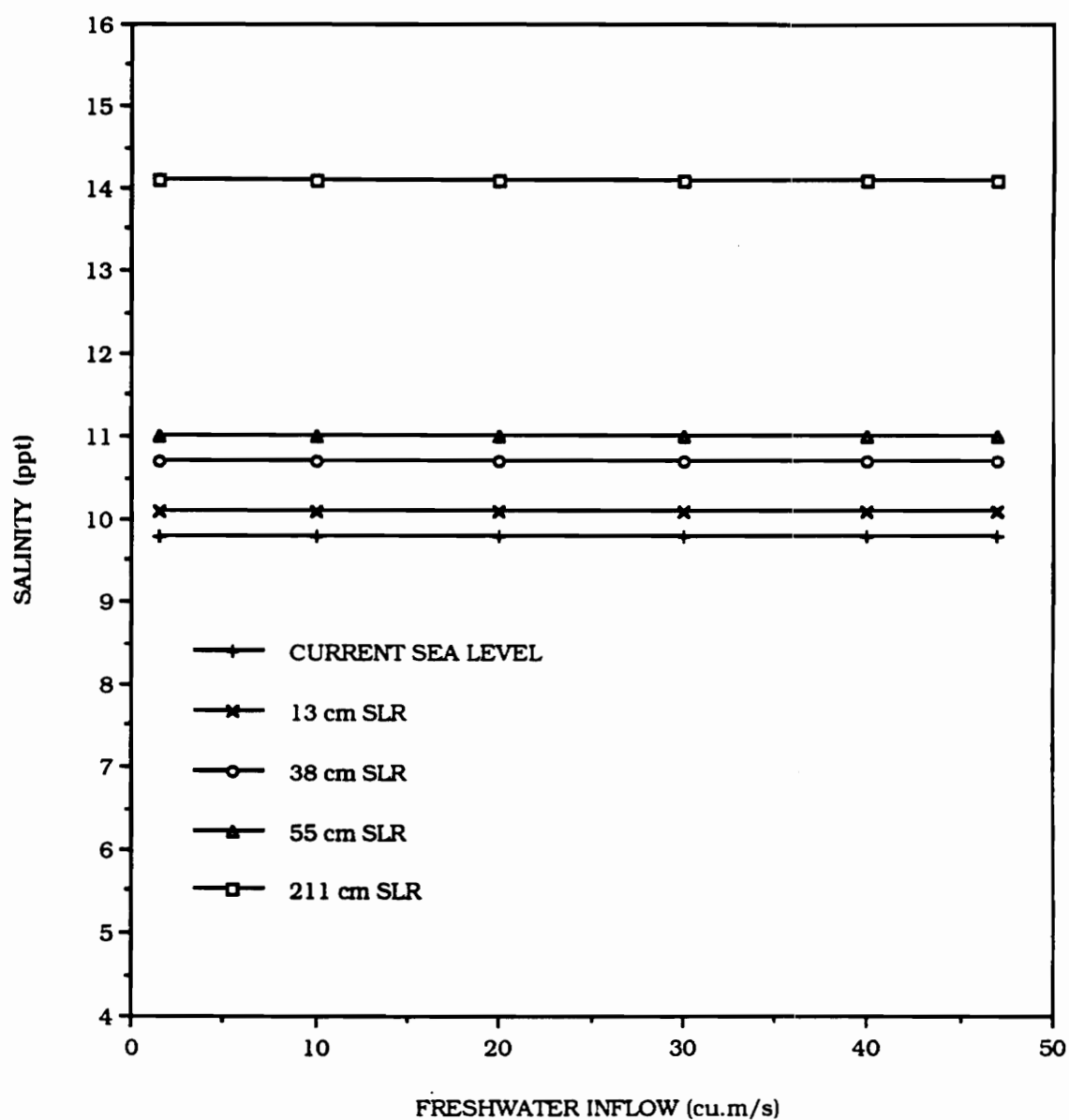


Figure 3.16 Average salinity in bottom layer of transect 27 for different conditions of freshwater inflow and sea level rise.

Figures

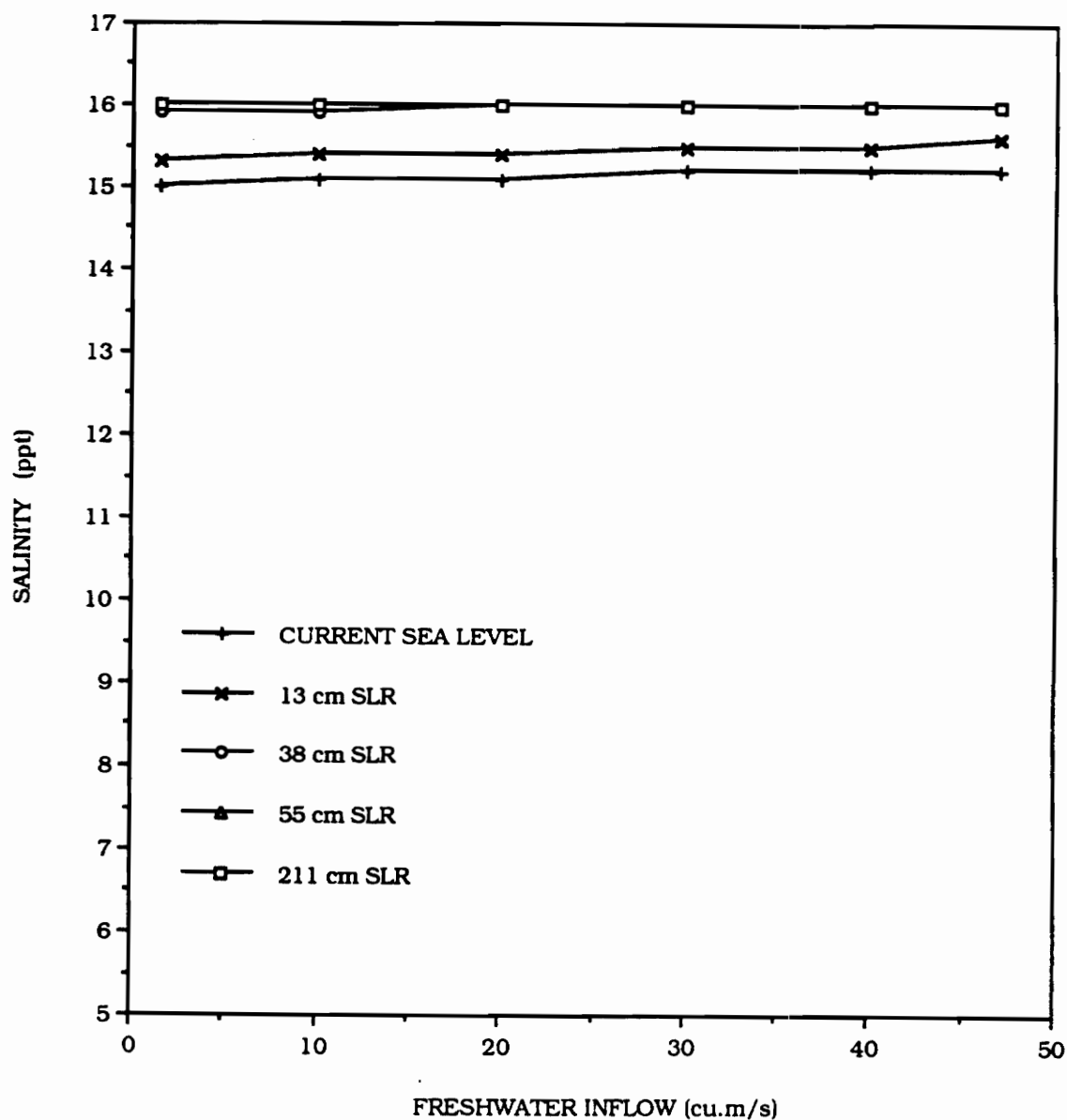


Figure 3.17 Average salinity in bottom layer of transect 28 for different conditions of freshwater inflow and sea level rise.

Figures

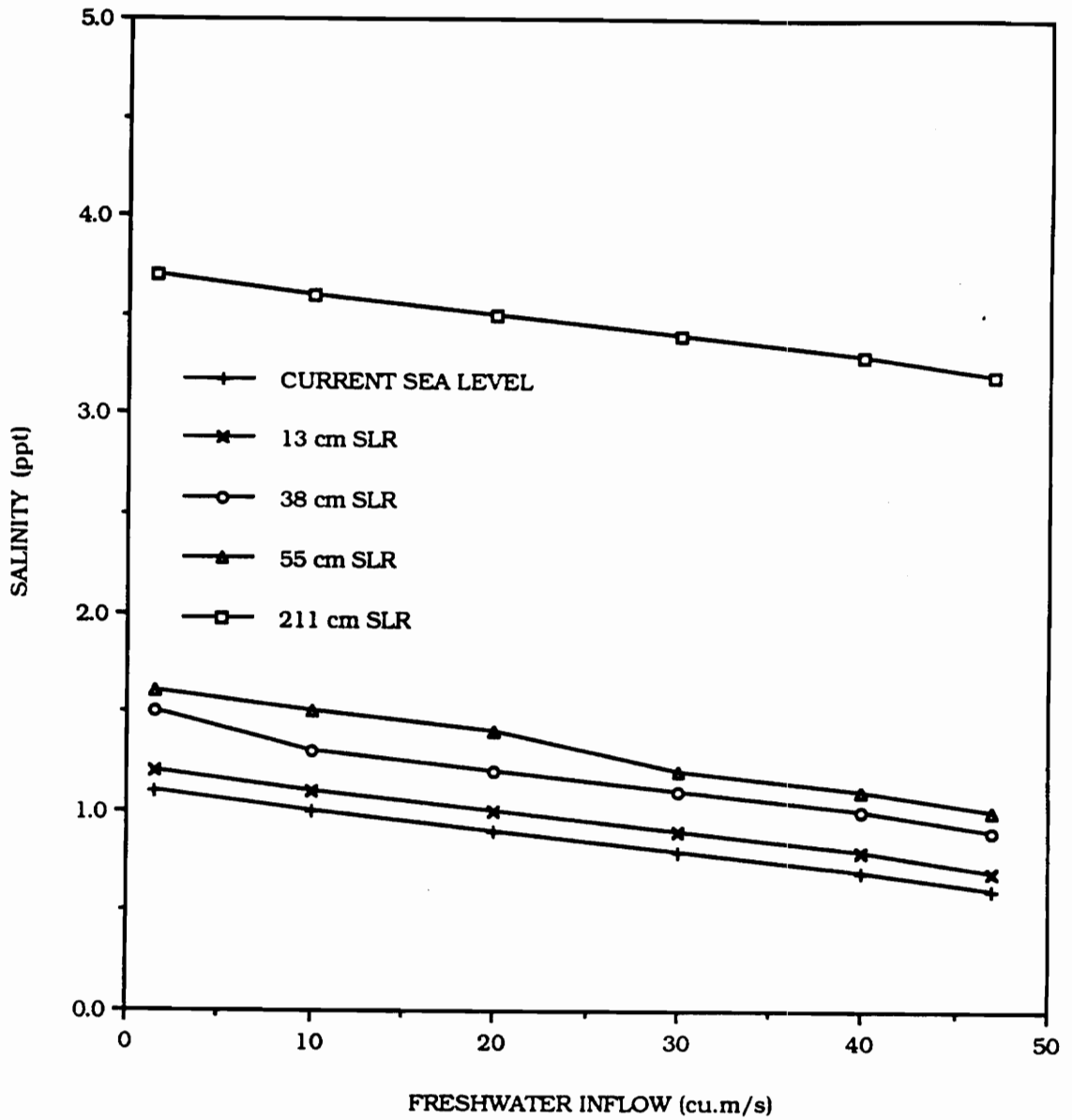


Figure 3.18 Average salinity in top layer of transect 25 for different conditions of freshwater inflow and sea level rise.

Figures

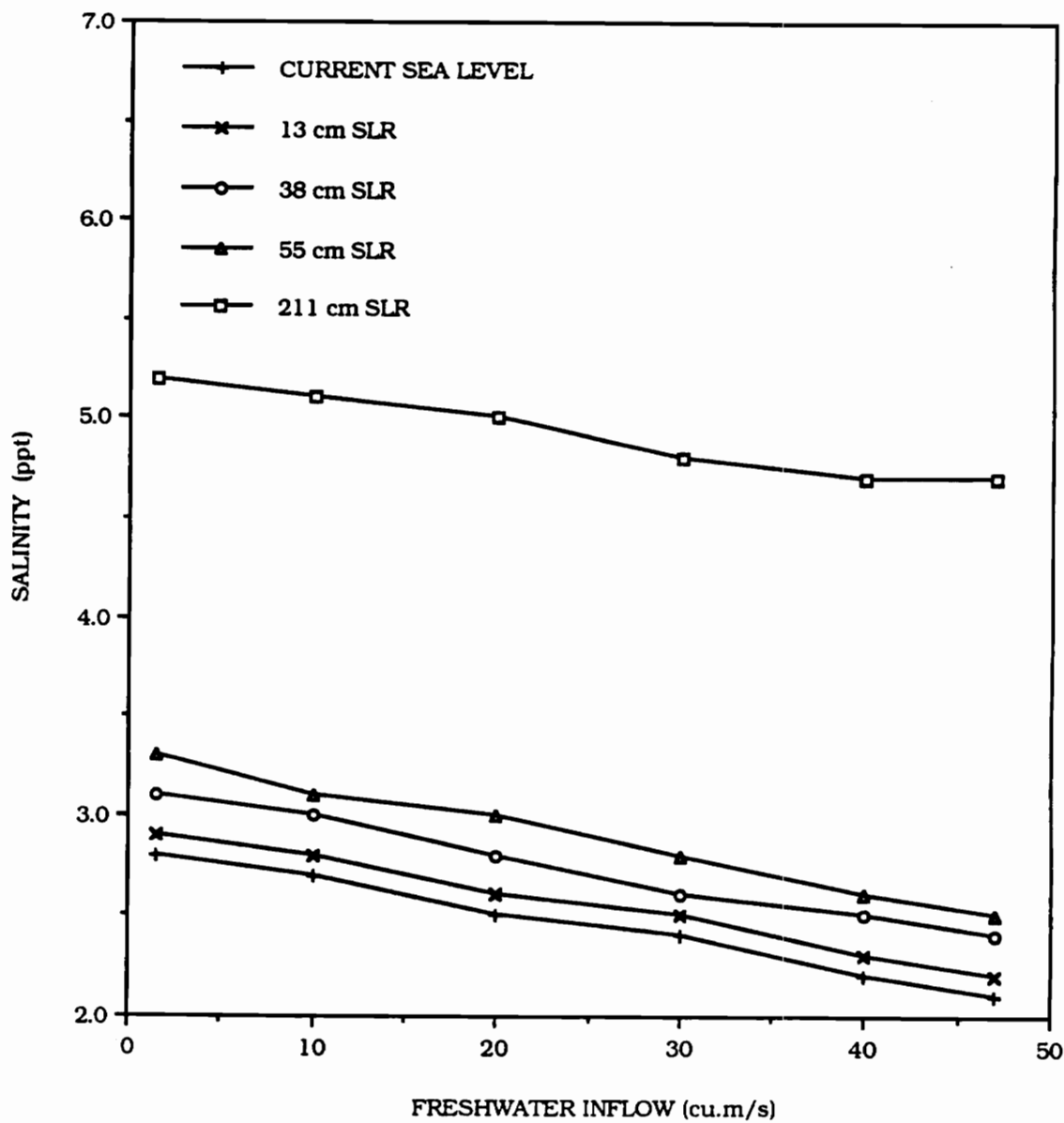


Figure 3.19 Average salinity in top layer of transect 26 for different conditions of freshwater inflow and sea level rise.

Figures

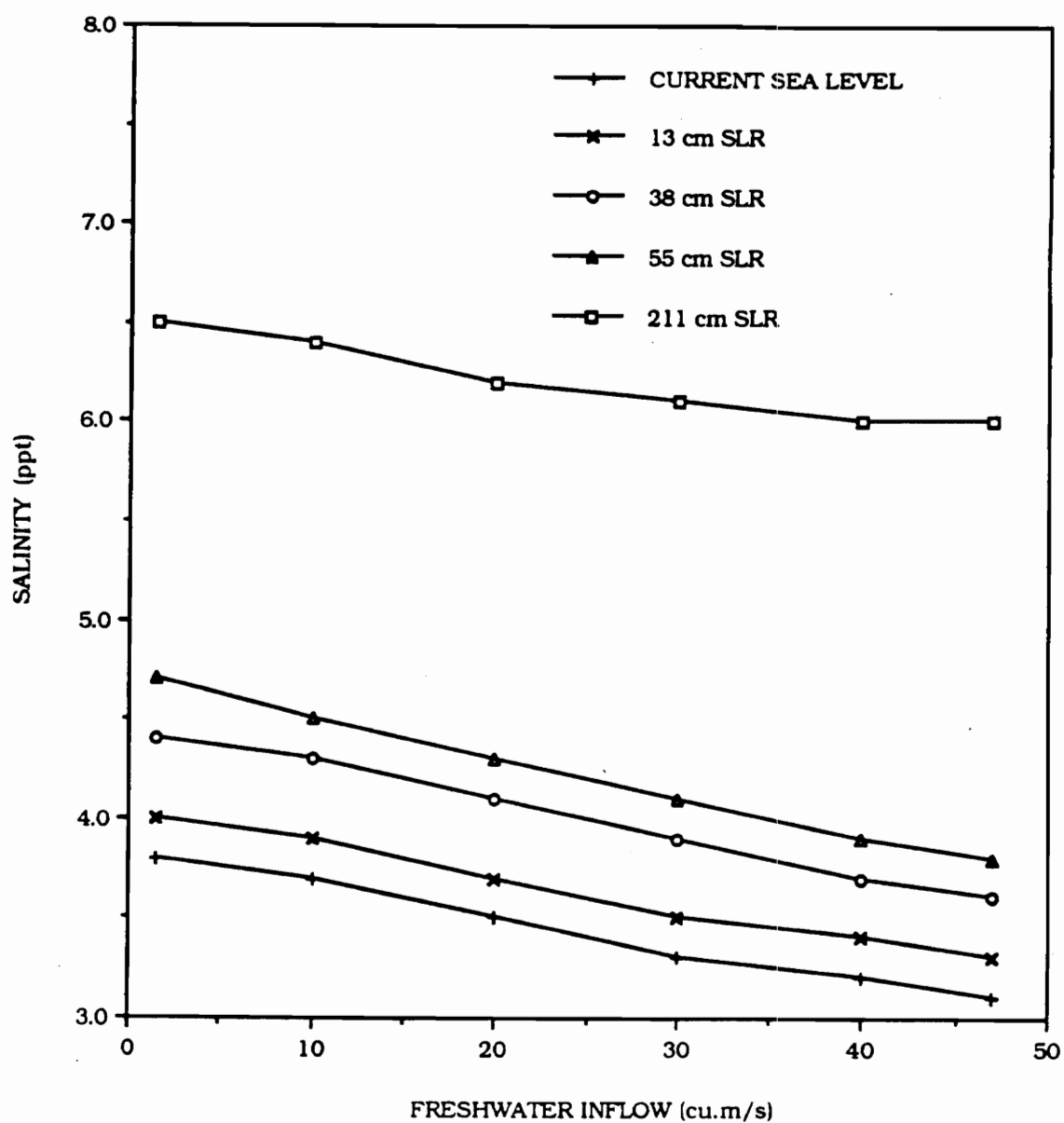


Figure 3.20 Average salinity in top layer of transect 27 for different conditions of freshwater inflow and sea level rise.

Figures

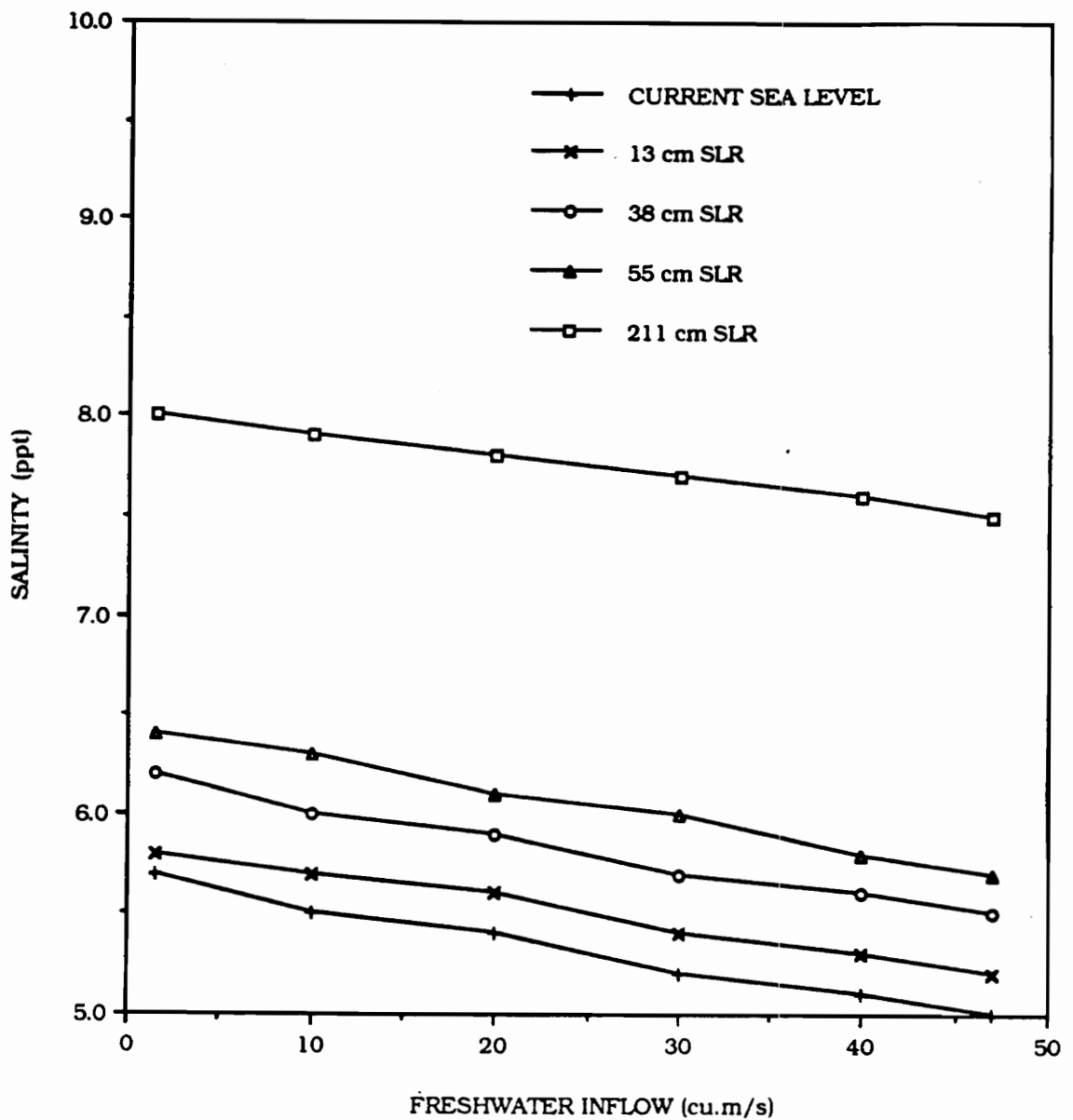


Figure 3.21 Average salinity in top layer of transect 28 for different conditions of freshwater inflow and sea level rise.

Figures

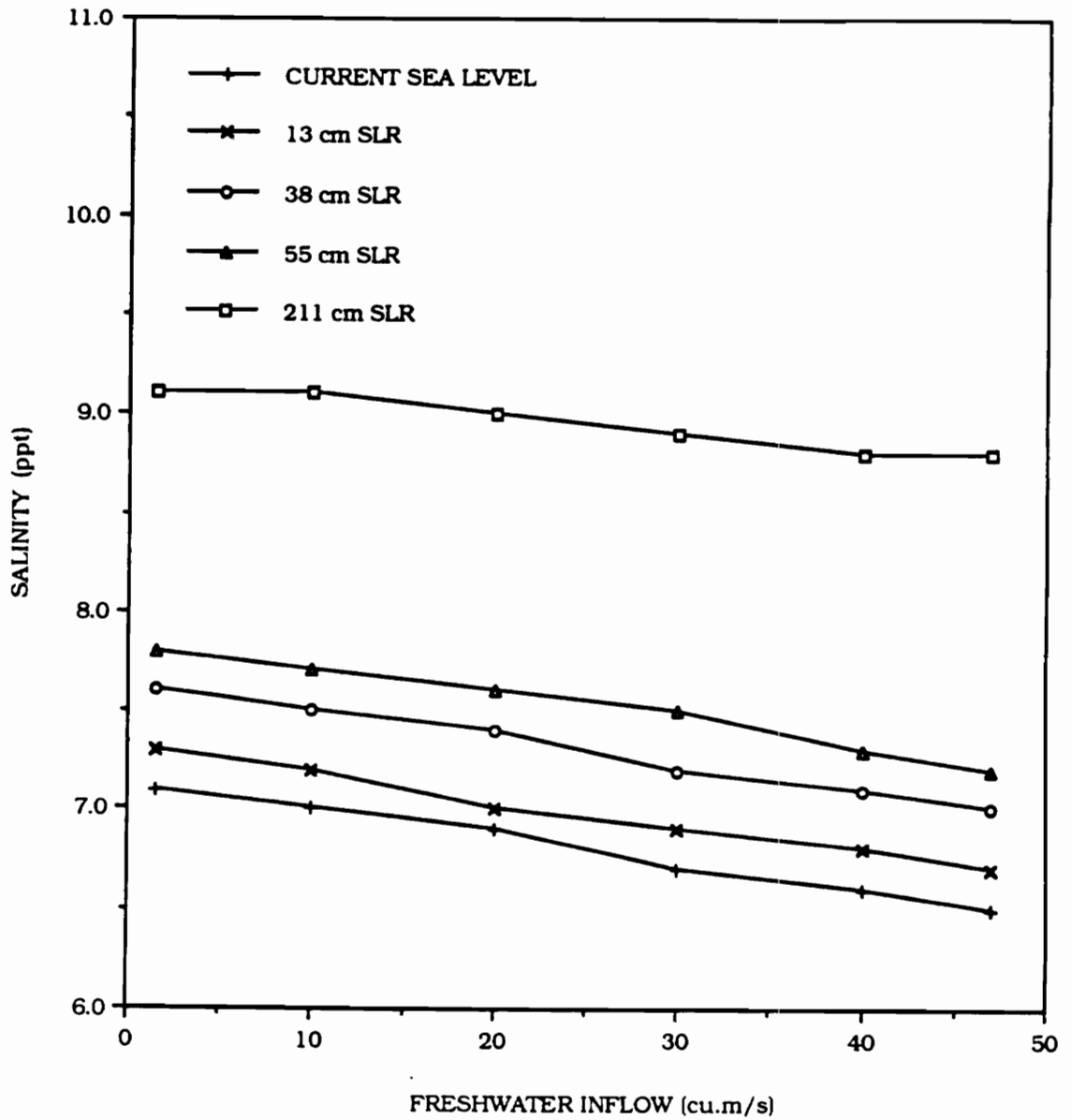


Figure 3.22 Average salinity in top layer of transect 29 for different conditions of freshwater inflow and sea level rise.

Figures

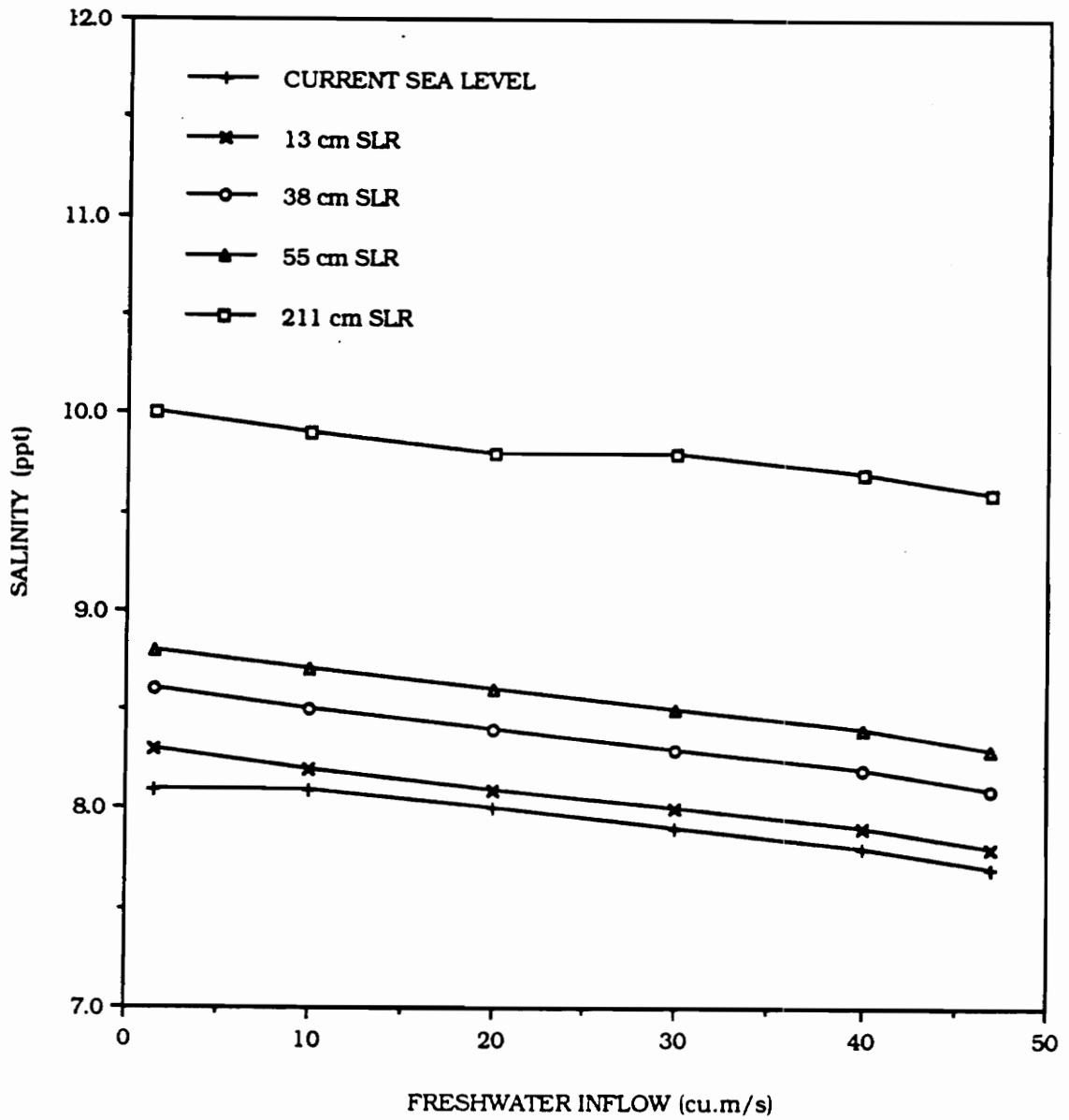


Figure 3.23 Average salinity in top layer of transect 30 for different conditions of freshwater inflow and sea level rise.

Figures

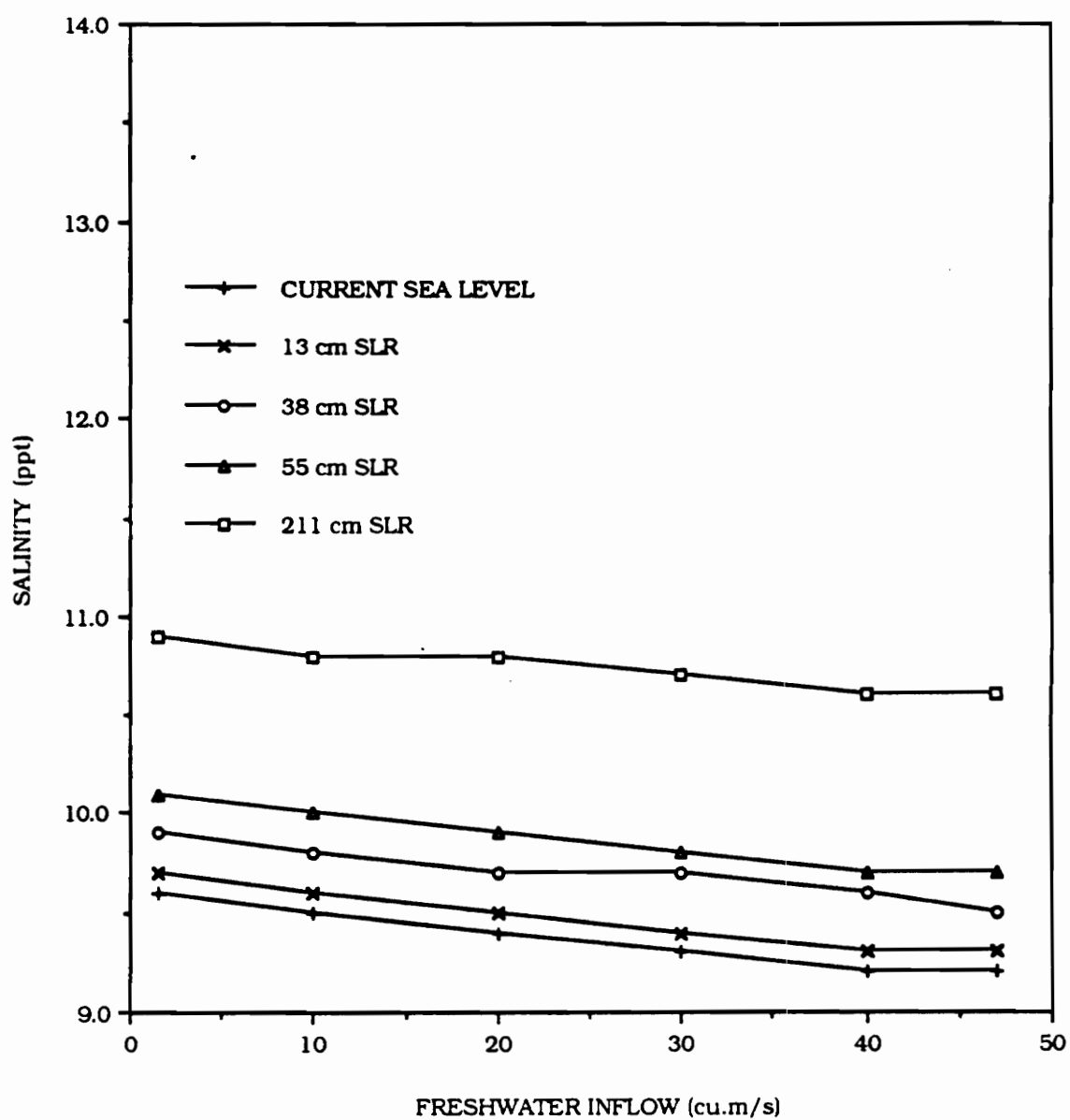


Figure 3.24 Average salinity in top layer of transect 31 for different conditions of freshwater inflow and sea level rise.

Figures

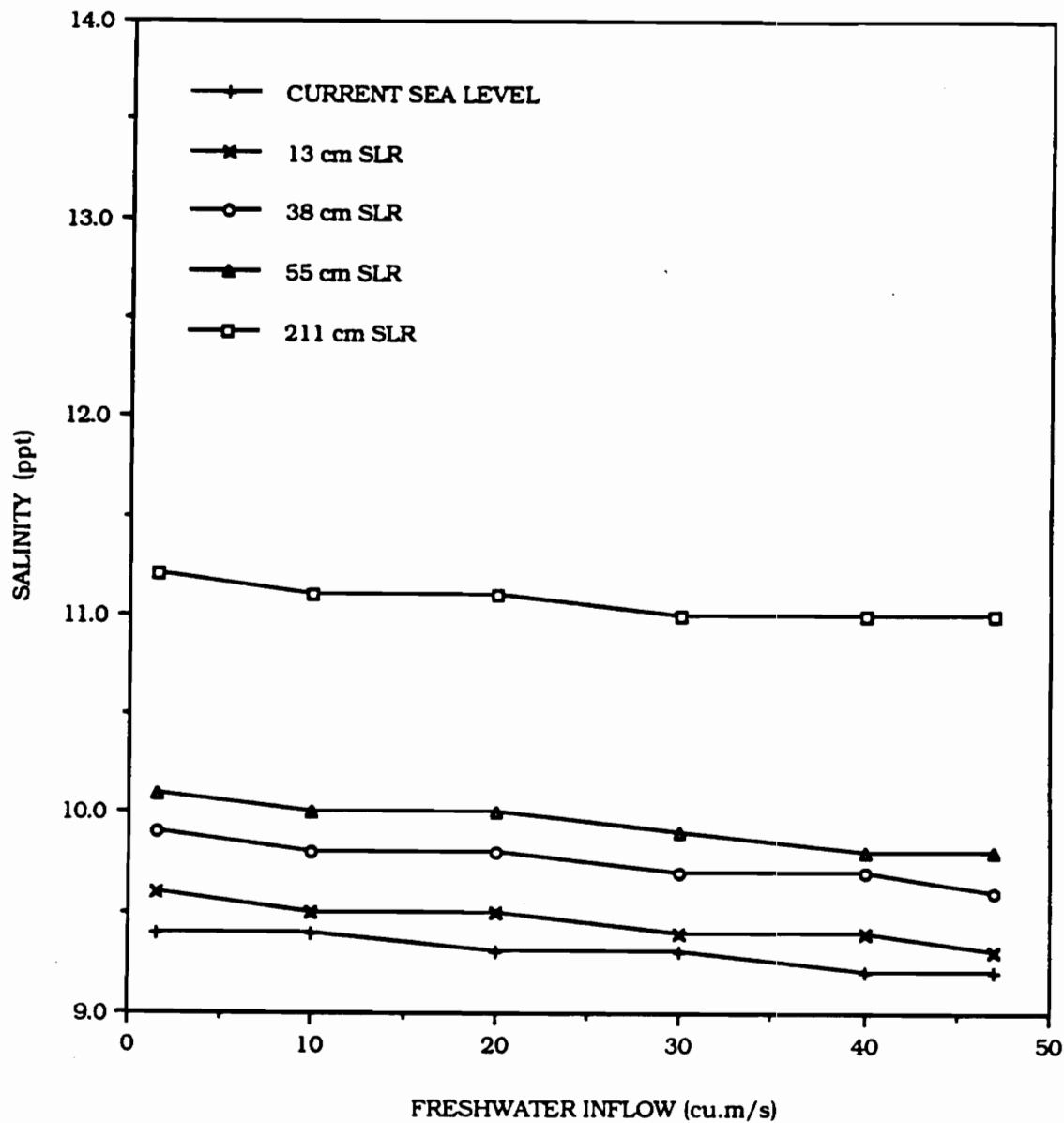


Figure 3.25 Average salinity in top layer of transect 32 for different conditions of freshwater inflow and sea level rise.

Figures

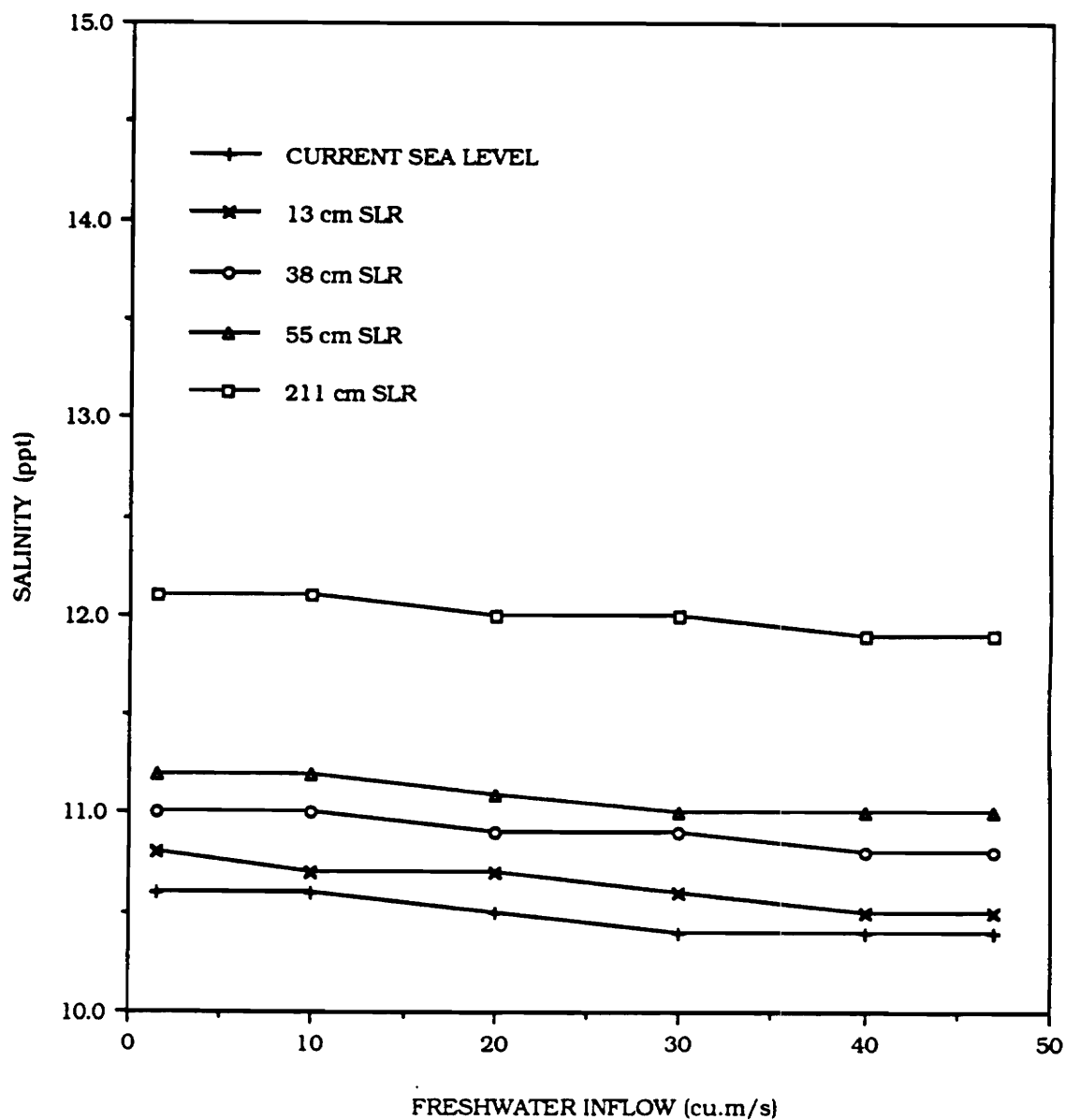


Figure 3.26 Average salinity in top layer of transect 33 for different conditions of freshwater inflow and sea level rise.

Figures

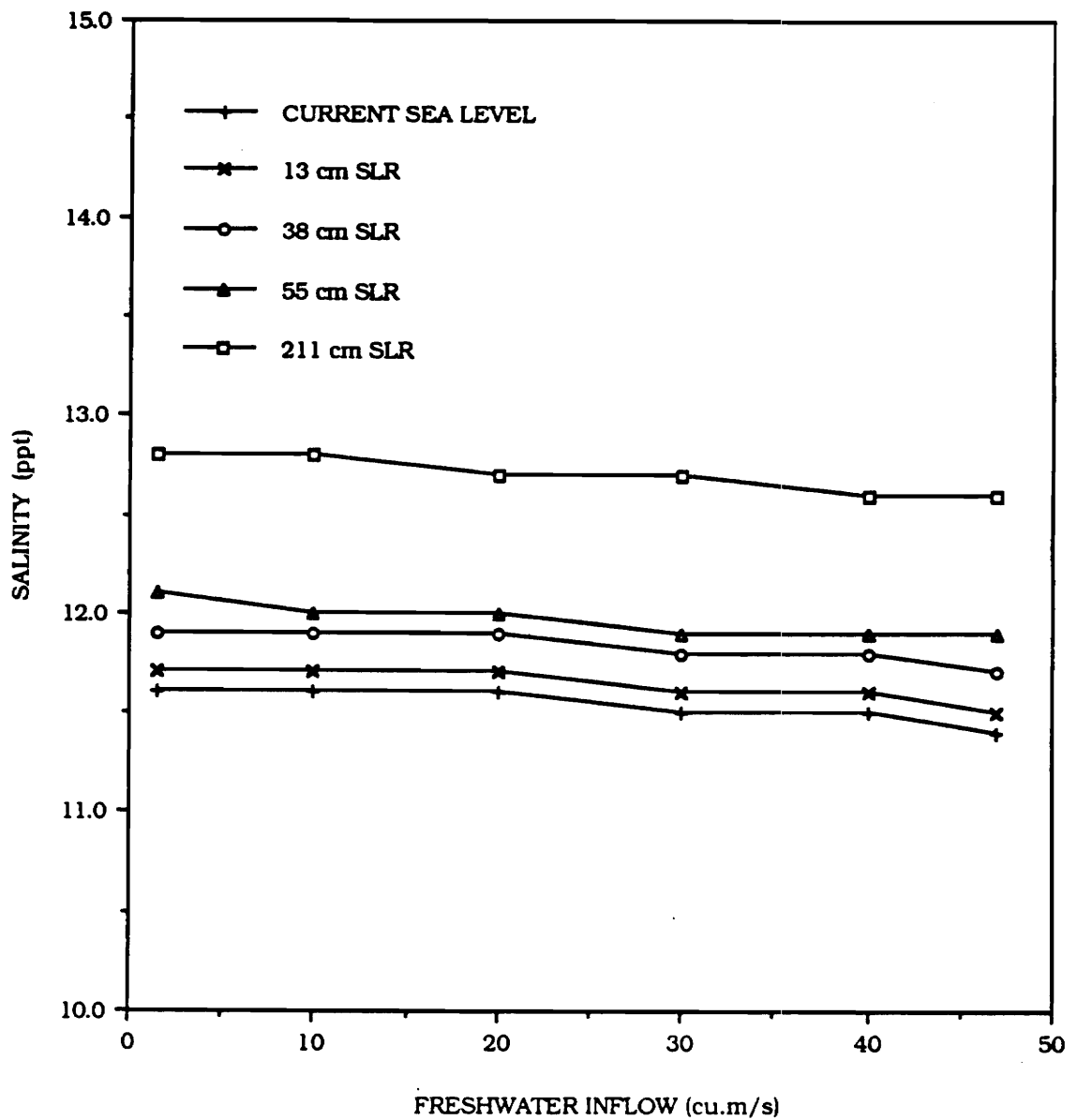


Figure 3.27 Average salinity in top layer of transect 34 for different conditions of freshwater inflow and sea level rise.

Figures

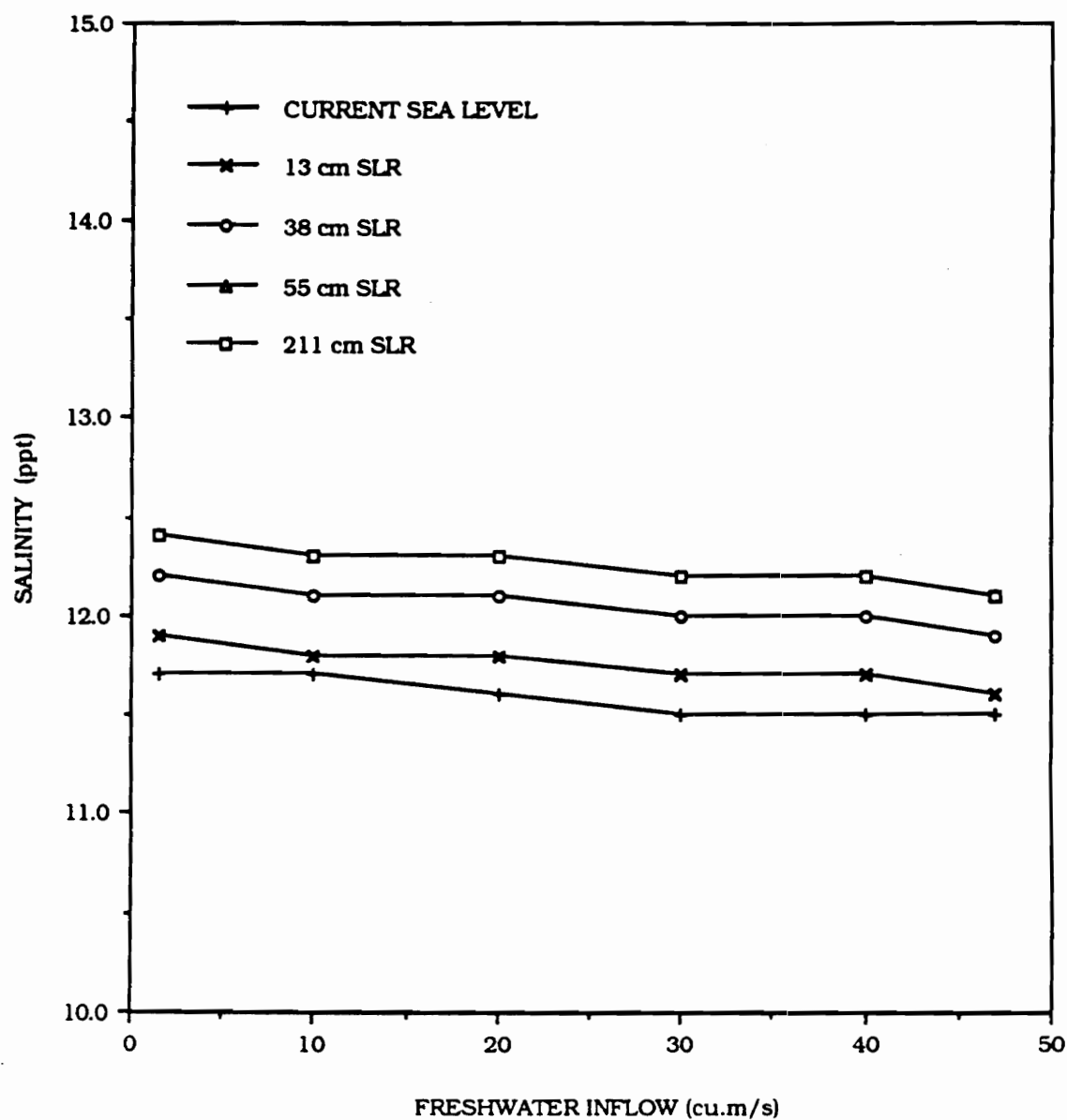


Figure 3.28 Average salinity in top layer of transect 35 for different conditions of freshwater inflow and sea level rise.

Figures

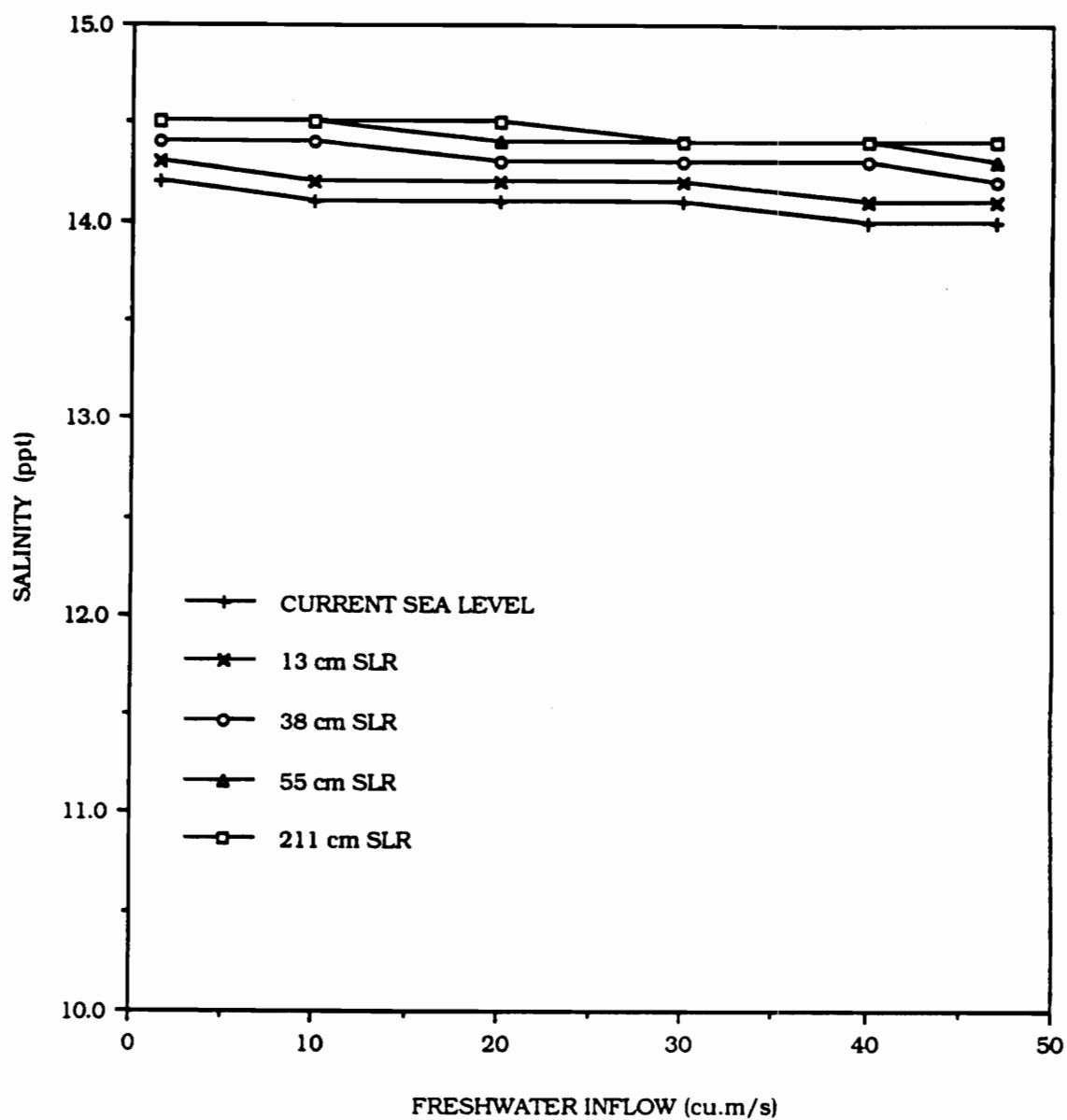


Figure 3.29 Average salinity in top layer of transect 36 for different conditions of freshwater inflow and sea level rise.

Figures

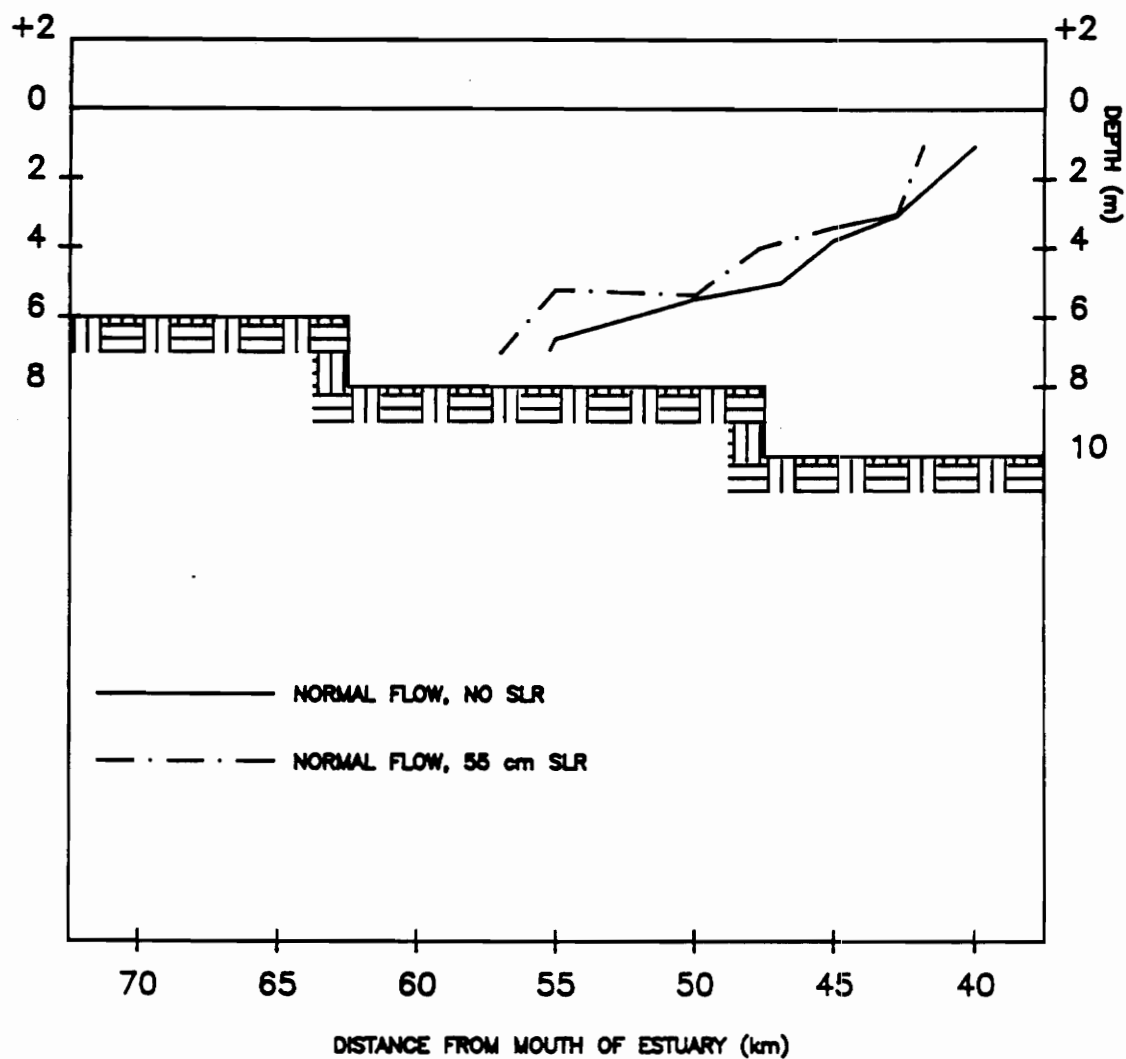


Figure 3.30 5 ppt isohalines for 55 cm vs. no SLR, for normal flow conditions.

Figures

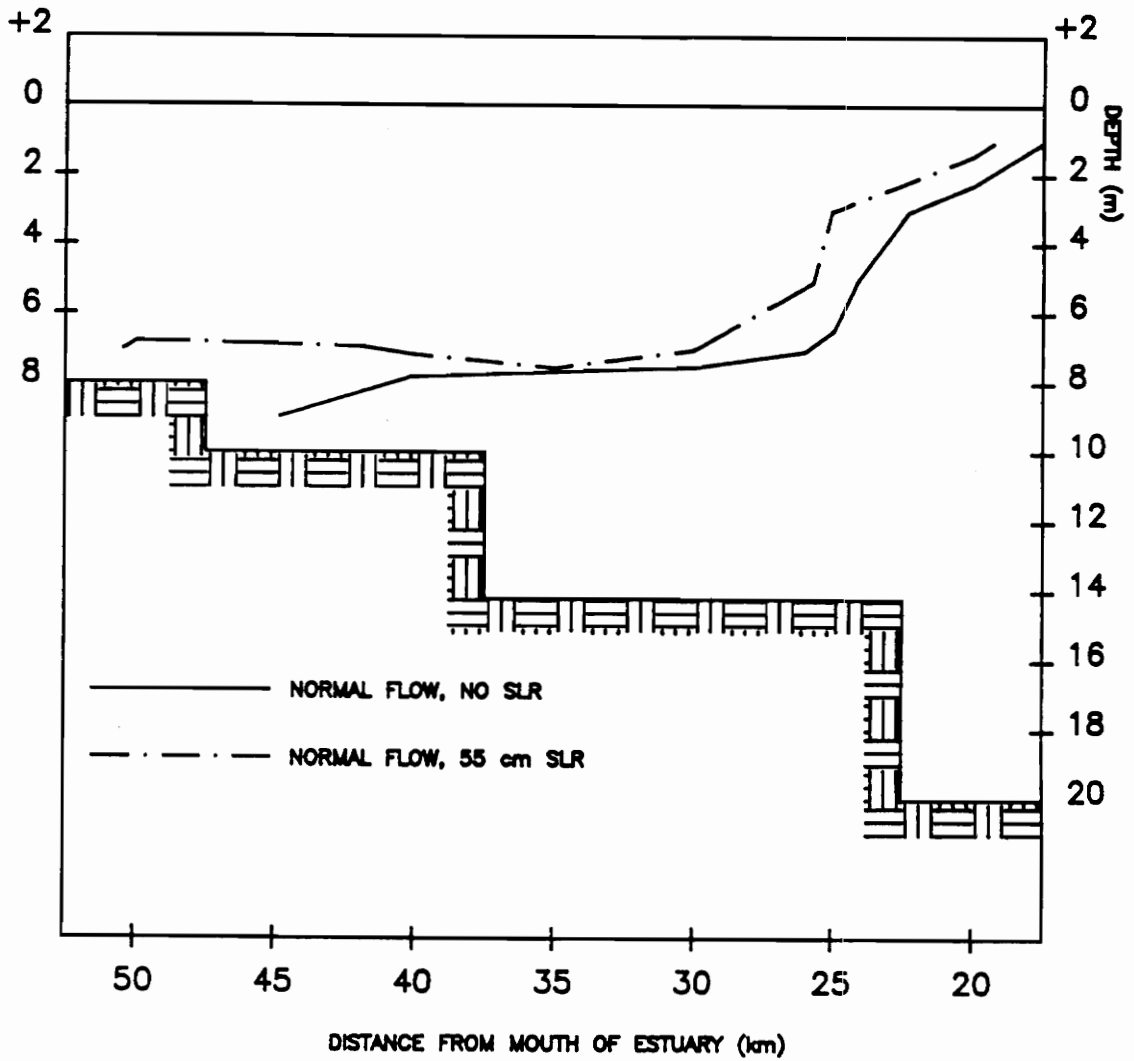


Figure 3.31 10 ppt isohalines for 55 cm vs. no SLR, for normal flow conditions.

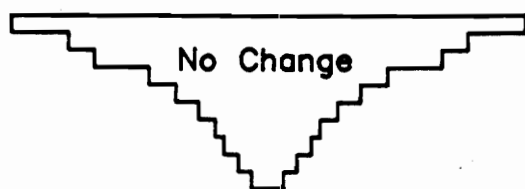
Figures

Transect 36



Case 1

Transect 35

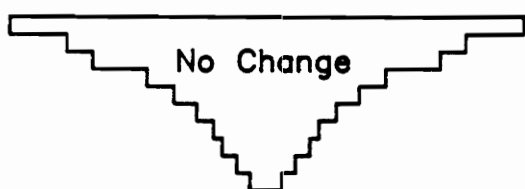


Transect 36

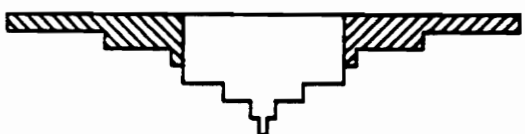


Case 2

Transect 35



Transect 36



Case 3

Transect 35

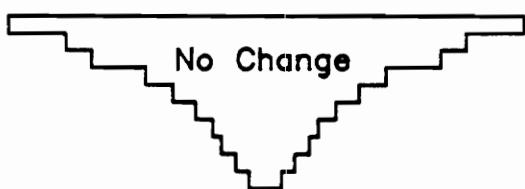
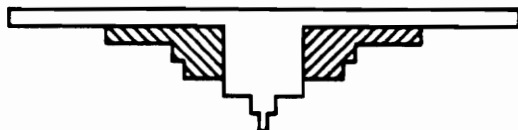


Figure 3.32 Cases 1, 2 and 3, of estuary constriction.

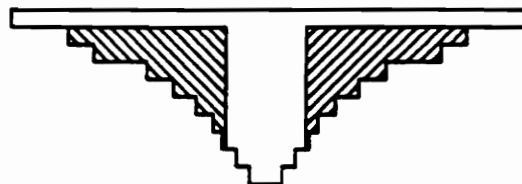
Figures

Transect 36

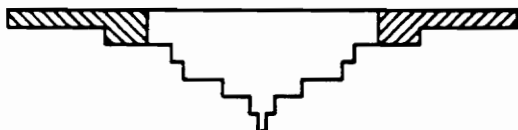


Case 4

Transect 35

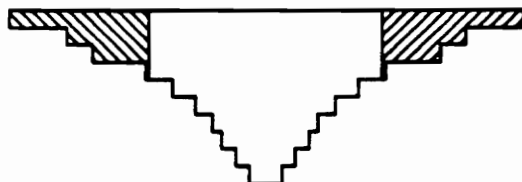


Transect 36

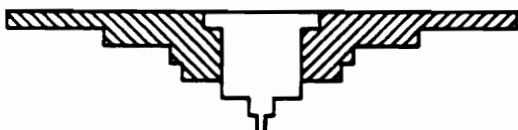


Case 5

Transect 35



Transect 36



Case 6

Transect 35

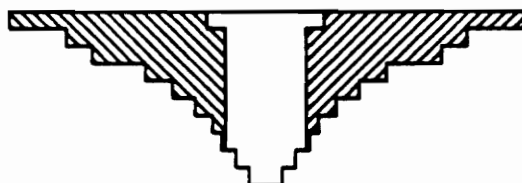


Figure 3.33 Cases 4, 5 and 6, of estuary constriction.

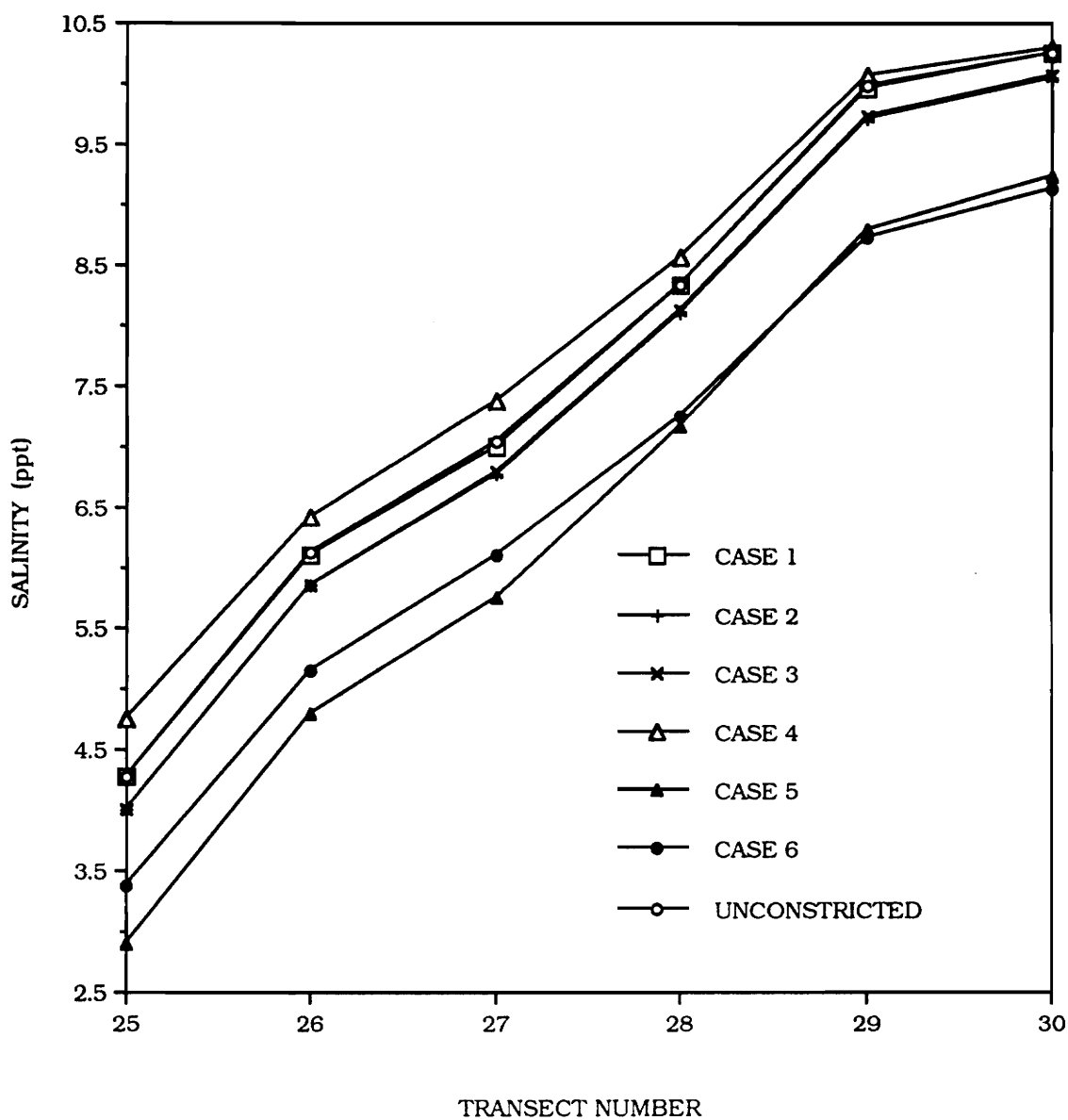


Figure 3.34 Depth-averaged salinities at transects 25 to 30, for different cases of estuary constriction.

Figures

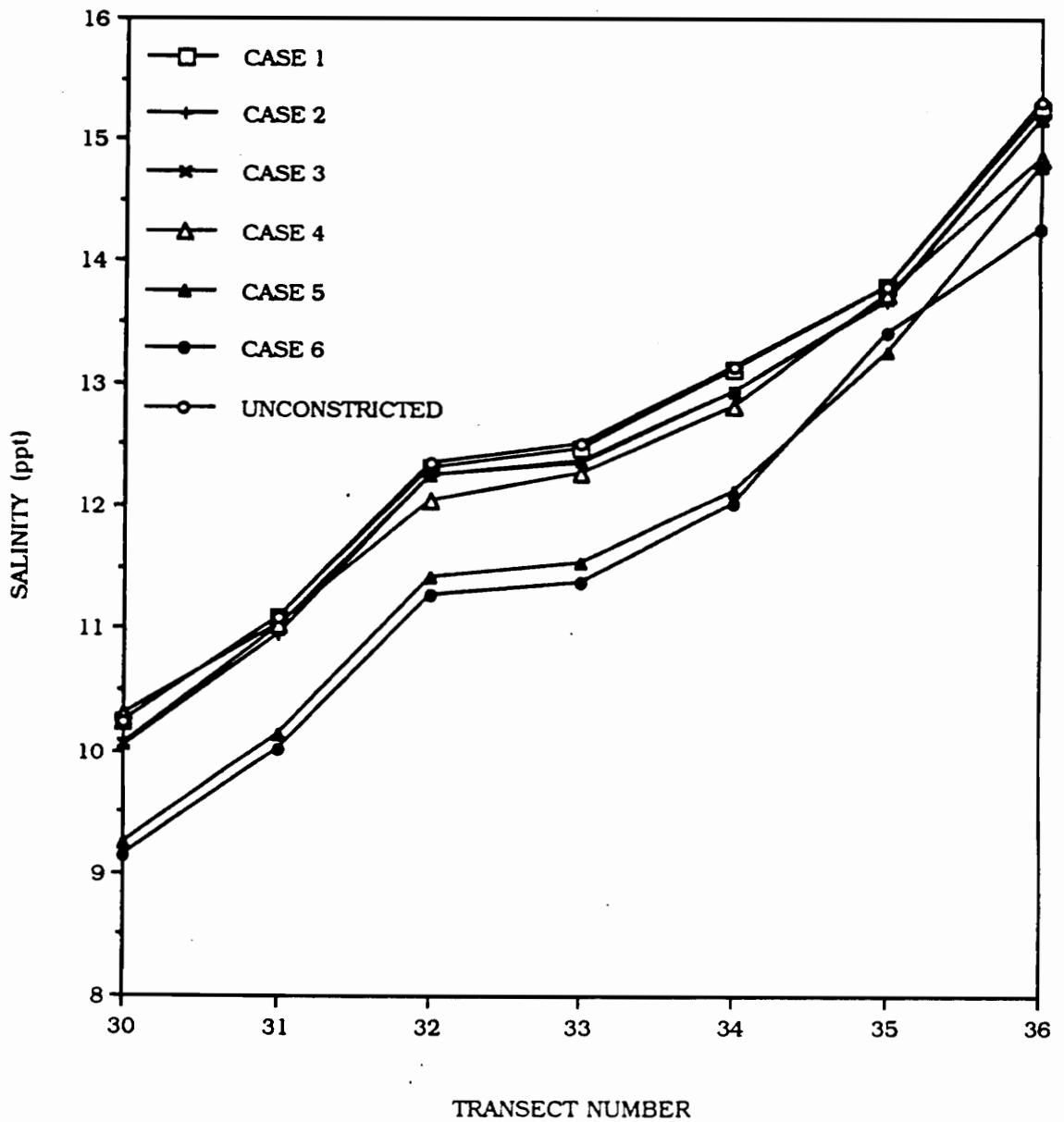


Figure 3.35 Depth-averaged salinities at transects 31 to 36, for different cases of estuary constriction.

Figures

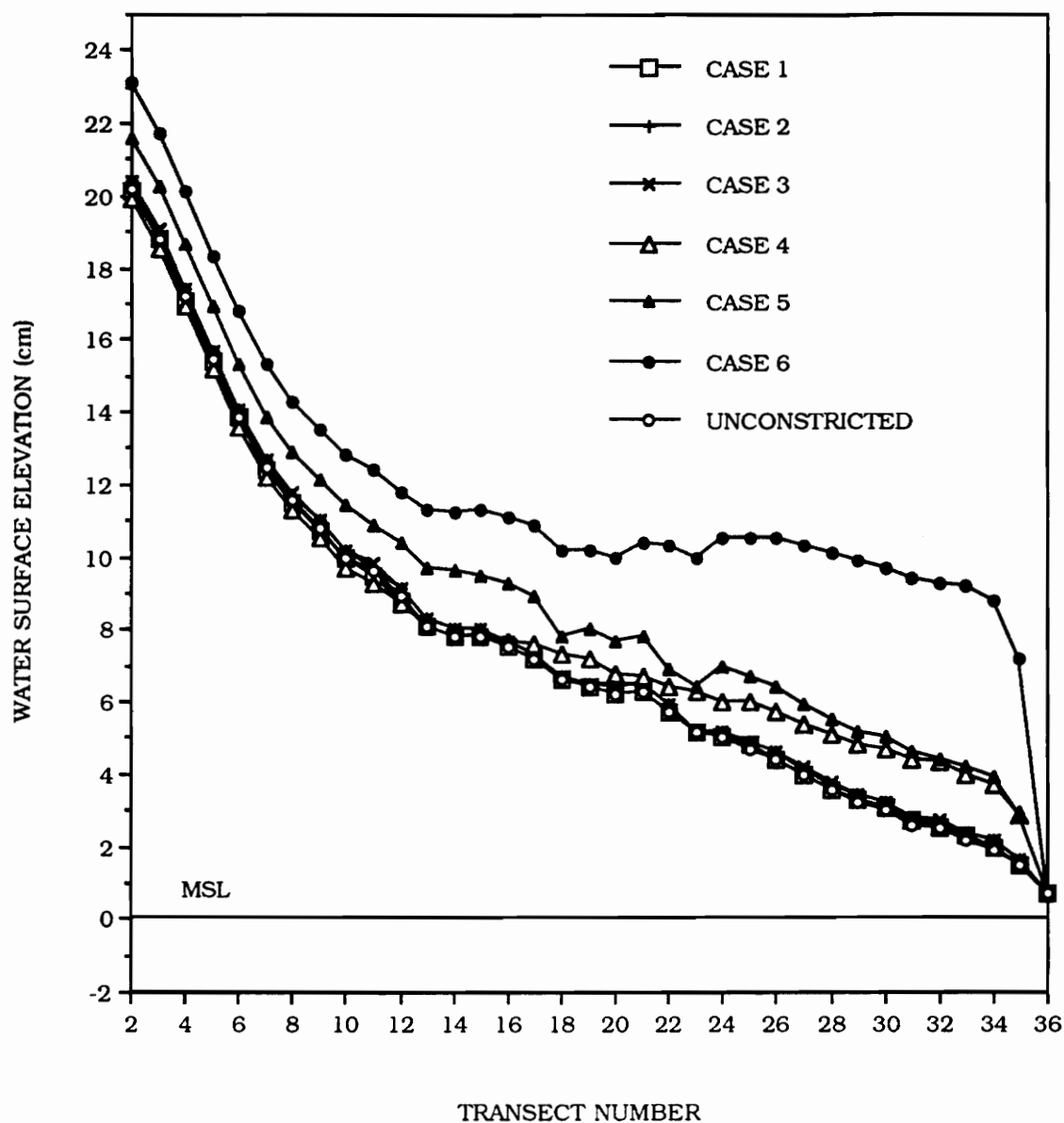


Figure 3.36 Water surface elevations at transects 2 to 36, for different cases of estuary constriction.

Figures

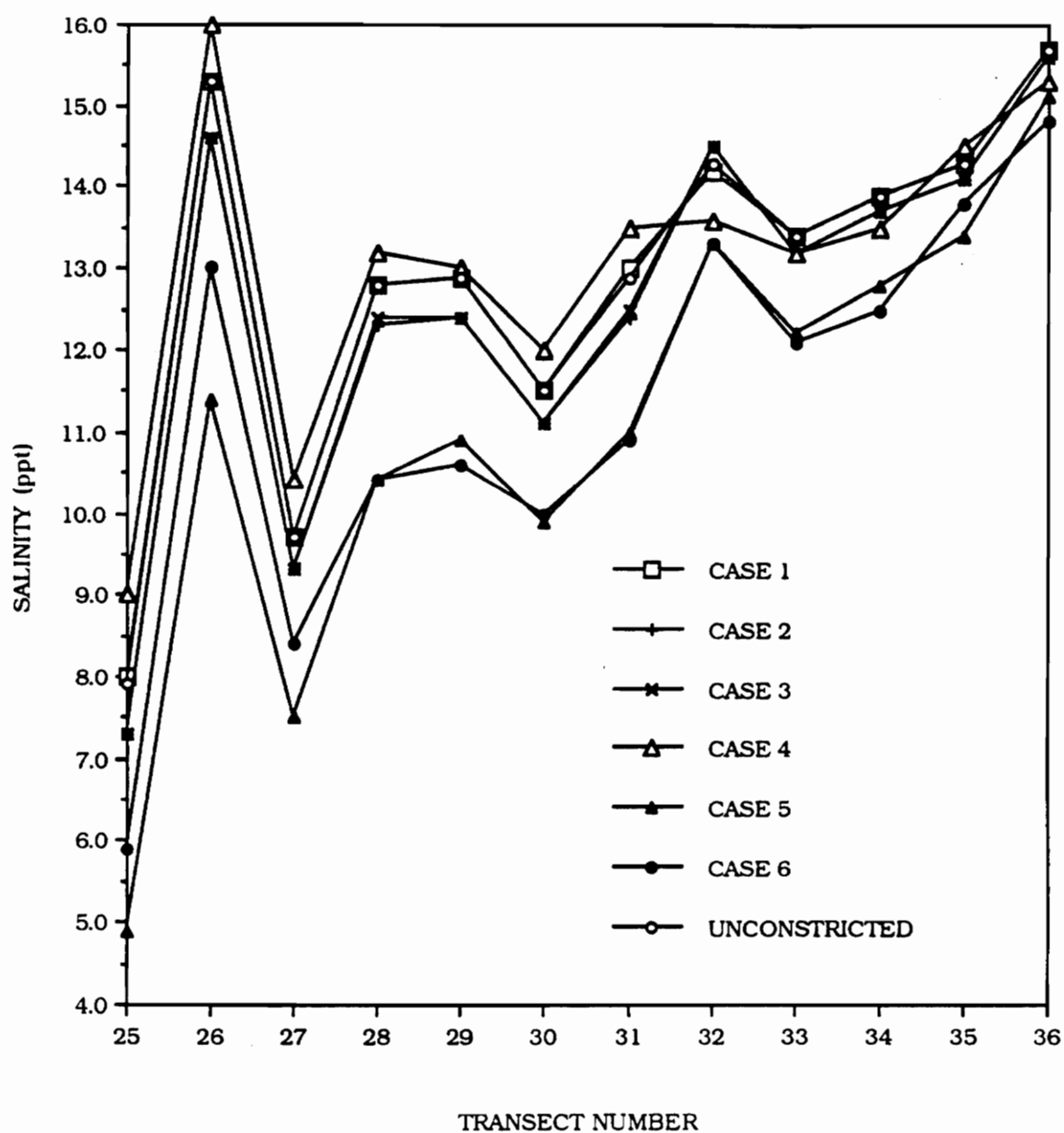


Figure 3.37 Average bottom layer salinities in transects 25 to 36, for different cases of estuary constriction.

Figures

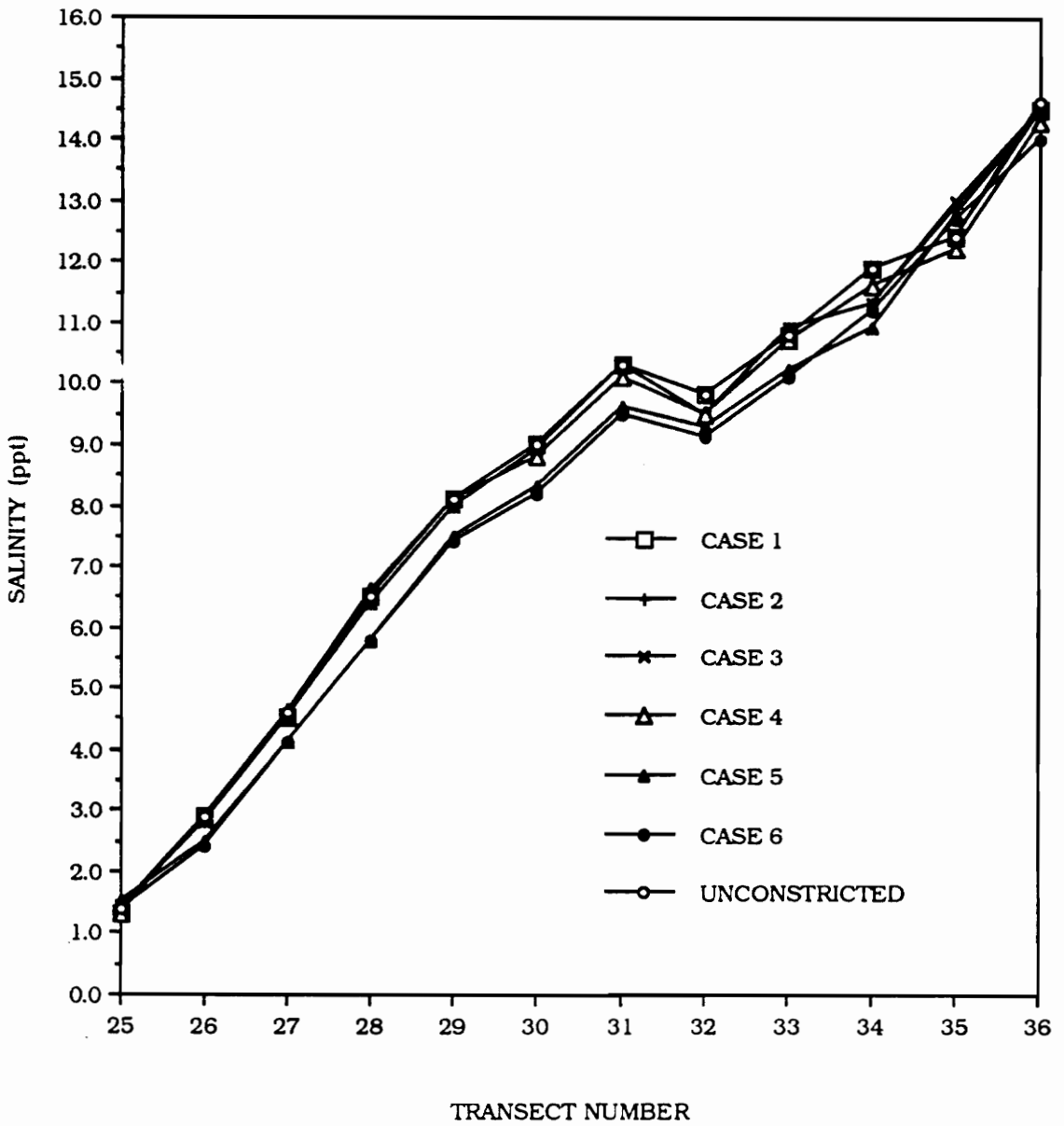


Figure 3.38 Average top layer salinities in transects 25 to 36, for different cases of estuary constriction.

Figures

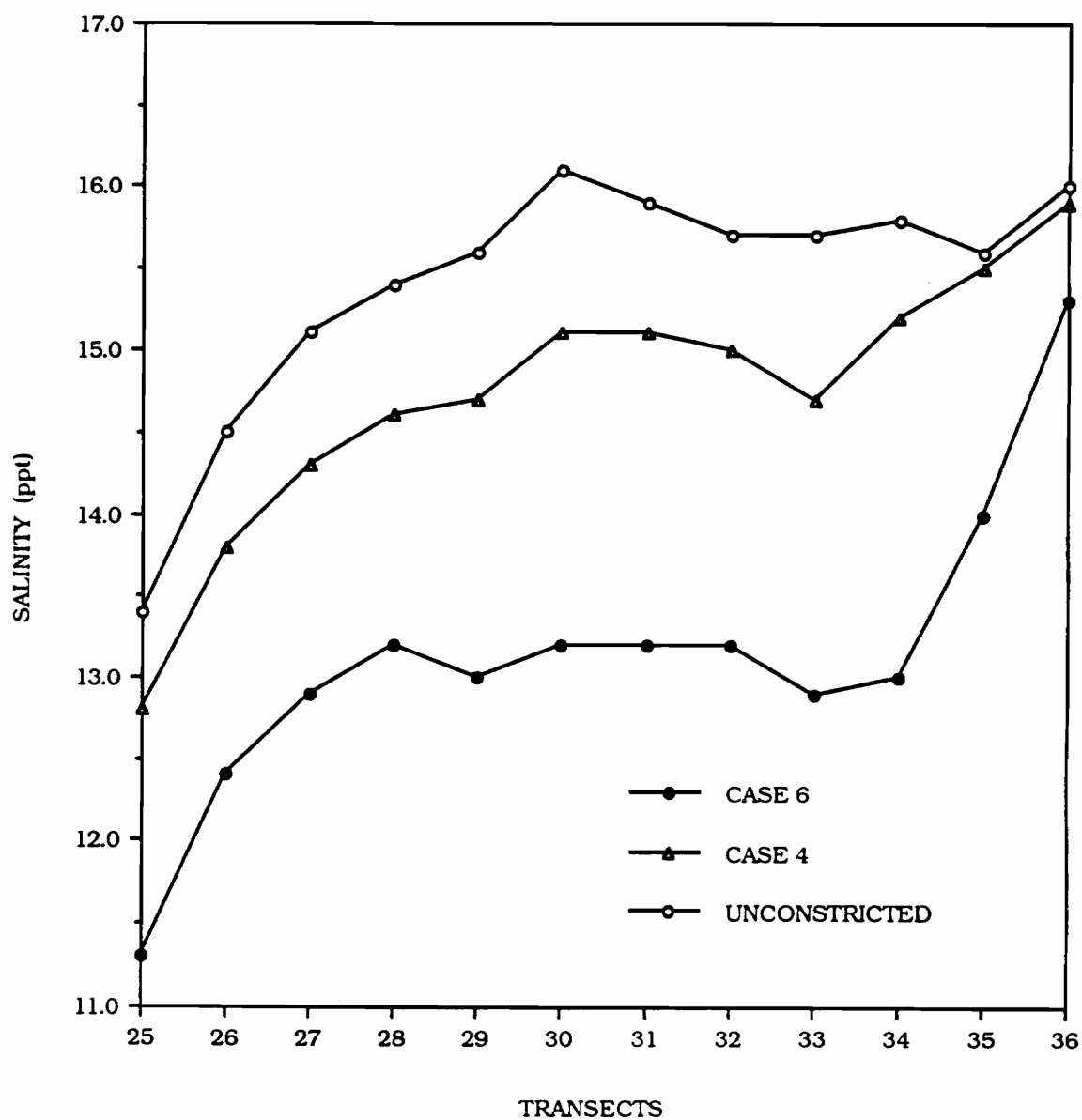


Figure 3.39 Average salinities in the bottom layer of transects 25 to 36, in a flat-bottom channel, for different cases of constriction.

Figures

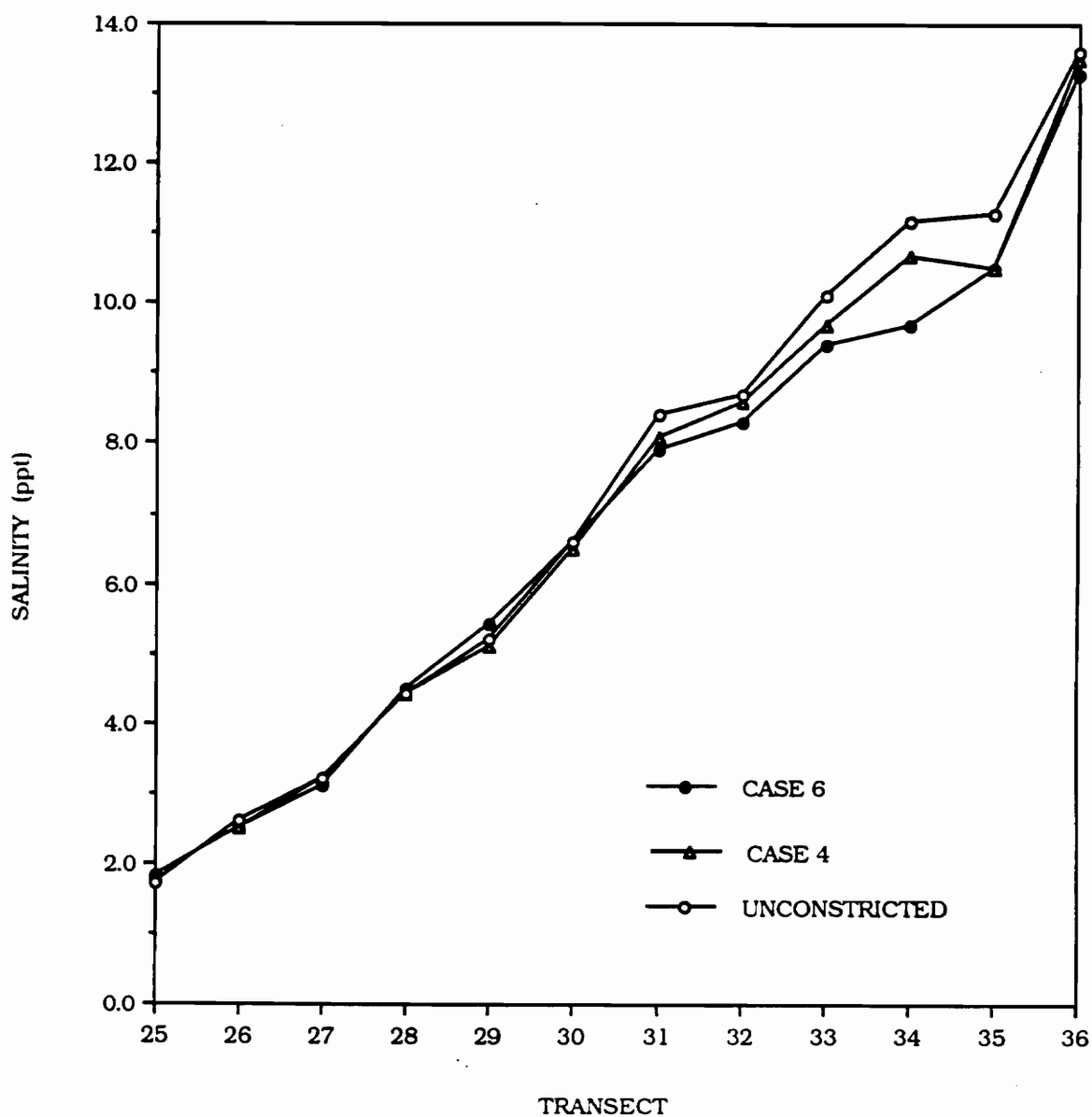


Figure 3.40 Average salinities in the top layer of transects 25 to 36, in a flat-bottom channel, for different cases of constriction.

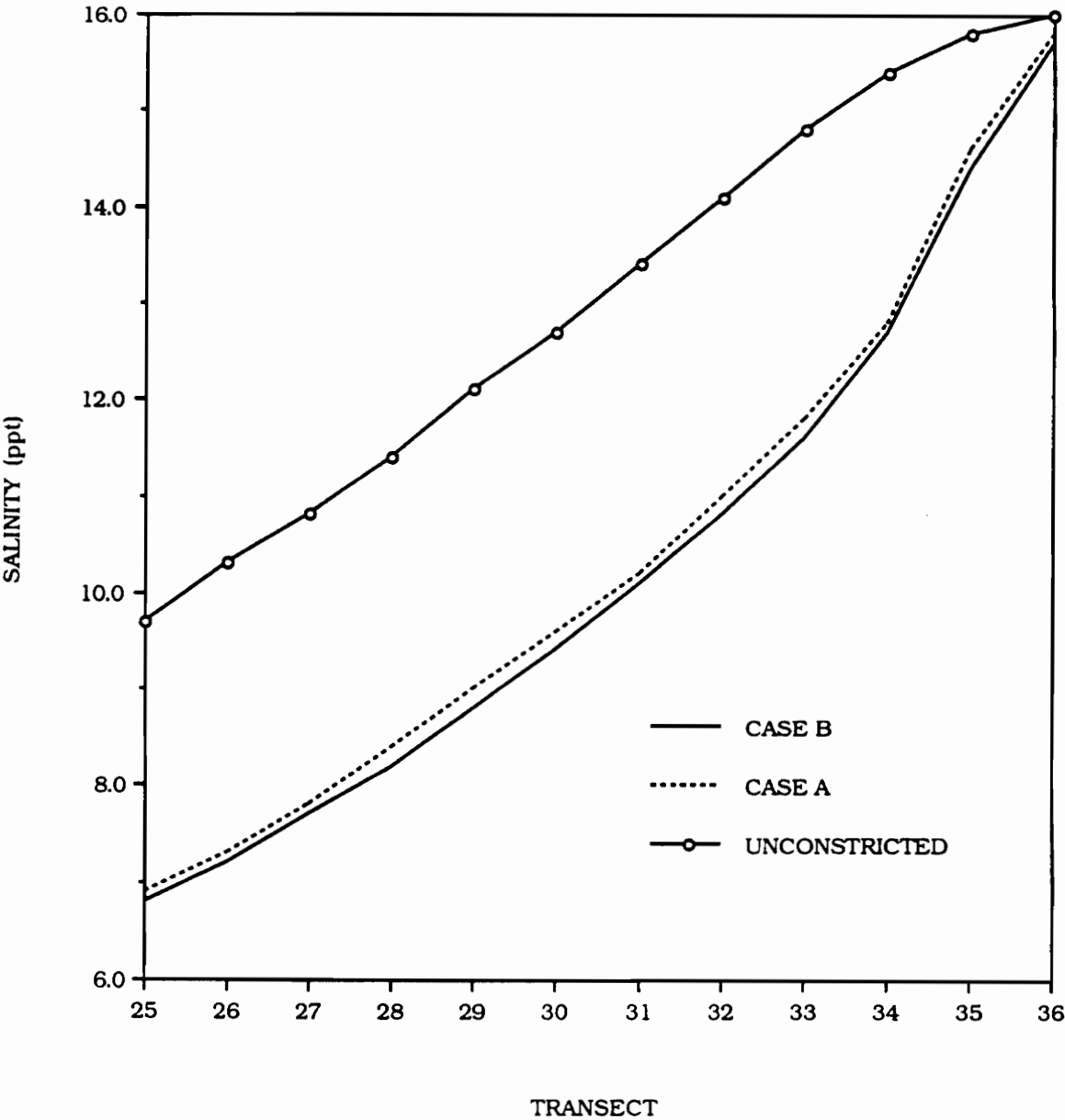


Figure 3.41 Average salinities in the bottom layer of transects 25 to 36, in a flat-bottom box shape channel, for different cases of constriction.

Figures

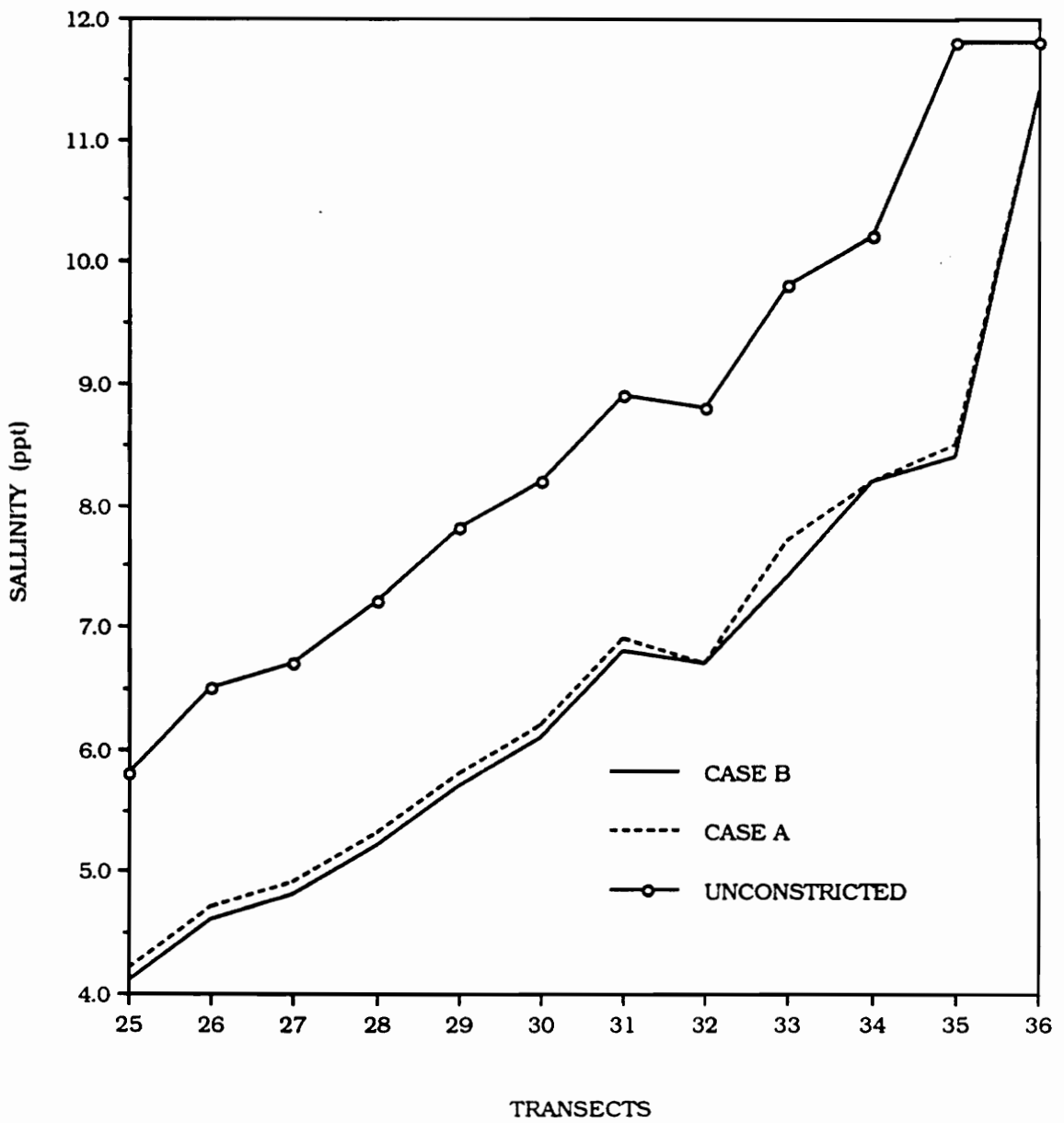


Figure 3.42 Average salinities in the top layer of transects 25 to 36, in a flat-bottom box shape channel, for different cases of constriction.

Figures

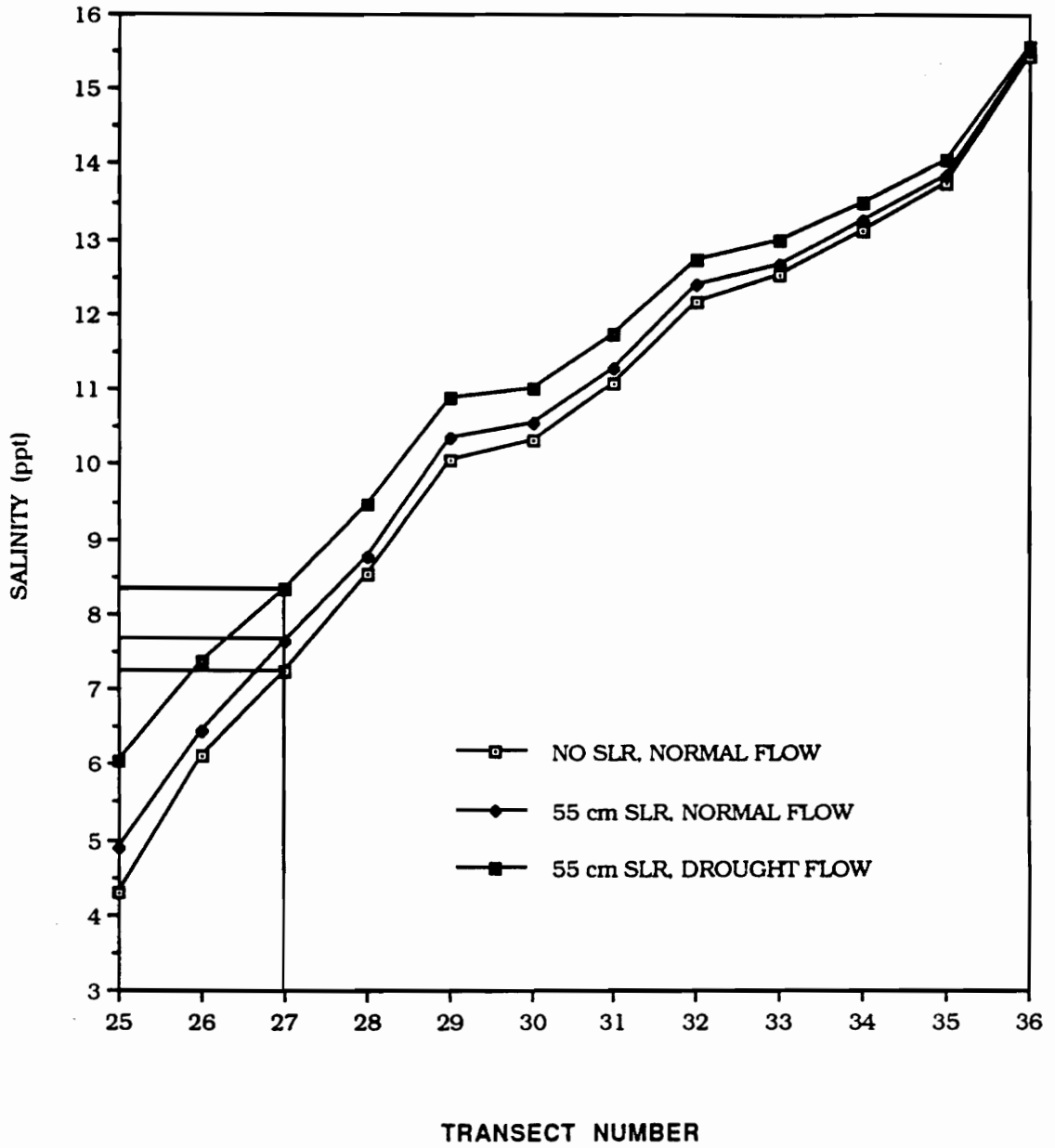


Figure 3.43 Depth-averaged salinity in an unconstricted channel, for no SLR vs. 55 cm SLR.

Figures

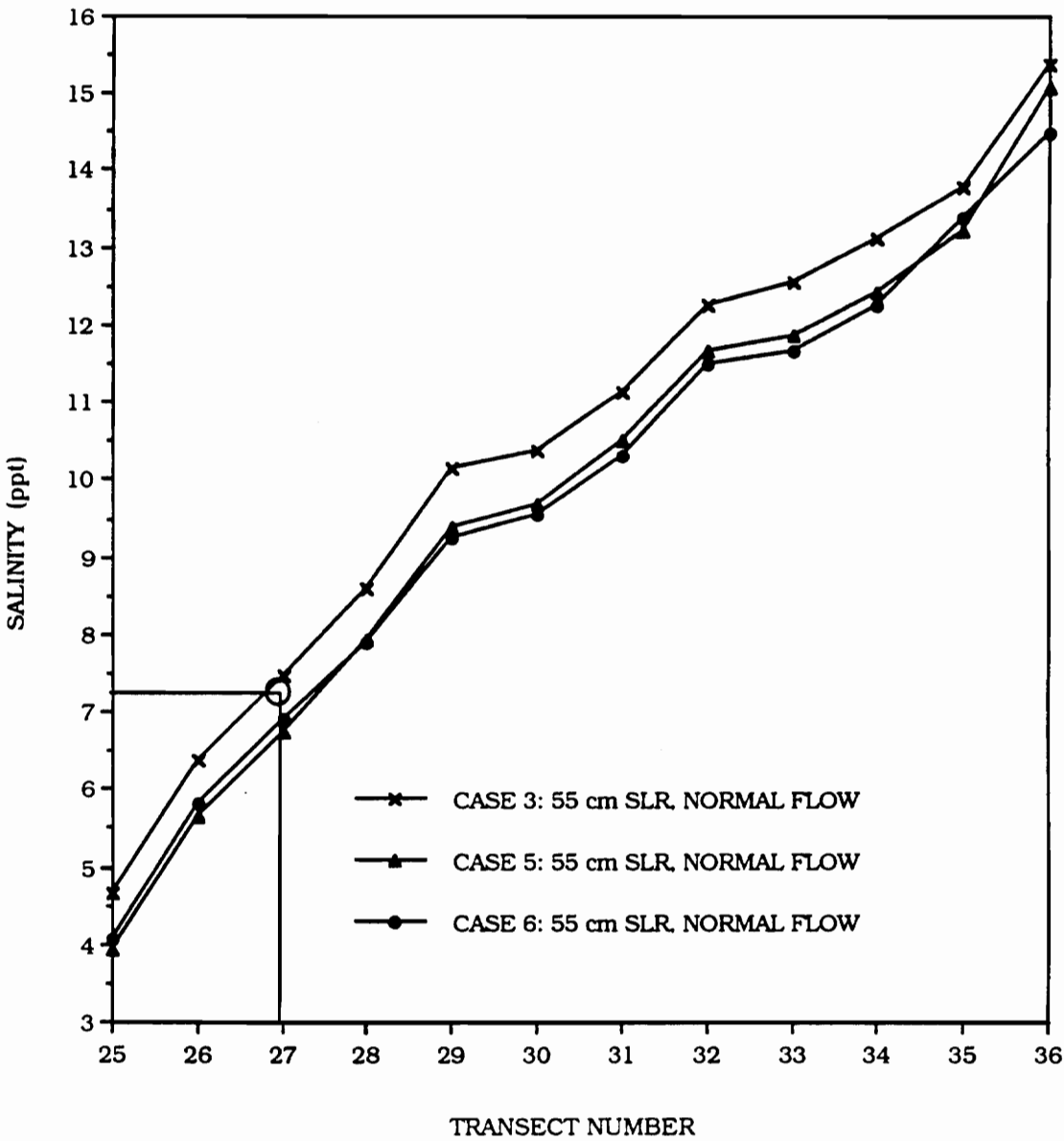


Figure 3.44 Depth-averaged salinity for cases 3, 5, and 6 for normal flow and 55 cm SLR.

Figures

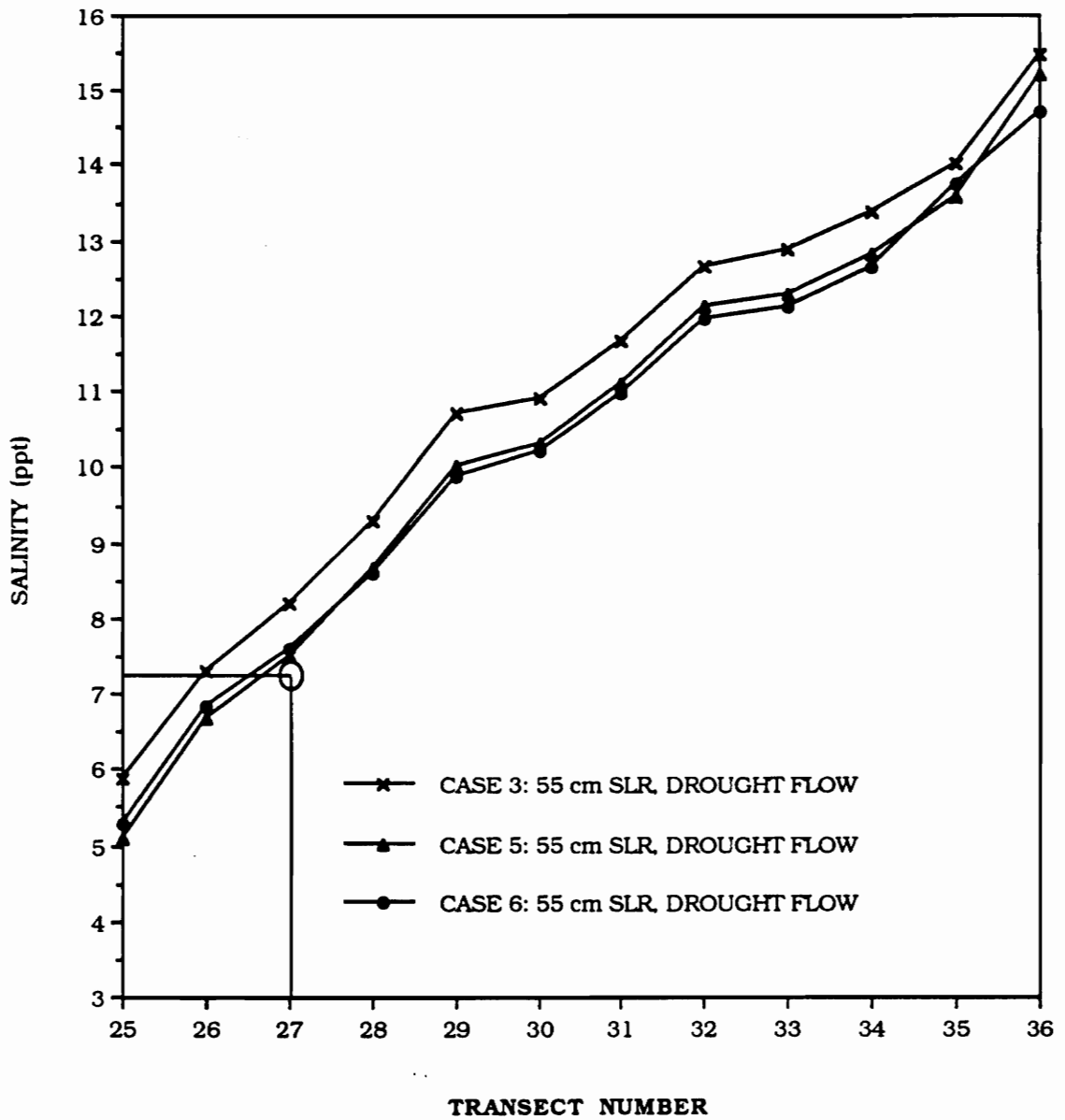


Figure 3.45 Depth-averaged salinity for cases 3, 5, and 6 for drought flow and 55 cm SLR.

Figures

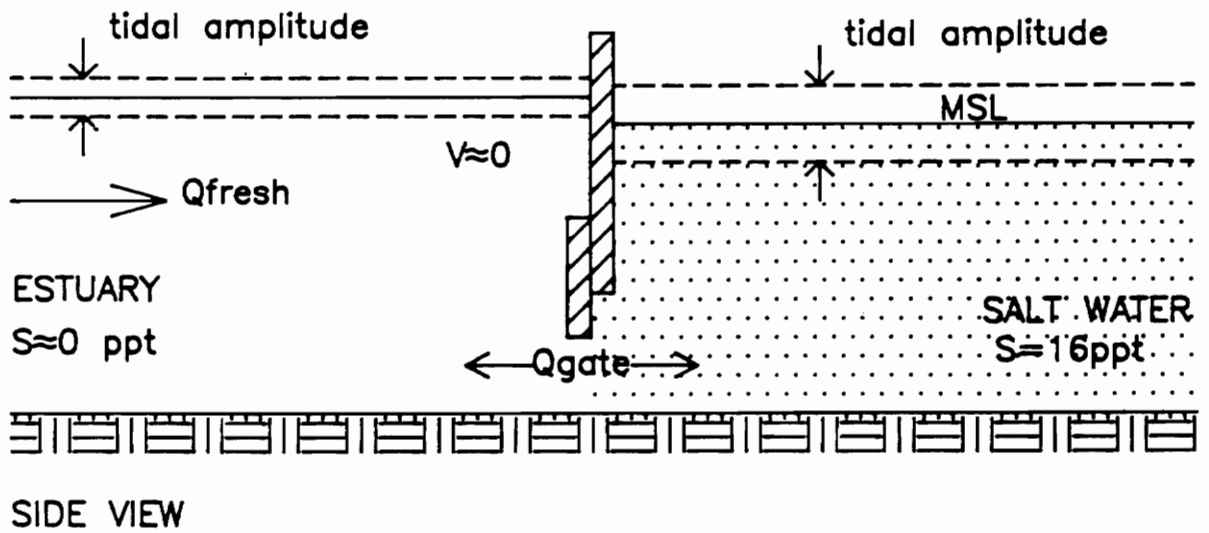
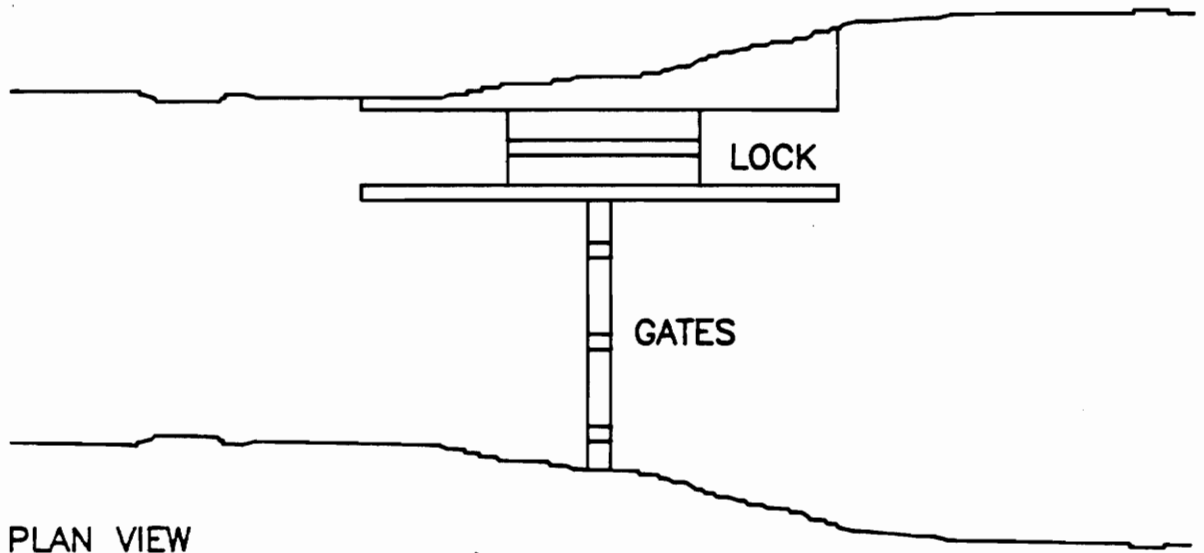


Figure 3.46 A schematic view of a tidal lock, with submerged gates, and a navigational channel.

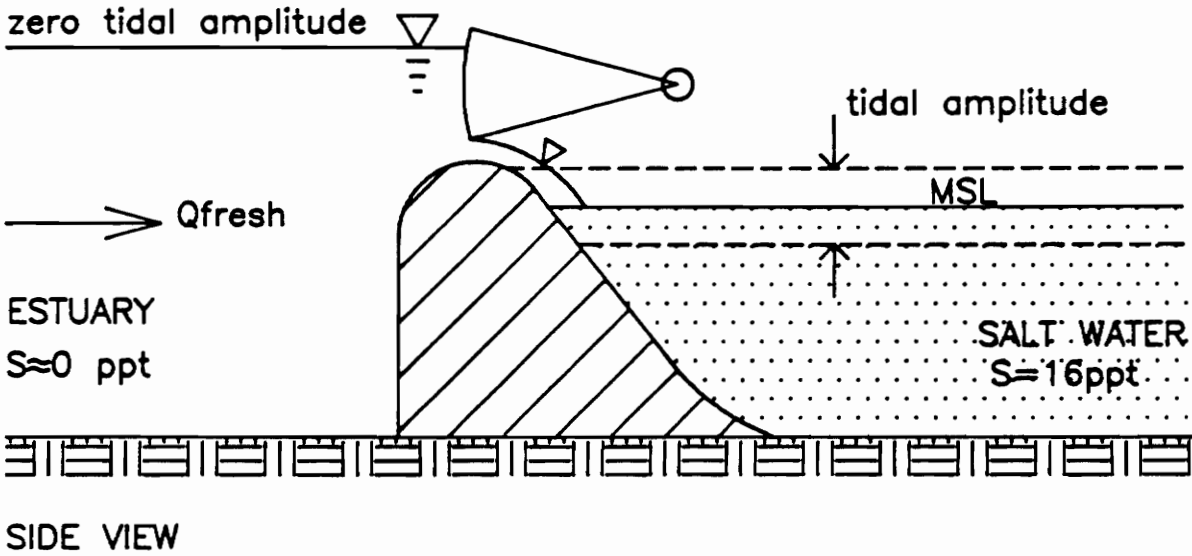
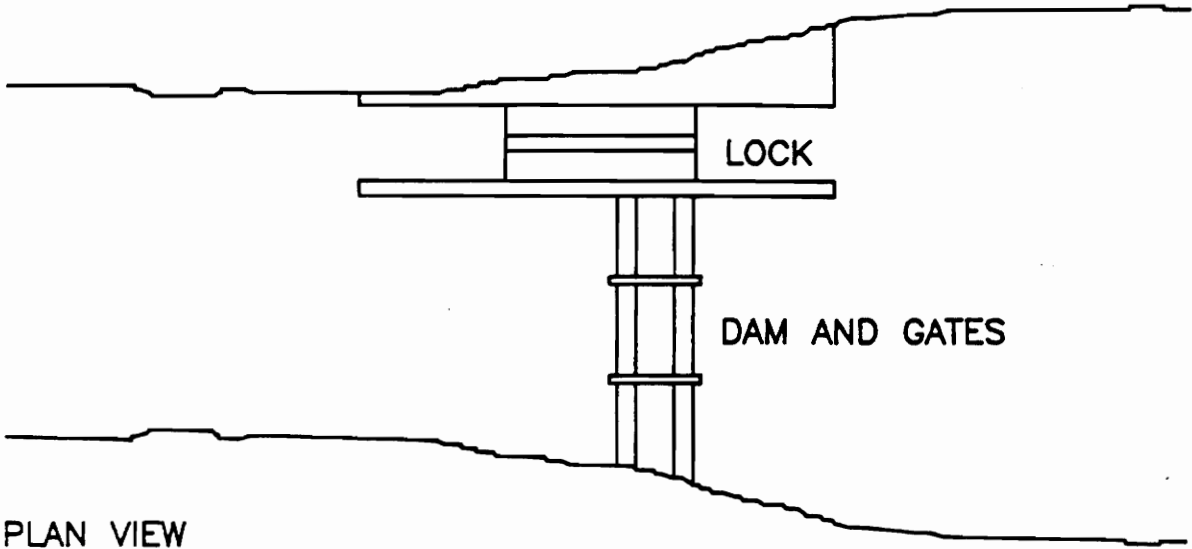


Figure 3.47 A schematic view of a tidal lock, with radial gates, and a navigational channel.

Figures

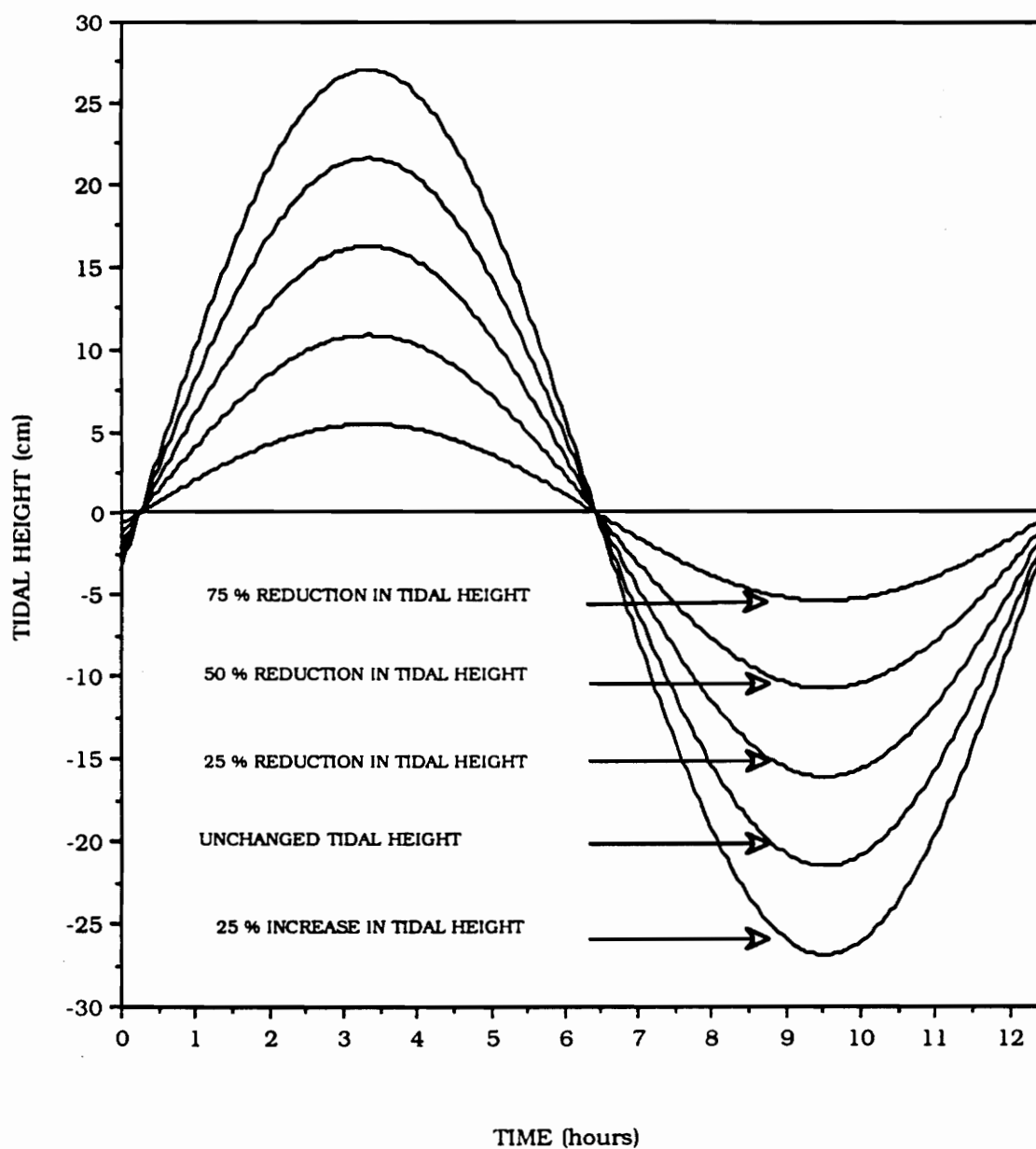


Figure 3.48 Tidal amplitudes prescribed at the downstream boundary for a tidal lock system.

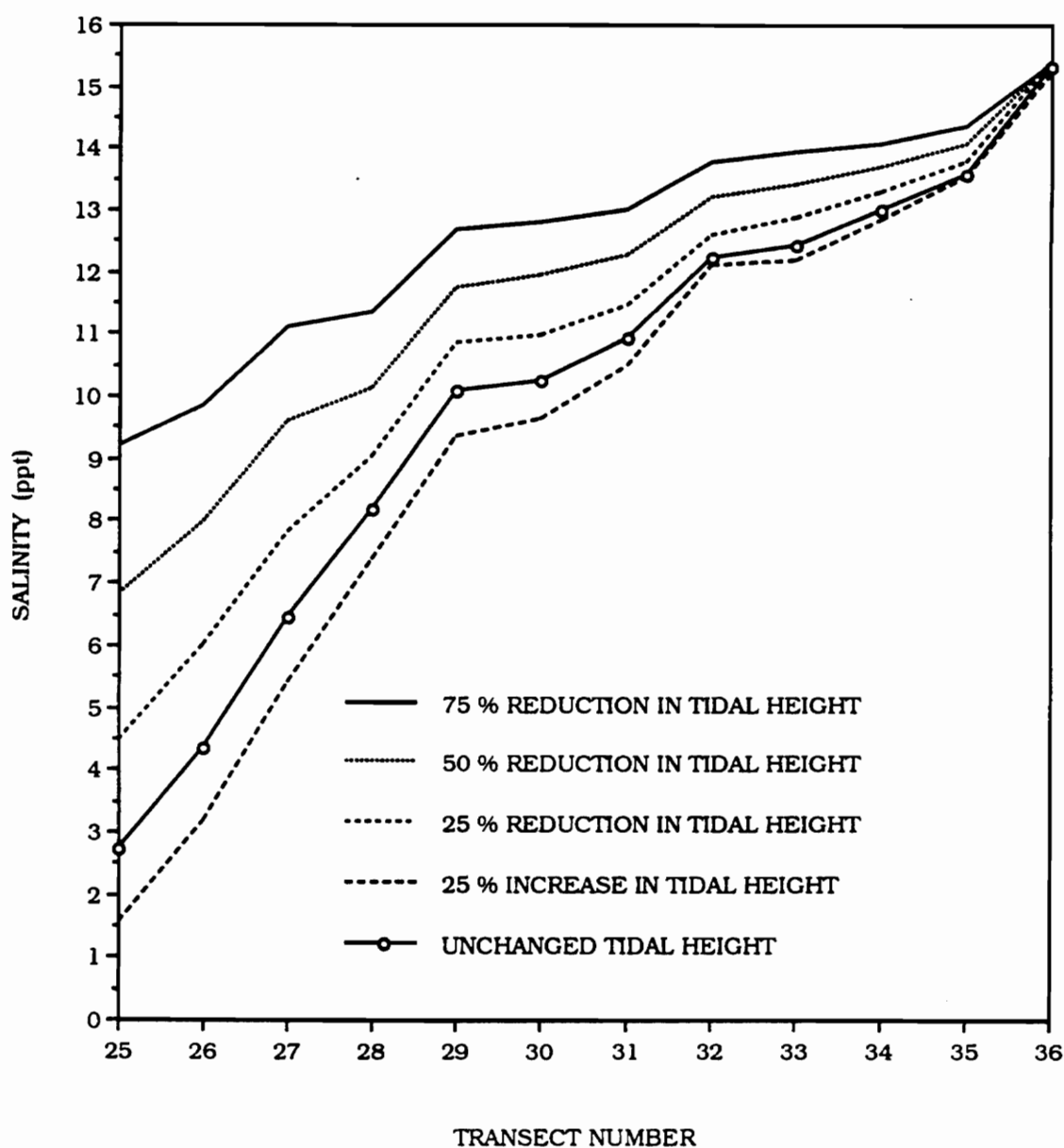


Figure 3.49 Depth averaged salinities at transect 25 to 36 for different tidal amplitudes (Flow = $47 \text{ m}^3/\text{s}$, no SLR).

Figures

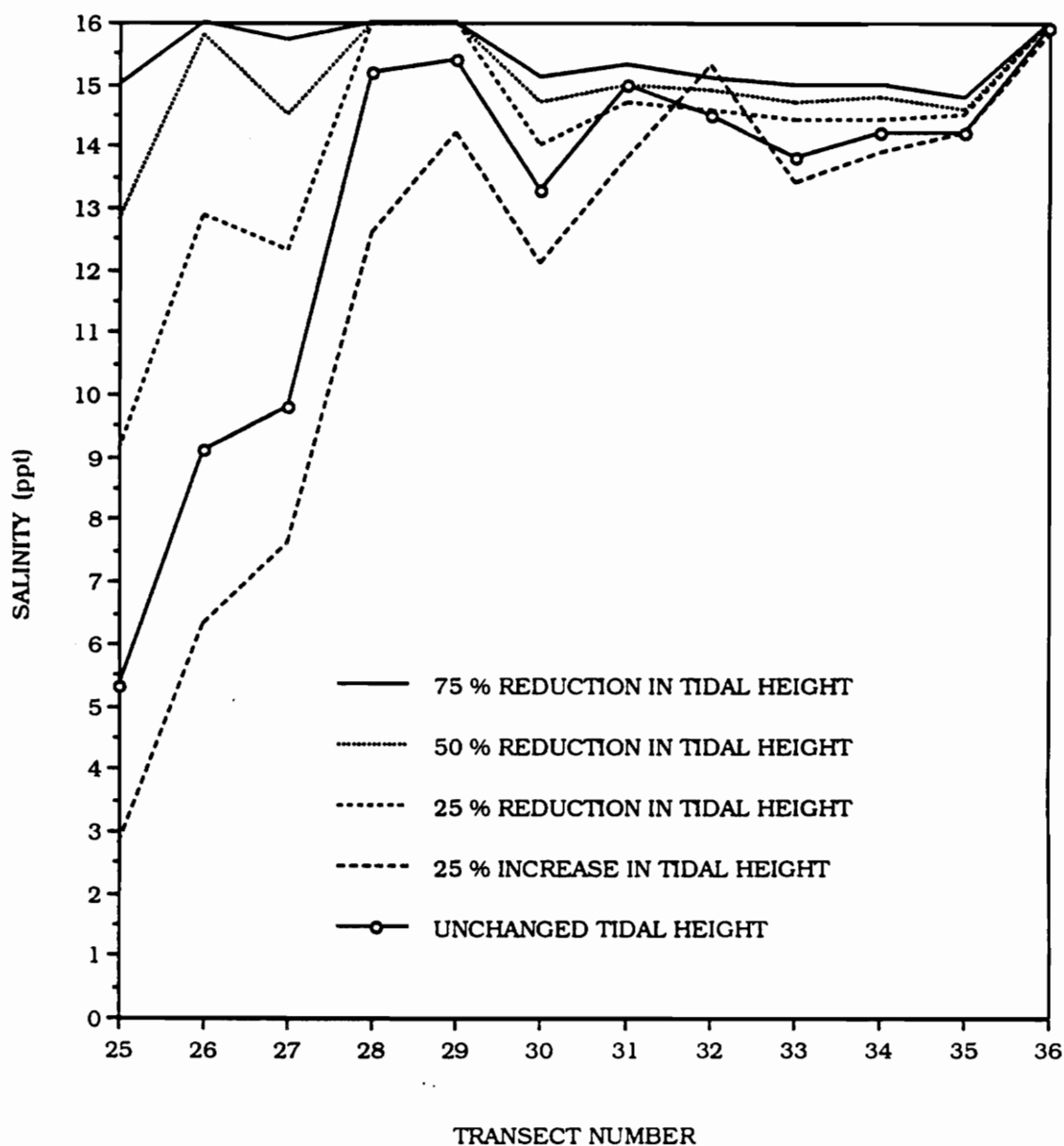


Figure 3.50 Average salinities in the bottom layer of transects 25 to 36 for different tidal amplitudes (Flow = $47 \text{ m}^3/\text{s}$, no SLR).

Figures

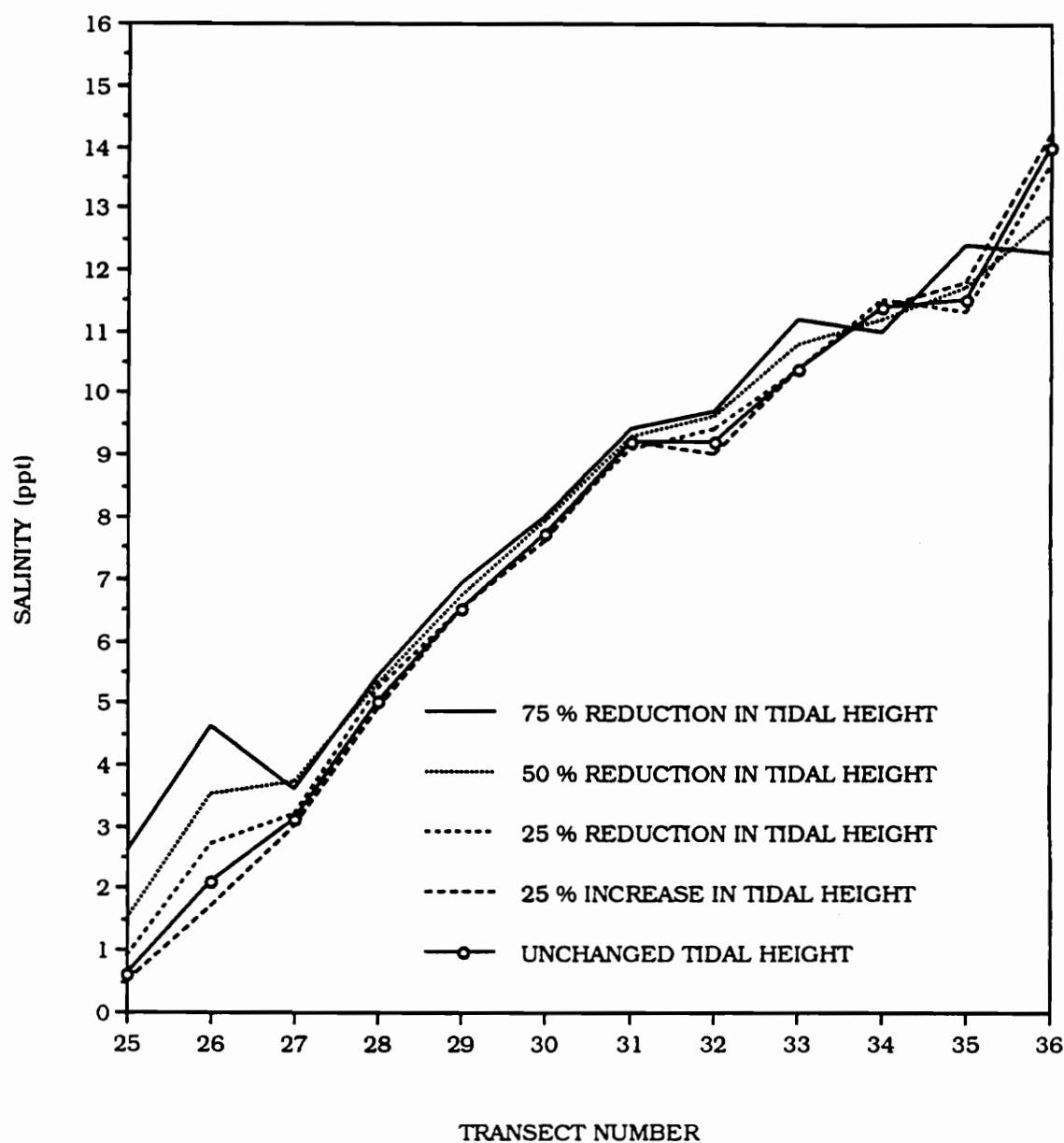


Figure 3.51 Average salinities in the top layer of transects 25 to 36 for different tidal amplitudes (Flow = $47 \text{ m}^3/\text{s}$, no SLR).

Figures

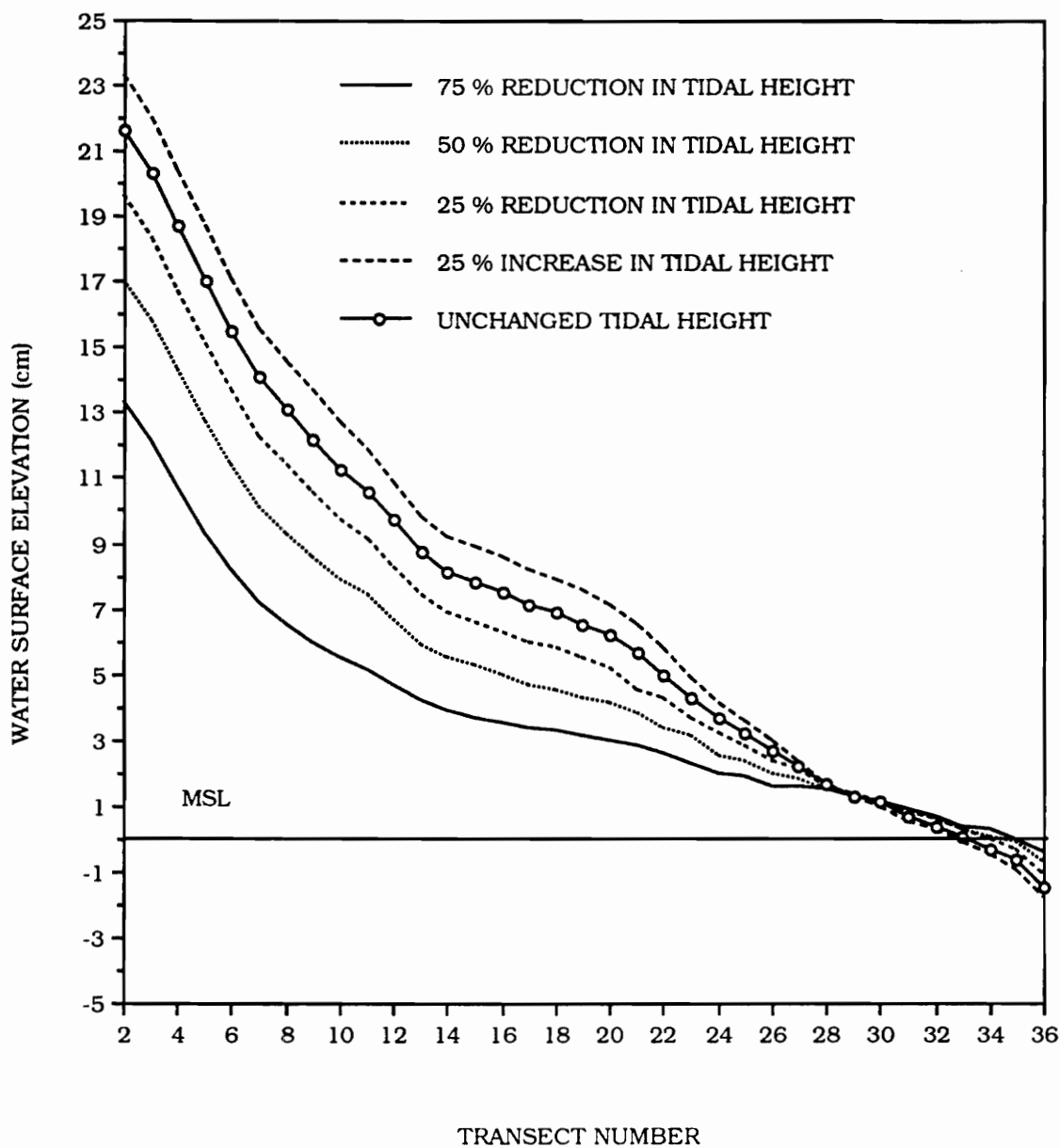


Figure 3.52 Water surface elevations at transects 2 to 36 for different tidal amplitudes (Flow = $47 \text{ m}^3/\text{s}$, no SLR).

Figures

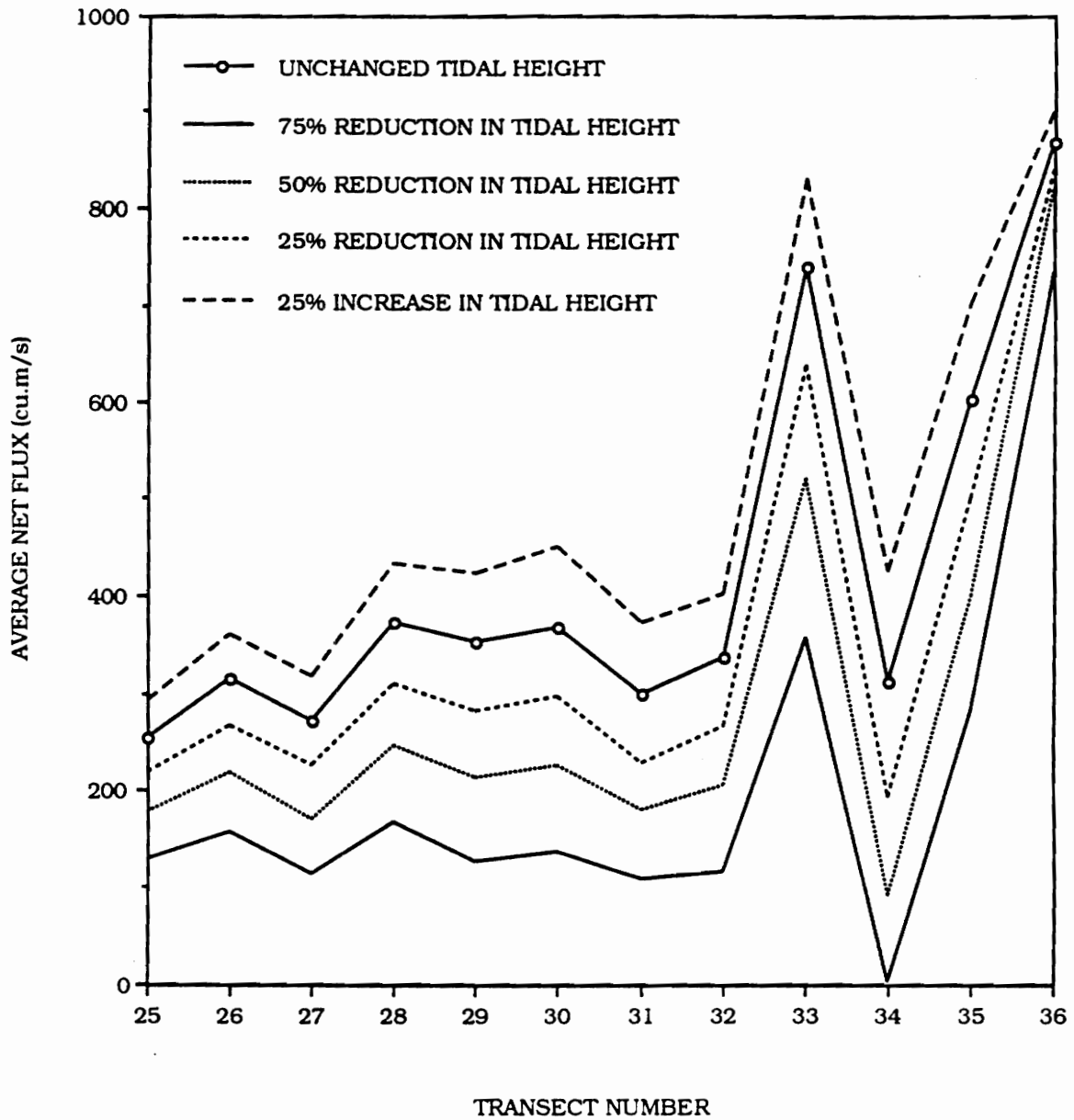


Figure 3.53 Average net flux/sec at transects 25 to 36 for different tidal amplitudes (Flow = $47 \text{ m}^3/\text{s}$, no SLR).

Figures

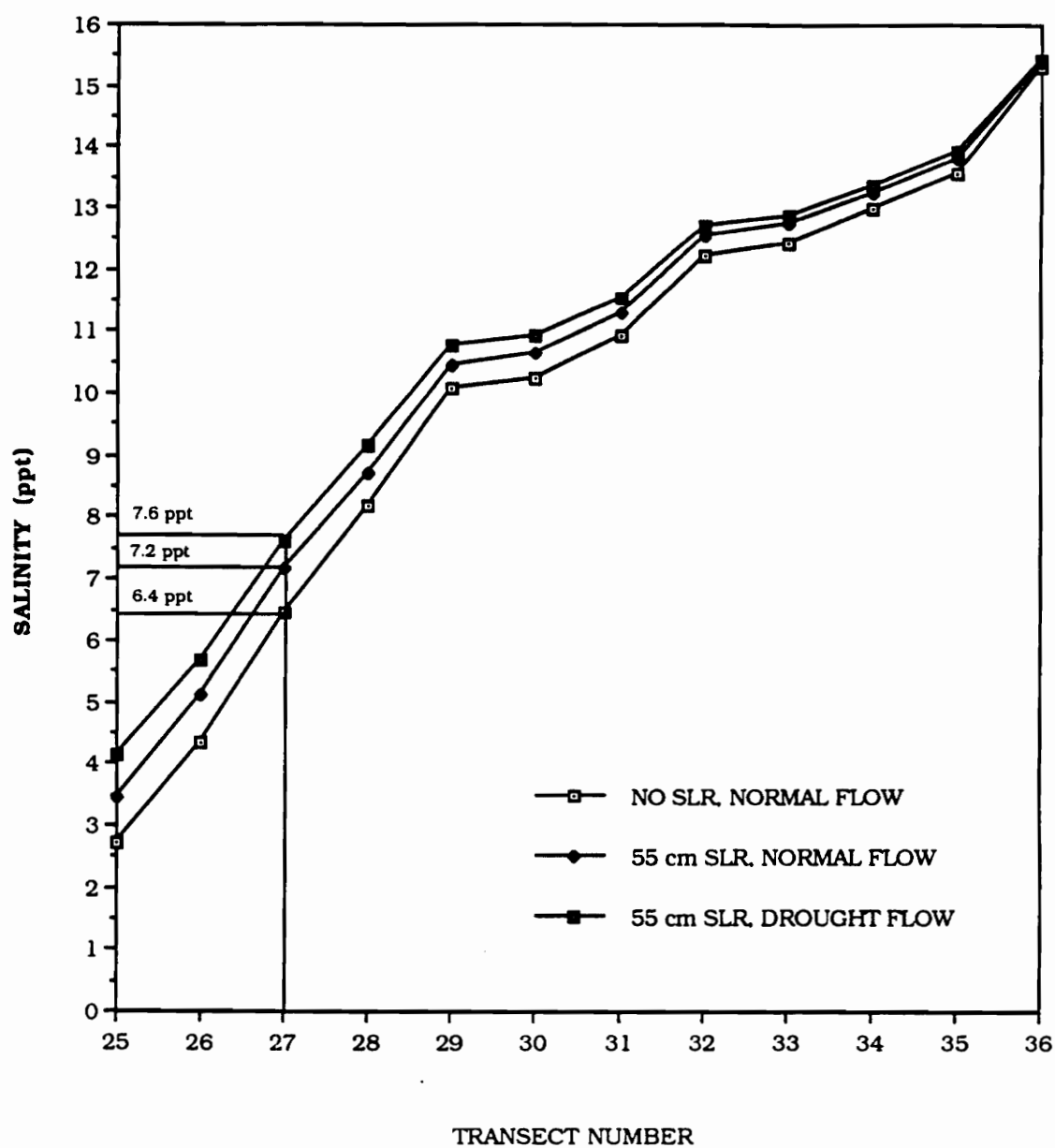


Figure 3.54 Depth averaged salinity for no SLR vs. 55 cm SLR.

Figures

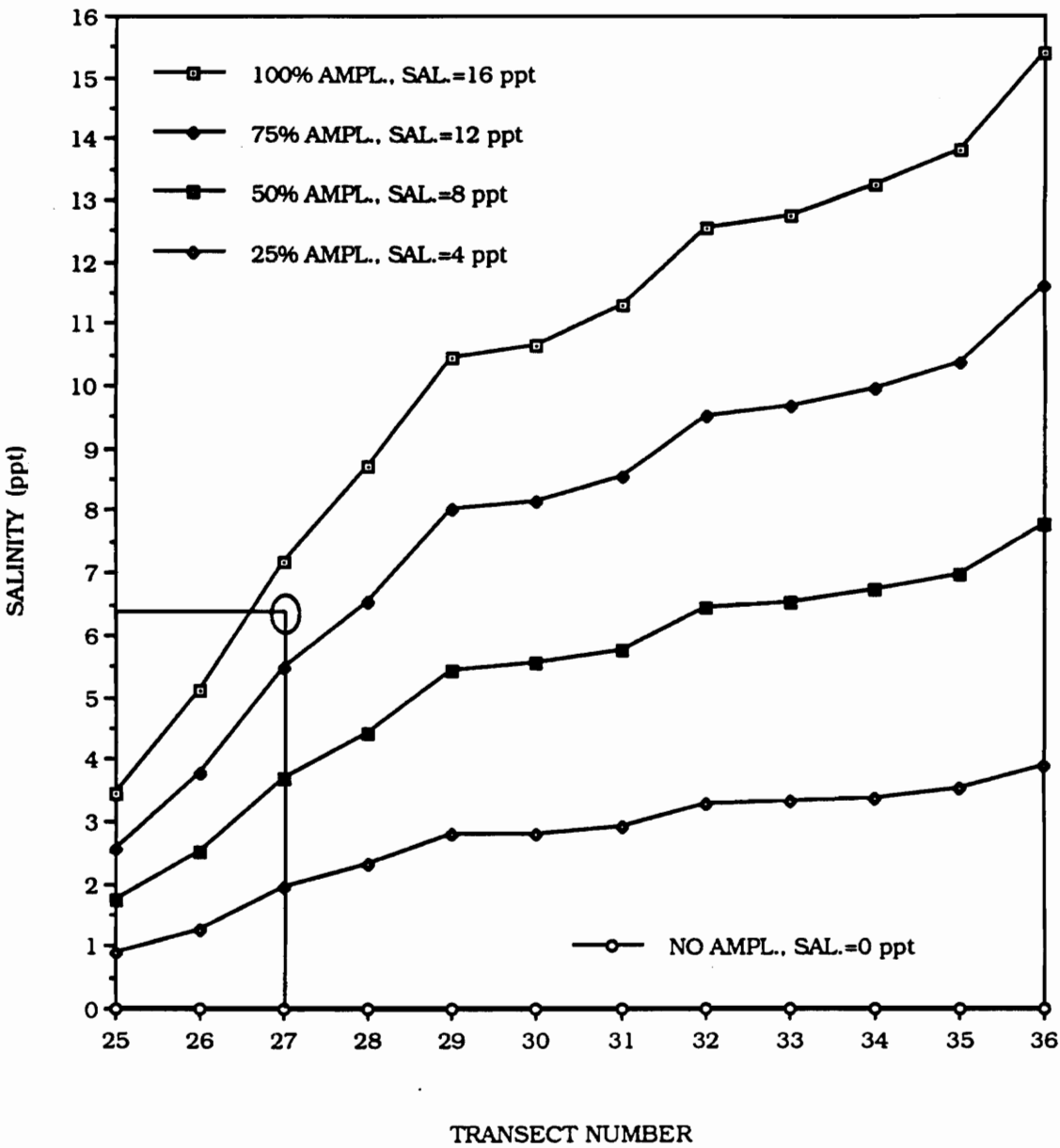


Figure 3.55 Average salinities at transects 25 to 36 for different tidal amplitudes (Flow = 47 m³/s, 55 cm SLR).

Figures

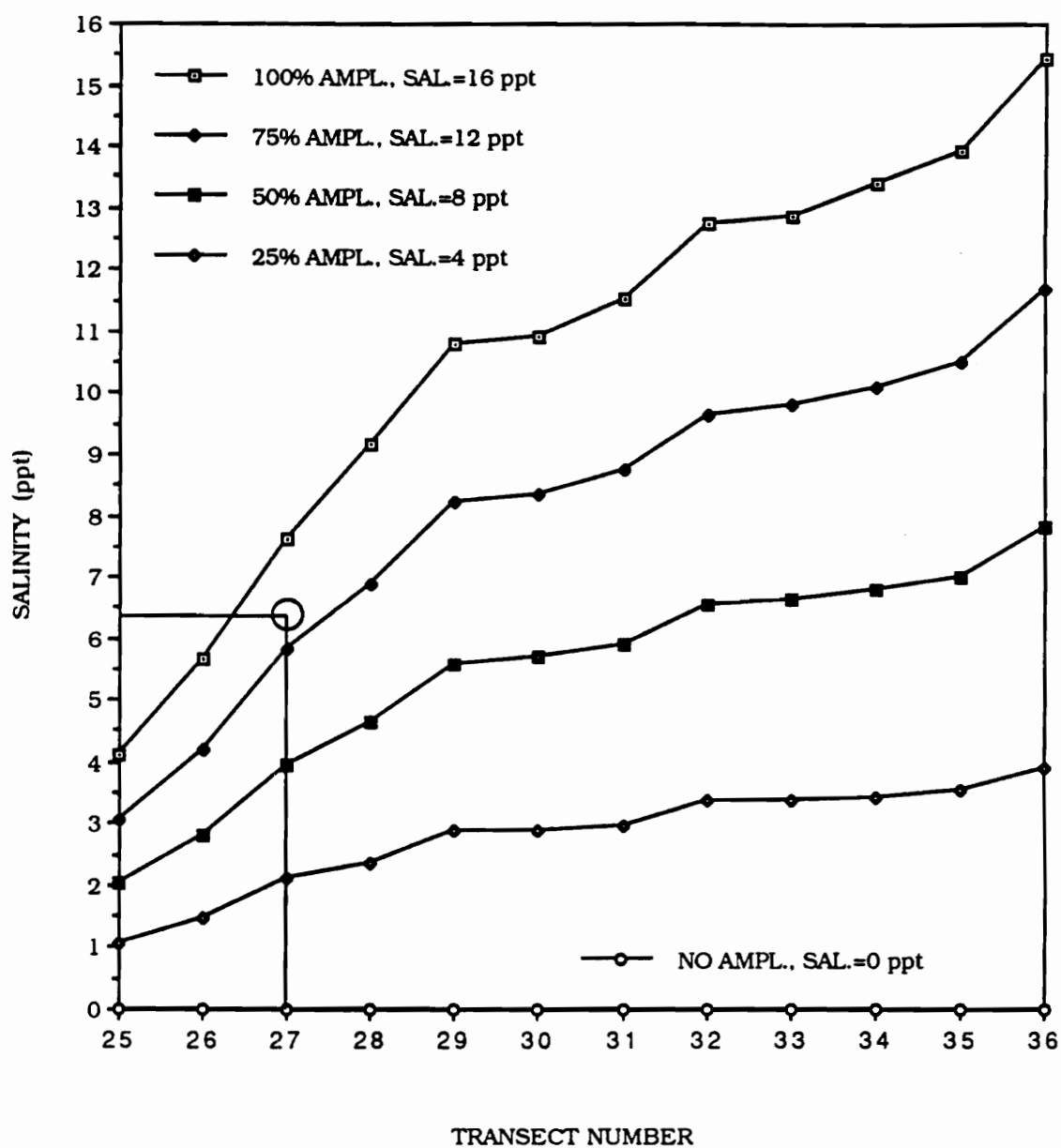


Figure 3.56 Average salinities at transects 25 to 36 for different tidal amplitudes (Flow = $1.52 \text{ m}^3/\text{s}$, 55 cm SLR).

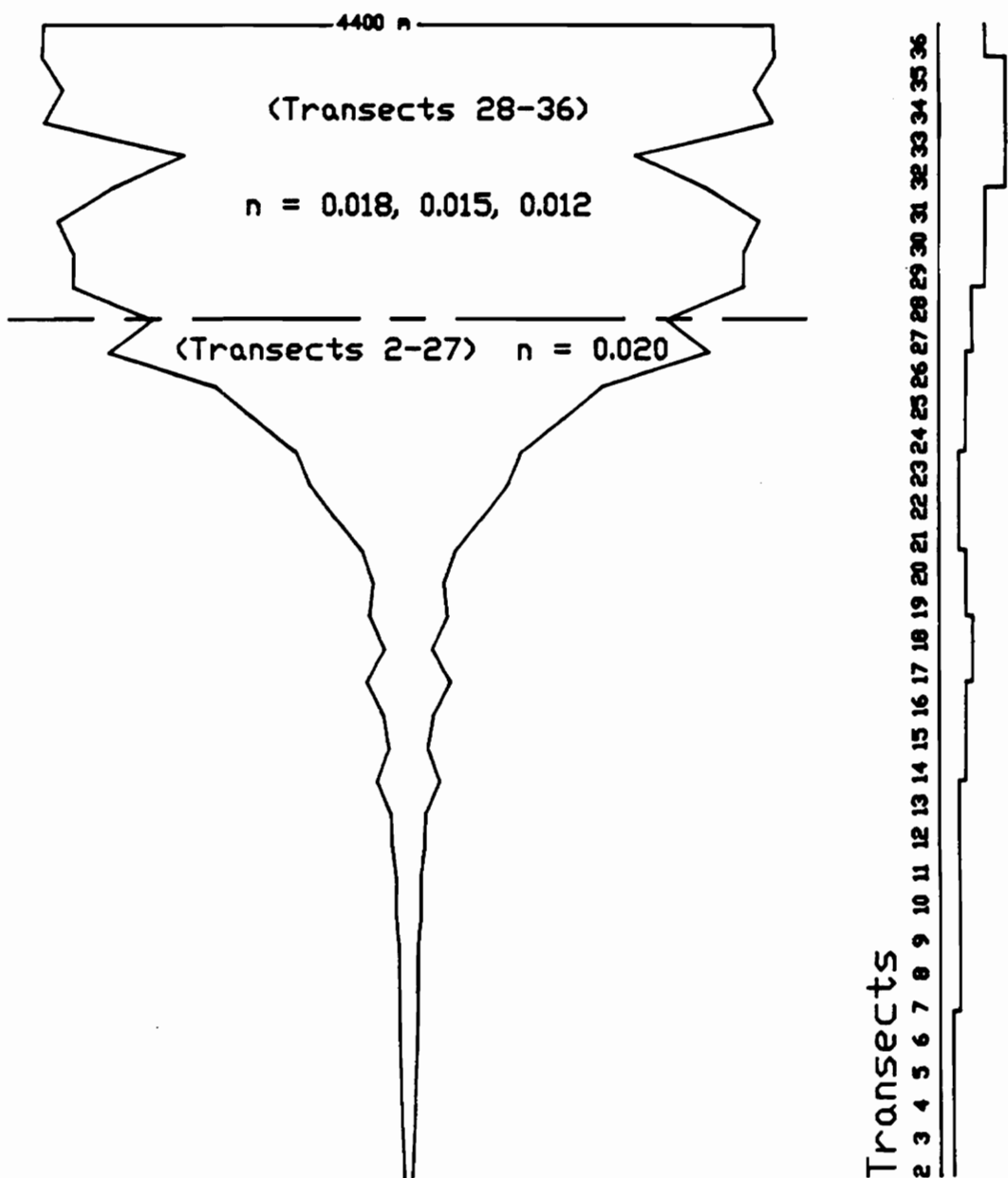


Figure 3.57 Potential change of Manning's n values in the Rappahannock River due to sea level rise.

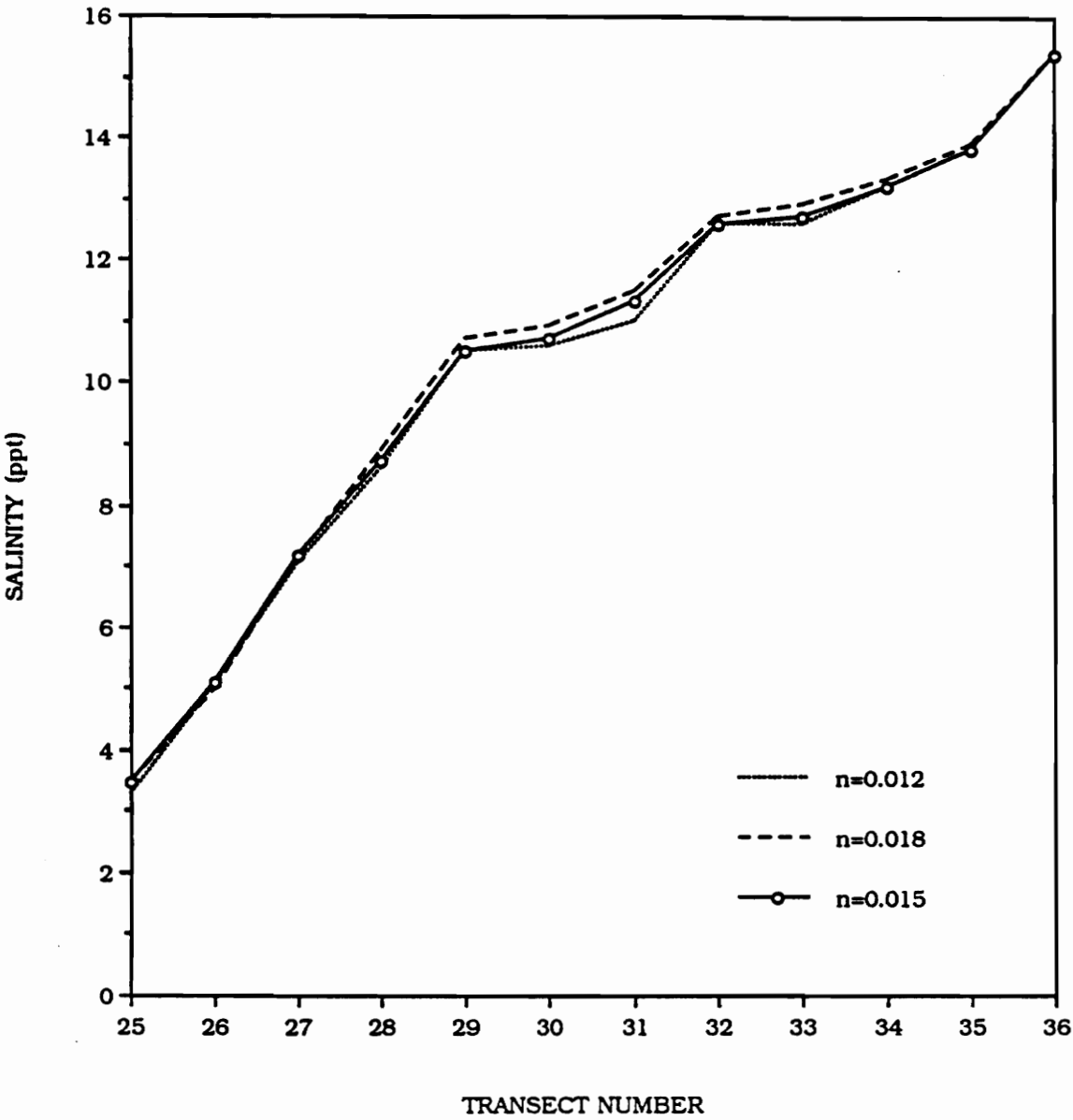


Figure 3.58 Depth averaged salinities at transects 25 to 36 for different values of Manning's n, and 55 cm SLR (Flow = 47 m³/s).

Figures

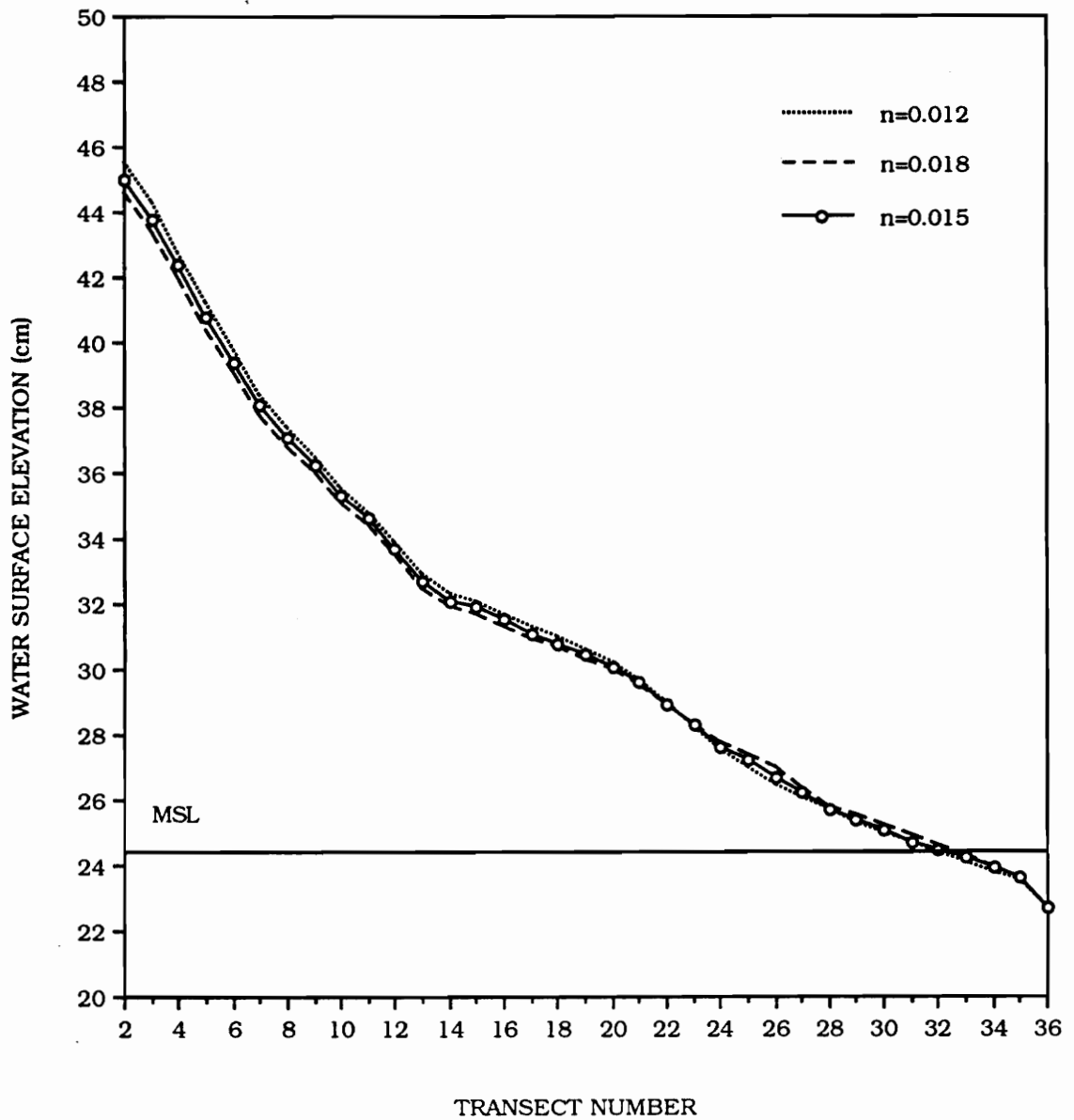


Figure 3.59 Water surface elevations at transects 2 to 36 for different values of Manning's n , and 55 cm SLR (Flow = $47 \text{ m}^3/\text{s}$).

Figures

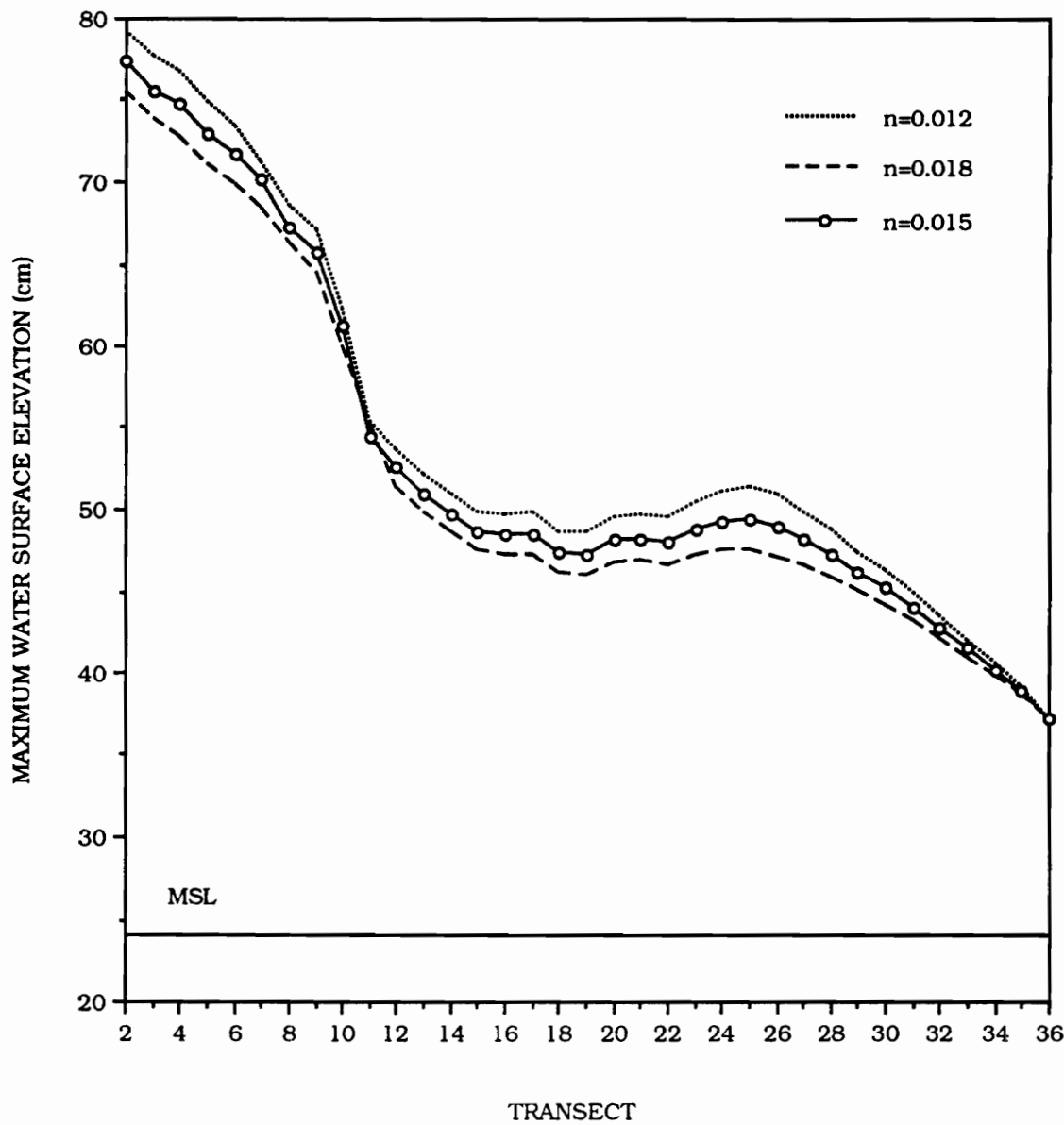


Figure 3.60 Maximum water surface elevations at transects 2 to 36 for different values of Manning's n, and 55 cm SLR (Flow = 47 m³/s).

Appendix A

Derivation of Governing Equations

A.1 Basic Equations

"To describe the time-varying tidal height, current and salinity distribution in an estuary, five equations are used in the computer model" (Kuo *et al.*, 1978; Yannaccone, 1987):

a) the equation of motion for an incompressible but non-homogeneous fluid

$$\begin{aligned} \frac{\partial u}{\partial t} + \frac{\partial(u^2)}{\partial X} + \frac{\partial(uv)}{\partial Y} + \frac{\partial(uw)}{\partial Z} = \\ -\frac{1}{\rho} \frac{\partial P}{\partial X} + \frac{\partial}{\partial X} \left[\epsilon_x \frac{\partial u}{\partial X} \right] + \frac{\partial}{\partial Y} \left[\epsilon_y \frac{\partial u}{\partial Y} \right] + \frac{\partial}{\partial Z} \left[\epsilon_z \frac{\partial u}{\partial Z} \right] \end{aligned} \quad (\text{A.1})$$

b) the hydrostatic equation

$$-g = \frac{1}{\rho} \frac{\partial P}{\partial Z} \quad (\text{A.2})$$

c) the continuity equation for an incompressible fluid

$$\frac{\partial u}{\partial X} + \frac{\partial v}{\partial Y} + \frac{\partial w}{\partial Z} = 0 \quad (\text{A.3})$$

d) the mass-balance equation for salts

$$\frac{\partial s}{\partial t} + \frac{\partial(us)}{\partial X} + \frac{\partial(vs)}{\partial Y} + \frac{\partial(ws)}{\partial Z} = \frac{\partial}{\partial X} \left[\epsilon_x \frac{\partial s}{\partial X} \right] + \frac{\partial}{\partial Y} \left[\epsilon_y \frac{\partial s}{\partial Y} \right] + \frac{\partial}{\partial Z} \left[\epsilon_z \frac{\partial s}{\partial Z} \right] \quad (\text{A.4})$$

e) an empirically derived equation of state

$$(P+P_o) \left[\frac{1}{\rho} - \frac{1}{\rho_o} \right] = \lambda \quad (\text{A.5})$$

where

Appendix A

u, v, w = velocity components in the X, Y, and Z directions, respectively

t = time

P = pressure

ρ = density of water

e_x, e_y, e_z = turbulent eddy viscosities (momentum exchange coefficients) in the X, Y, and Z directions, respectively

g = gravitational acceleration

s = salinity in parts per thousand

$\epsilon_x, \epsilon_y, \epsilon_z$ = turbulent mass diffusion coefficients in the X, Y, and Z directions, respectively

P_0, ρ_0, λ = empirical functions of temperature and salinity

A.2 Lateral Integration

Since lateral variations are not incorporated into the model, equations A.1, A.3, and A.4 are integrated with respect to the Y direction. This dimensional reduction is accomplished by assuming that the fluid is laterally homogeneous and that there is no flux of momentum through the lateral boundary of the estuary except at locations where tributaries enter. The equations reduce to (Kuo *et al.*, 1978):

$$\begin{aligned} \frac{\partial}{\partial t}(uB) + \frac{\partial}{\partial X}(uBu) + \frac{\partial}{\partial Z}(wBu) = \\ -\frac{B}{\rho} \frac{\partial P}{\partial X} + \frac{\partial}{\partial X}(e_x B \frac{\partial u}{\partial X}) + \frac{\partial}{\partial Z}(e_z B \frac{\partial u}{\partial Z}) + qu_t \end{aligned} \quad (A.6)$$

$$\frac{\partial}{\partial X}(uB) + \frac{\partial}{\partial Z}(wB) = q \quad (A.7)$$

$$\frac{\partial}{\partial t}(Bs) + \frac{\partial}{\partial X}(uBs) + \frac{\partial}{\partial Z}(wBs) = \frac{\partial}{\partial X}(\epsilon_X B \frac{\partial s}{\partial X}) + \frac{\partial}{\partial Z}(\epsilon_Z B \frac{\partial s}{\partial Z}) + qs_t \quad (\text{A.8})$$

where:

B = width of estuary

q = tributary inflow (or outflow) through unit area of X-Z plane

u_t, s_t = longitudinal velocity and salinity concentration of tributary flow, respectively.

To obtain the time-varying solution of the longitudinal and vertical velocity field, equation A.6 must be solved with the continuity equation (equation A.7) and the salt-balance equation (equation A.8). The equation of state is used in order to evaluate the pressure term in the longitudinal equation of motion (Kuo *et al.*, 1978).

A.3 Vertical Integration

Since variables in estuaries can change rapidly over a short vertical distance, they require a grid size that is much smaller in the vertical direction than in the longitudinal direction. To accomplish this, the fluid motion will be considered in horizontal slices with an exchange of mass and momentum between these slices. The geometry of the grid system used in the model and the location of variables within the grid system are shown in Figures 2.1 and 2.2, respectively, with η representing the surface elevation with respect to mean sea level. To determine the spatial location of a variable, a longitudinal and a vertical subscript are used. Integration over the height of the k^{th} layer can be performed by assuming that all variables are practically constant through the depth of any layer and that the fluxes of momentum and mass normal to the bottom of the

Appendix A

channel and to the surface are zero. Vertical integration gives the following equations (Kuo *et al.*, 1978):

$$\frac{\partial \eta}{\partial t} = \frac{1}{B_1} (w_b B_b - \frac{\partial}{\partial X} (u_1 B_1 h_1) + q_1 h_1) \quad (A.9)$$

$$w_T = \frac{1}{B_T} (w_b B_b - \frac{\partial}{\partial X} (u_k B_k h_k) + q_k h_k) \quad (A.10)$$

$$\begin{aligned} & \frac{\partial}{\partial t} (u_k B_k h_k) + \frac{\partial}{\partial X} (u_k B_k h_k u_k) + w_T u_T B_T - w_b u_b B_b = \\ & - \frac{B_k h_k}{\rho_k} \left(\frac{\partial P}{\partial X} \right)_k + \frac{\partial}{\partial X} \left(e_{X_k} B_k h_k \left(\frac{\partial u}{\partial X} \right)_k \right) + \tau_T - \tau_b + q_k u_t h_k \end{aligned} \quad (A.11)$$

$$\begin{aligned} & \frac{\partial}{\partial t} (s_k B_k h_k) + \frac{\partial}{\partial X} (u_k B_k h_k s_k) + w_T s_T B_T - w_b s_b B_b = \\ & \frac{\partial}{\partial X} (\epsilon_X h \frac{\partial s}{\partial X})_k + (\epsilon_Z B \frac{\partial s}{\partial Z})_T - (\epsilon_Z B \frac{\partial s}{\partial Z})_b + q_k s_t h_k \end{aligned} \quad (A.12)$$

where

B_k, u_k, h_k, q_k = width, longitudinal velocity, height, and tributary inflow for the k^{th} layer, respectively

u_b, w_b, B_b = longitudinal velocity, vertical velocity, and estuary width, respectively, at the bottom of a layer

u_T, w_T, B_T = longitudinal velocity, vertical velocity, and estuary width, respectively, at the top of a layer

Appendix A

η = water surface elevation with respect to mean sea level

$\tau_T = (e_z B \frac{\partial u}{\partial z})_T$ and $\tau_b = (e_z B \frac{\partial u}{\partial z})_b$ = interfacial shear stresses.

Equation A.9 is the continuity equation for the top layer, and equation A.10 is the continuity equation for all other layers. Equation A.11 is the longitudinal equation of motion, and equation A.12 is the mass-balance equation for salt (Kuo *et al.*, 1978).

A.4 Finite Difference Formulation

The finite difference approximations of equation A.9, A.10, A.11, and A.12 are (Kuo *et al.*, 1978):

a) continuity equations

$$\overline{\delta_t \eta}^t = \frac{1}{B_1} (w_1 B_1^{-Z} - \delta_x (u B^{-X} h^{-X})_1 + q_1 \cdot h_1) \quad (A.13)$$

$$h \delta_z (B^{-Z} w) = -\delta_x (u B^{-X} h^{-X}) + q_k \cdot h_k \quad (A.14)$$

b) equation of motion

$$\begin{aligned} \overline{\delta_t (u h^{-X} B^{-X})}^t &= -\delta_x \overline{(B^{-X} h^{-X} u u^{-X})}^X - h^{-Z} \delta_z (u^{-Z} w^{-X} B^{-XZ}) - \\ &\frac{B^{-X} h^{-X}}{\rho^{-X}} \cdot \left(\frac{\partial P}{\partial X} \right)_k + \delta_x \overline{(B^{-X} h^{-X} e_x \delta_x u)}^X + h^{-Z} \delta_z (\overline{e_z}^X B^{-XZ} \delta_z u) + q u_t h \end{aligned} \quad (A.15)$$

c) mass-balance equation for salt

$$\begin{aligned} \overline{\delta_t (shB)}^t &= -\delta_x (B^{-X} h^{-X} s^{-X} u) - h \delta_z (w s^{-Z} B^{-Z}) + \\ &\delta_x (E_x B^{-X} h^{-X} \delta_x s) + h \delta_z (E_z B^{-Z} \delta_z s) + q \cdot s_t h \end{aligned} \quad (A.16)$$

Appendix B

Sample Input for the Numerical Model

Appendix B

NUMBER OF TRANSECTS = 35

MAX. NUM. OF LAYERS IN ANY TRANSECT = 10

LAYER THICKNESS (M)

1	2.0
2	2.0
3	2.0
4	2.0
5	2.0
6	2.0
7	2.0
8	2.0
9	2.0
10	2.0

ESTUARY WIDTHS (M)

LAYERS

TRANSECT	1	2	3	4	5	6	7	8	9	10
----------	---	---	---	---	---	---	---	---	---	----

2	*	65.	50.							
3	*	82.	50.							
4	*	89.	49.							
5	*	103.	57.							
6	*	119.	69.							
7	*	109.	70.	35.						
8	*	117.	91.	47.						
9	*	153.	118.	39.						
10	*	146.	119.	68.						
11	*	197.	140.	45.						
12	*	210.	154.	42.						

Appendix B

13 * 383. 201. 23.
 14 * 235. 199. 143. 78.
 15 * 306. 268. 142. 68.
 16 * 510. 291. 132. 24.
 17 * 291. 239. 200. 145. 104.
 18 * 475. 306. 196. 132. 90.
 19 * 430. 342. 250. 122.
 20 * 567. 396. 238. 57.
 21 * 897. 461. 185.
 22 * 1199. 500. 111.
 23 * 1361. 546. 205.
 24 * 1879. 685. 234. 78.
 25 * 2347. 924. 345. 255.
 26 * 3617. 1270. 587. 357.
 27 * 3102. 1410. 739. 511. 128.
 28 * 4043. 2209. 864. 642. 498.
 29 * 4038. 2914. 1372. 835. 768. 606. 296.
 30 * 4230. 3382. 2113. 1329. 1071. 703. 433.
 31 * 3566. 3068. 2016. 1742. 1596. 791. 589.
 32 * 2720. 2309. 1810. 1501. 1120. 974. 793. 602. 396. 198.
 33 * 4390. 3734. 3190. 2347. 1195. 491. 395. 357. 299. 251.
 34 * 4167. 3073. 2475. 2230. 1793. 1280. 944. 704. 475. 256.
 35 * 4417. 3431. 2989. 2059. 1593. 1198. 902. 747. 506. 278.
 36 * 4400. 2730. 1585. 1378. 686. 216. 72.

****STORAGE SURFACE AREA****

0.000	0.000	0.000	0.000	0.000	0.000	0.500	0.800	0.600	0.900
5.060	1.280	0.790	1.000	1.300	3.300	3.680	3.890	9.770	12.830
10.000	6.130	2.900	5.800	2.000	9.400	4.000	0.000	2.550	3.570
33.100	3.450	6.160	6.100	0.000					

Appendix B

ESTUARINE TEMPERATURE = 20.0000

DISTANCE BETWEEN TRANSECTS (M) = 5000.0000

TIME INTERVAL BETWEEN TIME STEPS (SECS) = 46.0000

PRINTING OF VARIABLES WILL COMMENCE AT THE 19.00 TIDAL CYCLE, END AT
THE 20.00 TIDAL CYCLE,

PRINTING EVERY 972 TIME STEP(S)

WIND SPEED (M/S) = 0.0000

AIR DENSITY (GM/CC) = 0.0012

DRAG COEF = 0.0013

****MANNING FRICTION COEFFICIENTS****

0.0200	0.0200	0.0200	0.0200	0.0200	0.0200	0.0200	0.0200	0.0200
0.0150								
0.0150	0.0150	0.0150	0.0150	0.0150	0.0150	0.0150	0.0150	0.0150
0.0150								
0.0150	0.0150	0.0150	0.0150	0.0150	0.0150	0.0150	0.0150	0.0150
0.0150								
0.0150	0.0150	0.0150	0.0150	0.0150				

WIND WAVE CHARA: HEIGHT(CM)= 0.0000, LENGTH(CM)= 0.0000, PERIOD(SEC)=
0.0000

INITIAL UPSTREAM SALINITY = 0.0000

INITIAL DOWNSTREAM SALINITY= 16.0000

INITIAL SALT INTRUSION LIMIT IN TERMS TRANSECT NUMBER= 25

INITIAL UPSTREAM SED. CONCEN.= 30.00

INITIAL DOWNSTREAM SED. CONCEN.= 0.00

Appendix B

TIME INTERVAL FROM SBF TO REACH OCEAN CONDITIONS(HRS)= 5.00

****OCEAN SALINITIES ****

16.00 16.00 16.00 16.00 16.00 16.00 16.00

****OCEAN SEDIMENT CONCENTRATIONS****

0.00 0.00 0.00 0.00 0.00 0.00 0.00

COEFFICIENT FOR SETTLING VELOCITY IN CGS UNIT= 6000.0000

AVERAGE SED. PARTICLE SIZE IN MICRON= 6.50

VARIANCE OF PARTICLE SIZE DISTRIBUTION IN MICRON**2= 0.00

SED. SETTLING VELOCITY IN 0.01CM/S= 0.25

CRITICAL SHEAR STRESS FOR DEPOSITION= 0.30DYNE/CM**2

CRITICAL SHEAR STRESS FOR RESUSPENSION= 0.50DYNE/CM**2

RESUSPENSION CONSTANT= 0.3000 MICRO-GRAM/CM**2/SEC

TIDAL AMPLITUDES (CM) & PHASES (DEGREES)

O1	4.3	315.60
K1	5.0	127.80
M2	36.1	262.10
S2	6.9	285.40
N2	7.9	244.80

Appendix B

UPSTREAM TRANSECT BOUNDARY CONDITIONS:

LAYER HORZ. VEL. (CM/SEC)

1 20.4000

2 20.4000

FLOOD HYDROGRAPH AND SEDIMENTGRAPH

TIME (MG/L)

DOWNSTREAM BOUNDARY CONDITION

SEA LEVEL RISE (CM) = 55.00

STORM SURGE (CM) = 0.00

TIDE CONVERSION FACTOR = 0.44

Appendix C

Sample Output from the Numerical Model

Appendix C

SALINITY AT HOUR 235.98

		TRANSECT																	
LAYER		2	3	4	5	6	7	8	9	10	11	12	13	14	15	16	17	18	
19	20	21																	

1	*	0.0	0.0	0.0	0.0	0.0	0.0	0.0	0.0	0.0	0.0	0.0	0.0	0.0	0.0	0.0	0.0	0.0	0.0
0.1		0.0	0.1	0.0															
2	*	0.0	0.0	0.0	0.0	0.0	0.0	0.0	0.0	0.0	0.0	0.0	0.0	0.0	0.0	0.0	0.0	0.0	0.0
0.1		0.0	0.1	0.0															
3	*	30.0	30.0	30.0	30.0	30.0	0.0	0.0	0.0	0.0	0.0	0.0	0.0	0.0	0.0	0.0	0.0	0.0	0.0
0.0		0.1	0.0	0.1	0.0														
4	*	30.0	30.0	30.0	30.0	30.0	30.0	30.0	30.0	30.0	30.0	30.0	30.0	30.0	30.0	0.0	0.0	0.0	0.0
0.0		0.1	0.0	0.1	30.0														
5	*	30.0	30.0	30.0	30.0	30.0	30.0	30.0	30.0	30.0	30.0	30.0	30.0	30.0	30.0	30.0	30.0	30.0	30.0
30.0		0.0	0.1	30.0	30.0	30.0													
6	*	30.0	30.0	30.0	30.0	30.0	30.0	30.0	30.0	30.0	30.0	30.0	30.0	30.0	30.0	30.0	30.0	30.0	30.0
30.0		30.0	30.0	30.0	30.0	30.0													
7	*	30.0	30.0	30.0	30.0	30.0	30.0	30.0	30.0	30.0	30.0	30.0	30.0	30.0	30.0	30.0	30.0	30.0	30.0
30.0		30.0	30.0	30.0	30.0	30.0													
8	*	30.0	30.0	30.0	30.0	30.0	30.0	30.0	30.0	30.0	30.0	30.0	30.0	30.0	30.0	30.0	30.0	30.0	30.0
30.0		30.0	30.0	30.0	30.0	30.0													
9	*	30.0	30.0	30.0	30.0	30.0	30.0	30.0	30.0	30.0	30.0	30.0	30.0	30.0	30.0	30.0	30.0	30.0	30.0
30.0		30.0	30.0	30.0	30.0	30.0													
10	*	30.0	30.0	30.0	30.0	30.0	30.0	30.0	30.0	30.0	30.0	30.0	30.0	30.0	30.0	30.0	30.0	30.0	30.0
30.0		30.0	30.0	30.0	30.0	30.0													

		TRANSECT														
LAYER		22	23	24	25	26	27	28	29	30	31	32	33	34	35	36

1	*	0.2	0.0	0.7	0.8	2.3	3.4	5.3	6.9	8.1	9.5	9.5	10.8	11.7	11.9	13.4
2	*	0.2	0.0	0.7	0.8	2.3	3.9	5.8	7.5	8.6	9.7	10.4	11.4	12.1	12.8	14.4

Appendix C

3	*	0.2	0.0	0.9	4.1	3.9	5.2	6.6	8.3	9.1	10.0	10.8	11.8	12.5	13.3	14.9
4	*	30.0	30.0	0.9	5.8	9.9	9.8	7.9	8.9	9.8	10.3	11.3	12.1	12.8	13.6	15.3
5	*	30.0	30.0	30.0	30.0	30.0	9.4	16.0	11.9	11.3	10.8	11.7	12.5	13.1	13.8	15.6
6	*	30.0	30.0	30.0	30.0	30.0	30.0	30.0	11.8	13.2	12.4	12.1	13.0	13.3	14.0	15.8
7	*	30.0	30.0	30.0	30.0	30.0	30.0	30.0	15.7	13.7	15.0	14.1	13.7	13.5	14.2	15.9
8	*	30.0	30.0	30.0	30.0	30.0	30.0	30.0	30.0	30.0	30.0	14.1	14.0	13.7	14.3	30.0
9	*	30.0	30.0	30.0	30.0	30.0	30.0	30.0	30.0	30.0	30.0	14.6	14.0	14.2	14.4	30.0
10	*	30.0	30.0	30.0	30.0	30.0	30.0	30.0	30.0	30.0	30.0	15.0	14.1	14.3	14.3	30.0

SEDIMENT CONCENTRATION AT HOUR 235.98

TRANSECT

LAYER	2	3	4	5	6	7	8	9	10	11	12	13	14	15	16	17	18
19	20	21															

1	*	30.0	32.3	29.3	31.3	28.6	31.0	26.1	26.1	18.7	20.7	8.0	7.6	7.7	6.1	9.5	
9.4	9.6	8.2	6.4	0.0													
2	*	30.0	38.0	35.5	38.0	34.6	35.5	30.1	29.8	21.1	23.4	9.6	8.6	8.5	6.6	10.2	
10.0	9.8	8.1	5.9	0.0													
3	*	0.0	0.0	0.0	0.0	0.0	40.6	34.4	34.6	24.2	27.2	11.5	10.0	9.0	7.0	10.8	
10.5	10.0	8.2	5.9	0.0													
4	*	0.0	0.0	0.0	0.0	0.0	0.0	0.0	0.0	0.0	0.0	0.0	0.0	10.2	7.8	12.4	10.9
10.3	8.6	6.0	0.0														
5	*	0.0	0.0	0.0	0.0	0.0	0.0	0.0	0.0	0.0	0.0	0.0	0.0	0.0	0.0	0.0	12.3
11.2	0.0	0.0	0.0														
6	*	0.0	0.0	0.0	0.0	0.0	0.0	0.0	0.0	0.0	0.0	0.0	0.0	0.0	0.0	0.0	0.0
0.0	0.0	0.0	0.0														
7	*	0.0	0.0	0.0	0.0	0.0	0.0	0.0	0.0	0.0	0.0	0.0	0.0	0.0	0.0	0.0	0.0
0.0	0.0	0.0	0.0														
8	*	0.0	0.0	0.0	0.0	0.0	0.0	0.0	0.0	0.0	0.0	0.0	0.0	0.0	0.0	0.0	0.0
0.0	0.0	0.0	0.0														

Appendix C

9 * 0.0 0.0 0.0 0.0 0.0 0.0 0.0 0.0 0.0 0.0 0.0 0.0 0.0 0.0 0.0 0.0
0.0 0.0 0.0 0.0
10 * 0.0 0.0 0.0 0.0 0.0 0.0 0.0 0.0 0.0 0.0 0.0 0.0 0.0 0.0 0.0 0.0 0.0
0.0 0.0 0.0 0.0

TRANSECT																
LAYER	22	23	24	25	26	27	28	29	30	31	32	33	34	35	36	

1 *	0.0	1.2	9.5	5.6	4.7	3.2	1.8	1.2	2.0	1.2	0.6	0.6	0.4	0.3	0.2	
2 *	0.0	0.6	12.4	5.0	4.9	4.5	2.0	2.0	2.9	1.2	1.2	0.9	0.6	0.4	0.2	
3 *	0.2	0.0	22.0	70.1	17.0	3.7	1.0	2.8	3.6	1.1	1.6	1.0	0.6	0.5	0.2	
4 *	0.0	0.0	30.3	152.9	0.0	35.2	0.0	5.4	4.5	0.7	1.9	0.9	0.6	0.4	0.1	
5 *	0.0	0.0	0.0	0.0	0.0	40.7	30.0	0.0	6.0	0.3	2.2	0.8	0.5	0.4	0.1	
6 *	0.0	0.0	0.0	0.0	0.0	0.0	0.0	0.0	10.2	0.0	2.7	0.6	0.6	0.4	0.0	
7 *	0.0	0.0	0.0	0.0	0.0	0.0	0.0	2.0	14.4	0.0	3.8	0.4	0.6	0.4	0.0	
8 *	0.0	0.0	0.0	0.0	0.0	0.0	0.0	0.0	0.0	0.0	4.1	0.0	0.7	0.4	0.0	
9 *	0.0	0.0	0.0	0.0	0.0	0.0	0.0	0.0	0.0	0.0	5.0	0.0	1.2	0.3	0.0	
10 *	0.0	0.0	0.0	0.0	0.0	0.0	0.0	0.0	0.0	0.0	7.9	0.7	1.6	0.3	0.0	

TIDAL HEIGHT AT HOUR 235.98

TRANSECT																				
2	3	4	5	6	7	8	9	10	11	12	13	14	15	16	17	18	19	20	21	

75.5	75.3	74.8	73.0	71.6	70.1	67.0	63.9	58.6	54.4	49.1	41.9	36.7	33.3	30.4						
27.8	25.9	23.8	21.7	19.0																

TRANSECT																
LAYER	22	23	24	25	26	27	28	29	30	31	32	33	34	35	36	

	15.5	12.1	10.0	9.3	9.4	10.0	10.9	11.9	12.8	13.6	14.9	16.0	17.1	18.3	19.8	

Appendix C

VERTICAL VELOCITY AT HOUR 235.98

		TRANSECT																	
LAYER	2	3	4	5	6	7	8	9	10	11	12	13	14	15	16	17	18		
19	20	21																	

1	*	1.8	0.6	0.0	-0.5	-0.5	-2.2	-3.0	-2.2	-2.5	-3.6	-2.4	-2.9	-7.0	2.3	-2.0	-6.0		
		-0.8	-2.0	0.4	0.2														
2	*	0.0	0.0	0.0	0.0	0.0	-3.6	-0.9	-1.4	-1.1	0.2	1.2	-5.8	-7.8	3.4	-4.0	-7.3		
		2.4	0.3	3.5	2.4														
3	*	0.0	0.0	0.0	0.0	0.0	0.0	0.0	0.0	0.0	0.0	0.0	0.0	0.0	-6.7	3.5	-5.8	-7.7	
		6.2	2.1	5.1	0.0														
4	*	0.0	0.0	0.0	0.0	0.0	0.0	0.0	0.0	0.0	0.0	0.0	0.0	0.0	0.0	0.0	0.0	-6.7	
		7.5	0.0	0.0	0.0														
5	*	0.0	0.0	0.0	0.0	0.0	0.0	0.0	0.0	0.0	0.0	0.0	0.0	0.0	0.0	0.0	0.0	0.0	
		0.0	0.0	0.0	0.0														
6	*	0.0	0.0	0.0	0.0	0.0	0.0	0.0	0.0	0.0	0.0	0.0	0.0	0.0	0.0	0.0	0.0	0.0	
		0.0	0.0	0.0	0.0														
7	*	0.0	0.0	0.0	0.0	0.0	0.0	0.0	0.0	0.0	0.0	0.0	0.0	0.0	0.0	0.0	0.0	0.0	
		0.0	0.0	0.0	0.0														
8	*	0.0	0.0	0.0	0.0	0.0	0.0	0.0	0.0	0.0	0.0	0.0	0.0	0.0	0.0	0.0	0.0	0.0	
		0.0	0.0	0.0	0.0														
9	*	0.0	0.0	0.0	0.0	0.0	0.0	0.0	0.0	0.0	0.0	0.0	0.0	0.0	0.0	0.0	0.0	0.0	
		0.0	0.0	0.0	0.0														
10	*	0.0	0.0	0.0	0.0	0.0	0.0	0.0	0.0	0.0	0.0	0.0	0.0	0.0	0.0	0.0	0.0	0.0	
		0.0	0.0	0.0	0.0														

		TRANSECT															
LAYER		22	23	24	25	26	27	28	29	30	31	32	33	34	35	36	

1 *		-0.7	-0.5	-0.9	-0.1	0.0	0.6	1.2	0.6	1.7	0.5	5.2	1.9	1.1	1.9	0.1	
2 *		-0.4	-1.1	-2.2	-1.0	-0.1	1.0	2.0	0.9	2.3	0.6	5.4	2.2	1.3	0.8	-1.6	

Appendix C

3 *	0.0	0.0	-6.5	-1.1	0.1	0.0	2.4	1.8	3.3	1.3	5.0	2.6	1.8	-1.1	-3.6
4 *	0.0	0.0	0.0	0.0	0.0	0.4	-0.9	2.7	3.6	1.8	4.3	3.5	2.8	-4.2	-7.7
5 *	0.0	0.0	0.0	0.0	0.0	0.0	0.0	2.0	1.8	2.3	4.8	5.8	3.6	-7.2	-16.4
6 *	0.0	0.0	0.0	0.0	0.0	0.0	0.0	1.4	1.3	1.4	5.8	8.8	3.9	-10.0	-28.3
7 *	0.0	0.0	0.0	0.0	0.0	0.0	0.0	0.0	0.0	0.0	6.6	7.7	3.6	-12.8	0.0
8 *	0.0	0.0	0.0	0.0	0.0	0.0	0.0	0.0	0.0	0.0	4.8	5.3	2.6	-9.0	0.0
9 *	0.0	0.0	0.0	0.0	0.0	0.0	0.0	0.0	0.0	0.0	3.0	2.5	0.8	-4.7	0.0
10 *	0.0	0.0	0.0	0.0	0.0	0.0	0.0	0.0	0.0	0.0	0.0	0.0	0.0	0.0	0.0

HORIZONTAL VELOCITY AT HOUR 235.98

TRANSECT

LAYER	2	3	4	5	6	7	8	9	10	11	12	13	14	15	16	17	18
19	20	21															

1 *	20.4	20.7	17.9	15.7	13.5	12.3	9.5	12.0	14.1	17.9	27.0	32.3	30.9	27.0			
	24.1	24.5	23.1	27.1	30.0	32.9											
2 *	20.4	15.2	13.4	12.7	12.1	12.7	11.3	14.8	16.9	20.0	28.2	31.3	30.4	28.0			
	23.6	24.5	23.5	26.8	29.1	30.5											
3 *	0.0	0.0	0.0	0.0	0.0	0.0	11.4	14.6	16.8	20.3	25.4	24.6	29.1	27.3	22.3		
	24.2	23.8	25.8	26.8	26.8												
4 *	0.0	0.0	0.0	0.0	0.0	0.0	0.0	0.0	0.0	0.0	0.0	0.0	0.0	25.3	20.1	24.3	
	23.8	22.5	20.9	0.0													
5 *	0.0	0.0	0.0	0.0	0.0	0.0	0.0	0.0	0.0	0.0	0.0	0.0	0.0	0.0	0.0	0.0	
	21.5	0.0	0.0	0.0													
6 *	0.0	0.0	0.0	0.0	0.0	0.0	0.0	0.0	0.0	0.0	0.0	0.0	0.0	0.0	0.0	0.0	
	0.0	0.0	0.0	0.0													
7 *	0.0	0.0	0.0	0.0	0.0	0.0	0.0	0.0	0.0	0.0	0.0	0.0	0.0	0.0	0.0	0.0	
	0.0	0.0	0.0	0.0													
8 *	0.0	0.0	0.0	0.0	0.0	0.0	0.0	0.0	0.0	0.0	0.0	0.0	0.0	0.0	0.0	0.0	
	0.0	0.0	0.0	0.0													

Appendix C

9 * 0.0 0.0 0.0 0.0 0.0 0.0 0.0 0.0 0.0 0.0 0.0 0.0 0.0 0.0 0.0 0.0
0.0 0.0 0.0 0.0
10 * 0.0 0.0 0.0 0.0 0.0 0.0 0.0 0.0 0.0 0.0 0.0 0.0 0.0 0.0 0.0 0.0
0.0 0.0 0.0 0.0

TRANSECT																
LAYER	22	23	24	25	26	27	28	29	30	31	32	33	34	35	36	

1 *	35.2	35.6	31.3	24.3	17.2	14.3	11.8	9.7	8.0	8.7	7.7	7.0	6.1	3.9	3.3	
2 *	30.5	30.3	25.9	20.1	13.6	10.7	7.5	4.7	3.6	3.5	4.1	2.0	1.6	1.5	-2.3	
3 *	25.0	25.1	22.9	17.5	12.5	9.3	4.4	0.4	0.3	-0.3	1.1	-1.9	-2.0	-1.3	-7.5	
4 *	0.0	0.0	0.0	15.1	10.9	7.5	6.3	-2.9	-1.7	-3.5	-2.5	-5.6	-5.7	-4.6	-12.6	
5 *	0.0	0.0	0.0	0.0	0.0	0.0	-1.0	1.4	-1.1	-5.7	-6.4	-8.7	-9.0	-7.9	-17.0	
6 *	0.0	0.0	0.0	0.0	0.0	0.0	0.0	0.0	-2.8	-5.4	-9.4	-11.0	-11.9	-11.1	-21.3	
7 *	0.0	0.0	0.0	0.0	0.0	0.0	0.0	0.0	-4.4	-6.9	-8.6	-12.1	-14.5	-14.1	-26.7	
8 *	0.0	0.0	0.0	0.0	0.0	0.0	0.0	0.0	0.0	0.0	0.0	-11.6	-16.1	-16.8	0.0	
9 *	0.0	0.0	0.0	0.0	0.0	0.0	0.0	0.0	0.0	0.0	0.0	-10.7	-16.4	-19.3	0.0	
10 *	0.0	0.0	0.0	0.0	0.0	0.0	0.0	0.0	0.0	0.0	0.0	-10.0	-15.5	-17.4	0.0	

SALINITY AT HOUR 248.40

TRANSECT																	
LAYER	2	3	4	5	6	7	8	9	10	11	12	13	14	15	16	17	18
19	20	21															

1	*	0.0	0.0	0.0	0.0	0.0	0.0	0.0	0.0	0.0	0.0	0.0	0.0	0.0	0.0	0.0	0.0
0.1	0.0	0.2	0.0														
2	*	0.0	0.0	0.0	0.0	0.0	0.0	0.0	0.0	0.0	0.0	0.0	0.0	0.0	0.0	0.0	0.0
0.1	0.0	0.1	0.0														
3	*	30.0	30.0	30.0	30.0	30.0	0.0	0.0	0.0	0.0	0.0	0.0	0.0	0.0	0.0	0.0	0.0
0.0	0.1	0.0	0.1	0.0													

Appendix C

```

4 * 30.0 30.0 30.0 30.0 30.0 30.0 30.0 30.0 30.0 30.0 30.0 30.0 30.0 0.0 0.0 0.0
0.0 0.1 0.0 0.1 30.0
5 * 30.0 30.0 30.0 30.0 30.0 30.0 30.0 30.0 30.0 30.0 30.0 30.0 30.0 30.0 30.0
30.0 0.0 0.1 30.0 30.0 30.0
6 * 30.0 30.0 30.0 30.0 30.0 30.0 30.0 30.0 30.0 30.0 30.0 30.0 30.0 30.0 30.0
30.0 30.0 30.0 30.0 30.0 30.0
7 * 30.0 30.0 30.0 30.0 30.0 30.0 30.0 30.0 30.0 30.0 30.0 30.0 30.0 30.0 30.0
30.0 30.0 30.0 30.0 30.0 30.0
8 * 30.0 30.0 30.0 30.0 30.0 30.0 30.0 30.0 30.0 30.0 30.0 30.0 30.0 30.0 30.0
30.0 30.0 30.0 30.0 30.0 30.0
9 * 30.0 30.0 30.0 30.0 30.0 30.0 30.0 30.0 30.0 30.0 30.0 30.0 30.0 30.0 30.0
30.0 30.0 30.0 30.0 30.0 30.0
10 * 30.0 30.0 30.0 30.0 30.0 30.0 30.0 30.0 30.0 30.0 30.0 30.0 30.0 30.0 30.0
30.0 30.0 30.0 30.0 30.0 30.0

```

TRANSECT

LAYER	22	23	24	25	26	27	28	29	30	31	32	33	34	35	36
1 *	0.3	0.0	0.7	0.7	2.1	3.2	5.2	6.8	8.0	9.4	9.5	10.6	11.7	11.7	13.1
2 *	0.3	0.0	0.7	0.7	2.1	3.5	5.6	7.4	8.5	9.6	10.2	11.3	12.0	12.7	14.3
3 *	0.3	0.0	0.6	3.9	3.7	4.7	6.2	7.9	8.9	9.8	10.7	11.7	12.4	13.2	14.8
4 *	30.0	30.0	0.4	5.5	10.1	10.1	7.6	8.9	9.7	10.2	11.2	12.0	12.7	13.4	15.1
5 *	30.0	30.0	30.0	30.0	30.0	9.5	15.8	12.0	11.3	10.7	11.6	12.3	13.0	13.7	15.4
6 *	30.0	30.0	30.0	30.0	30.0	30.0	30.0	11.8	13.1	12.3	12.0	12.8	13.2	13.9	15.6
7 *	30.0	30.0	30.0	30.0	30.0	30.0	30.0	15.6	13.7	15.0	14.2	13.6	13.4	14.0	15.8
8 *	30.0	30.0	30.0	30.0	30.0	30.0	30.0	30.0	30.0	30.0	14.1	14.0	13.6	14.1	30.0
9 *	30.0	30.0	30.0	30.0	30.0	30.0	30.0	30.0	30.0	30.0	14.5	14.0	14.2	14.3	30.0
10 *	30.0	30.0	30.0	30.0	30.0	30.0	30.0	30.0	30.0	30.0	14.8	14.0	14.3	14.3	30.0

Appendix C

SEDIMENT CONCENTRATION AT HOUR 248.40

		TRANSECT																			
LAYER	2	3	4	5	6	7	8	9	10	11	12	13	14	15	16	17	18	19	20	21	

1	*	30.0	32.1	29.3	32.1	29.4	32.2	26.7	26.7	18.8	21.4	8.7	8.1	8.4	6.3	9.6	10.3	10.4	8.7	5.8	0.0
2	*	30.0	37.4	35.5	39.1	35.8	36.2	30.6	30.4	21.2	24.0	10.3	8.9	9.0	6.8	10.1	10.4	10.4	8.6	5.6	0.0
3	*	0.0	0.0	0.0	0.0	0.0	41.4	35.8	35.3	24.1	27.3	12.0	9.8	9.4	7.1	10.5	10.7	10.5	8.6	5.7	0.0
4	*	0.0	0.0	0.0	0.0	0.0	0.0	0.0	0.0	0.0	0.0	0.0	0.0	10.8	7.9	11.7	11.0	10.7	8.9	6.0	0.0
5	*	0.0	0.0	0.0	0.0	0.0	0.0	0.0	0.0	0.0	0.0	0.0	0.0	0.0	0.0	0.0	12.0	11.4	0.0	0.0	0.0
6	*	0.0	0.0	0.0	0.0	0.0	0.0	0.0	0.0	0.0	0.0	0.0	0.0	0.0	0.0	0.0	0.0	0.0	0.0	0.0	0.0
7	*	0.0	0.0	0.0	0.0	0.0	0.0	0.0	0.0	0.0	0.0	0.0	0.0	0.0	0.0	0.0	0.0	0.0	0.0	0.0	0.0
8	*	0.0	0.0	0.0	0.0	0.0	0.0	0.0	0.0	0.0	0.0	0.0	0.0	0.0	0.0	0.0	0.0	0.0	0.0	0.0	0.0
9	*	0.0	0.0	0.0	0.0	0.0	0.0	0.0	0.0	0.0	0.0	0.0	0.0	0.0	0.0	0.0	0.0	0.0	0.0	0.0	0.0
10	*	0.0	0.0	0.0	0.0	0.0	0.0	0.0	0.0	0.0	0.0	0.0	0.0	0.0	0.0	0.0	0.0	0.0	0.0	0.0	0.0

		TRANSECT															
LAYER	22	23	24	25	26	27	28	29	30	31	32	33	34	35	36		

1 *	0.6	0.5	10.5	4.8	4.4	3.3	1.5	1.0	2.0	1.1	0.6	0.5	0.4	0.3	0.2		
2 *	1.0	0.0	12.7	4.2	4.3	4.2	1.5	1.8	2.9	1.2	1.2	0.8	0.6	0.4	0.2		

Appendix C

3	*	1.5	0.0	13.3	64.9	27.2	1.8	0.7	2.4	3.5	1.1	1.6	0.8	0.6	0.4	0.2
4	*	0.0	0.0	10.0	182.2	0.0	41.3	0.0	5.3	4.5	0.8	1.9	0.8	0.6	0.4	0.1
5	*	0.0	0.0	0.0	0.0	0.0	48.5	33.2	2.1	5.9	0.5	2.1	0.7	0.6	0.4	0.1
6	*	0.0	0.0	0.0	0.0	0.0	0.0	0.0	0.0	10.6	1.1	2.4	0.5	0.7	0.4	0.1
7	*	0.0	0.0	0.0	0.0	0.0	0.0	0.0	0.5	15.0	0.0	4.5	0.2	0.7	0.3	0.0
8	*	0.0	0.0	0.0	0.0	0.0	0.0	0.0	0.0	0.0	0.0	4.7	0.0	0.8	0.3	0.0
9	*	0.0	0.0	0.0	0.0	0.0	0.0	0.0	0.0	0.0	0.0	5.8	0.0	1.5	0.2	0.0
10	*	0.0	0.0	0.0	0.0	0.0	0.0	0.0	0.0	0.0	0.0	8.9	0.4	2.2	0.0	0.0

TIDAL HEIGHT AT HOUR 248.40

TRANSECT

2	3	4	5	6	7	8	9	10	11	12	13	14	15	16	17	18	19	20	21

75.0	74.5	73.4	71.0	68.8	66.0	61.9	57.8	51.7	46.9	42.2	36.5	32.3	29.5	26.8	24.0	21.8	19.4	17.0	13.7

TRANSECT

LAYER	22	23	24	25	26	27	28	29	30	31	32	33	34	35	36

9.6	5.7	3.1	2.3	2.5	3.3	4.5	5.7	6.8	7.9	9.4	10.8	12.2	13.7	15.6	

VERTICAL VELOCITY AT HOUR 248.40

TRANSECT

LAYER	2	3	4	5	6	7	8	9	10	11	12	13	14	15	16	17	18
19	20	21															

1	*	1.5	0.2	-0.4	-0.8	-1.1	-4.0	-3.9	-3.9	-3.4	-3.1	-1.0	-3.2	-7.7	2.3	-2.7	-
6.9	0.0	-1.6	0.4	0.3													
2	*	0.0	0.0	0.0	0.0	0.0	-5.1	-0.9	-2.1	-1.4	1.0	1.9	-6.4	-8.3	3.4	-5.1	-8.5

Appendix C

```

3.5 0.6 3.7 2.7
 3 * 0.0 0.0 0.0 0.0 0.0 0.0 0.0 0.0 0.0 0.0 0.0 0.0 0.0 -6.7 3.4 -7.2 -8.9
7.4 2.5 5.4 0.0
 4 * 0.0 0.0 0.0 0.0 0.0 0.0 0.0 0.0 0.0 0.0 0.0 0.0 0.0 0.0 0.0 0.0 -7.5
8.4 0.0 0.0 0.0
 5 * 0.0 0.0 0.0 0.0 0.0 0.0 0.0 0.0 0.0 0.0 0.0 0.0 0.0 0.0 0.0 0.0 0.0
0.0 0.0 0.0 0.0
 6 * 0.0 0.0 0.0 0.0 0.0 0.0 0.0 0.0 0.0 0.0 0.0 0.0 0.0 0.0 0.0 0.0 0.0
0.0 0.0 0.0 0.0
 7 * 0.0 0.0 0.0 0.0 0.0 0.0 0.0 0.0 0.0 0.0 0.0 0.0 0.0 0.0 0.0 0.0 0.0
0.0 0.0 0.0 0.0
 8 * 0.0 0.0 0.0 0.0 0.0 0.0 0.0 0.0 0.0 0.0 0.0 0.0 0.0 0.0 0.0 0.0 0.0
0.0 0.0 0.0 0.0
 9 * 0.0 0.0 0.0 0.0 0.0 0.0 0.0 0.0 0.0 0.0 0.0 0.0 0.0 0.0 0.0 0.0 0.0
0.0 0.0 0.0 0.0
10 * 0.0 0.0 0.0 0.0 0.0 0.0 0.0 0.0 0.0 0.0 0.0 0.0 0.0 0.0 0.0 0.0 0.0
0.0 0.0 0.0 0.0

```

```

                                TRANSECT
LAYER   22   23   24   25   26   27   28   29   30   31   32   33   34   35   36
*****
 1 * -0.8 -0.6 -0.9 0.1 0.1 1.1 1.6 1.3 1.9 0.9 7.0 2.1 1.3 1.9 -0.1
 2 * -0.5 -1.3 -2.5 -0.9 -0.4 1.5 2.4 2.0 2.3 1.0 7.5 2.1 1.4 0.4 -2.3
 3 * 0.0 0.0 -7.3 -1.1 -0.3 0.3 2.8 3.7 3.1 1.7 7.1 2.4 1.9 -1.8 -4.3
 4 * 0.0 0.0 0.0 0.0 0.0 0.2 -0.6 4.5 3.2 2.0 6.2 3.1 3.0 -5.1 -8.7
 5 * 0.0 0.0 0.0 0.0 0.0 0.0 0.0 3.3 1.7 2.1 7.0 4.7 3.8 -8.1 -17.7
 6 * 0.0 0.0 0.0 0.0 0.0 0.0 0.0 2.2 1.3 1.3 7.9 6.8 3.9 -10.9 -30.0
 7 * 0.0 0.0 0.0 0.0 0.0 0.0 0.0 0.0 0.0 0.0 8.6 6.0 3.6 -13.6 0.0
 8 * 0.0 0.0 0.0 0.0 0.0 0.0 0.0 0.0 0.0 0.0 6.3 4.2 2.6 -9.7 0.0
 9 * 0.0 0.0 0.0 0.0 0.0 0.0 0.0 0.0 0.0 0.0 4.0 2.0 0.7 -5.2 0.0
10 * 0.0 0.0 0.0 0.0 0.0 0.0 0.0 0.0 0.0 0.0 0.0 0.0 0.0 0.0 0.0

```

Appendix C

HORIZONTAL VELOCITY AT HOUR 248.40

		TRANSECT																			
LAYER	2	3	4	5	6	7	8	9	10	11	12	13	14	15	16	17	18	19	20	21	

1	*	20.4	21.7	20.4	19.9	18.8	19.7	18.5	22.5	28.2	31.8	40.2	41.3	38.2	34.4	30.0	30.5	28.1	31.3	33.6	36.1
2	*	20.4	15.9	15.3	15.7	15.7	17.9	18.2	22.3	27.4	31.2	38.0	36.6	35.1	32.9	27.7	29.5	28.2	30.4	32.1	33.4
3	*	0.0	0.0	0.0	0.0	0.0	0.0	16.2	18.9	22.9	27.6	30.3	26.4	31.9	30.3	25.1	28.6	28.2	28.9	29.3	29.2
4	*	0.0	0.0	0.0	0.0	0.0	0.0	0.0	0.0	0.0	0.0	0.0	0.0	0.0	25.5	21.2	28.1	27.9	24.8	22.4	0.0
5	*	0.0	0.0	0.0	0.0	0.0	0.0	0.0	0.0	0.0	0.0	0.0	0.0	0.0	0.0	0.0	0.0	24.1	0.0	0.0	0.0
6	*	0.0	0.0	0.0	0.0	0.0	0.0	0.0	0.0	0.0	0.0	0.0	0.0	0.0	0.0	0.0	0.0	0.0	0.0	0.0	0.0
7	*	0.0	0.0	0.0	0.0	0.0	0.0	0.0	0.0	0.0	0.0	0.0	0.0	0.0	0.0	0.0	0.0	0.0	0.0	0.0	0.0
8	*	0.0	0.0	0.0	0.0	0.0	0.0	0.0	0.0	0.0	0.0	0.0	0.0	0.0	0.0	0.0	0.0	0.0	0.0	0.0	0.0
9	*	0.0	0.0	0.0	0.0	0.0	0.0	0.0	0.0	0.0	0.0	0.0	0.0	0.0	0.0	0.0	0.0	0.0	0.0	0.0	0.0
10	*	0.0	0.0	0.0	0.0	0.0	0.0	0.0	0.0	0.0	0.0	0.0	0.0	0.0	0.0	0.0	0.0	0.0	0.0	0.0	0.0

		TRANSECT														
LAYER		22	23	24	25	26	27	28	29	30	31	32	33	34	35	36

1	*	38.1	38.7	33.9	25.9	17.9	14.1	11.1	8.6	7.3	7.3	5.4	5.2	3.8	0.6	-1.2
2	*	33.1	33.0	28.3	21.6	14.3	10.8	6.9	3.6	2.7	2.0	2.0	-0.1	-0.9	-1.4	-6.5

Appendix C

3	*	27.0	27.5	25.4	19.3	13.4	10.1	3.9	-0.6	-0.7	-1.7	-1.0	-4.4	-4.6	-4.1	-11.3
4	*	0.0	0.0	0.0	17.1	11.9	9.3	6.5	-3.2	-3.2	-4.8	-4.3	-8.3	-8.2	-7.1	-15.7
5	*	0.0	0.0	0.0	0.0	0.0	0.0	-0.4	1.2	-3.0	-6.5	-7.8	-11.0	-11.2	-10.1	-19.4
6	*	0.0	0.0	0.0	0.0	0.0	0.0	0.0	0.0	-4.8	-6.6	-10.3	-13.5	-13.9	-12.9	-23.2
7	*	0.0	0.0	0.0	0.0	0.0	0.0	0.0	0.0	-6.8	-8.6	-9.5	-15.2	-16.3	-15.5	-28.3
8	*	0.0	0.0	0.0	0.0	0.0	0.0	0.0	0.0	0.0	0.0	0.0	-14.8	-17.6	-17.9	0.0
9	*	0.0	0.0	0.0	0.0	0.0	0.0	0.0	0.0	0.0	0.0	0.0	-14.1	-17.9	-20.6	0.0
10	*	0.0	0.0	0.0	0.0	0.0	0.0	0.0	0.0	0.0	0.0	0.0	-13.2	-17.3	-18.9	0.0

AVERAGE SALINITY FOR THE 20TH TIDAL CYCLE

		TRANSECT																
LAYER		2	3	4	5	6	7	8	9	10	11	12	13	14	15	16	17	18
19	20	21																

1	*	0.0	0.0	0.0	0.0	0.0	0.0	0.0	0.0	0.0	0.0	0.0	0.0	0.0	0.0	0.0	0.0	0.0
0.0	-0.1	0.1	0.0															
2	*	0.0	0.0	0.0	0.0	0.0	0.0	0.0	0.0	0.0	0.0	0.0	0.0	0.0	0.0	0.0	0.0	0.0
0.0	-0.1	0.1	0.0															
3	*	0.0	0.0	0.0	0.0	0.0	0.0	0.0	0.0	0.0	0.0	0.0	0.0	0.0	0.0	0.0	0.0	0.0
0.0	-0.1	0.1	0.0															
4	*	0.0	0.0	0.0	0.0	0.0	0.0	0.0	0.0	0.0	0.0	0.0	0.0	0.0	0.0	0.0	0.0	0.0
0.0	-0.1	0.1	0.0															
5	*	0.0	0.0	0.0	0.0	0.0	0.0	0.0	0.0	0.0	0.0	0.0	0.0	0.0	0.0	0.0	0.0	0.0
0.0	0.0	0.0	0.0															
6	*	0.0	0.0	0.0	0.0	0.0	0.0	0.0	0.0	0.0	0.0	0.0	0.0	0.0	0.0	0.0	0.0	0.0
0.0	0.0	0.0	0.0															
7	*	0.0	0.0	0.0	0.0	0.0	0.0	0.0	0.0	0.0	0.0	0.0	0.0	0.0	0.0	0.0	0.0	0.0
0.0	0.0	0.0	0.0															
8	*	0.0	0.0	0.0	0.0	0.0	0.0	0.0	0.0	0.0	0.0	0.0	0.0	0.0	0.0	0.0	0.0	0.0
0.0	0.0	0.0	0.0															

Appendix C

```

 9 * 0.0 0.0 0.0 0.0 0.0 0.0 0.0 0.0 0.0 0.0 0.0 0.0 0.0 0.0 0.0 0.0
0.0 0.0 0.0 0.0
10 * 0.0 0.0 0.0 0.0 0.0 0.0 0.0 0.0 0.0 0.0 0.0 0.0 0.0 0.0 0.0 0.0
0.0 0.0 0.0 0.0

```

TRANSECT

```

LAYER  22  23  24  25  26  27  28  29  30  31  32  33  34  35  36
*****
*****
1 * 0.2 0.0 0.8 1.0 2.5 3.8 5.7 7.2 8.3 9.7 9.8 11.0 11.9 12.1 14.3
2 * 0.2 0.0 0.8 1.2 2.9 4.7 6.3 7.9 8.9 10.0 10.7 11.6 12.4 13.1 15.1
3 * 0.2 0.0 1.8 4.8 4.2 6.0 7.3 8.9 9.4 10.2 11.2 11.9 12.7 13.5 15.4
4 * 0.0 0.0 2.2 6.8 10.8 10.3 8.2 9.4 10.0 10.5 11.6 12.2 13.0 13.8 15.6
5 * 0.0 0.0 0.0 0.0 0.0 11.0 16.4 12.0 11.2 10.9 12.0 12.7 13.2 14.0 15.7
6 * 0.0 0.0 0.0 0.0 0.0 0.0 0.0 12.1 13.2 12.6 12.4 13.0 13.4 14.2 15.8
7 * 0.0 0.0 0.0 0.0 0.0 0.0 0.0 15.8 13.6 15.1 14.2 13.3 13.5 14.3 15.9
8 * 0.0 0.0 0.0 0.0 0.0 0.0 0.0 0.0 0.0 0.0 14.2 13.8 13.7 14.3 0.0
9 * 0.0 0.0 0.0 0.0 0.0 0.0 0.0 0.0 0.0 0.0 14.6 13.9 14.2 14.4 0.0
10 * 0.0 0.0 0.0 0.0 0.0 0.0 0.0 0.0 0.0 0.0 14.8 14.0 14.3 14.3 0.0

```

AVERAGE SEDIMENT CONCENTRATIONS FOR THE 20TH TIDAL CYCLE

TRANSECT

```

LAYER  2  3  4  5  6  7  8  9  10  11  12  13  14  15  16  17  18
19  20  21
*****
1 * 30.0 31.4 29.5 31.7 29.4 32.0 27.1 27.4 19.7 23.2 12.0 8.6 7.9 5.5 7.4
6.9 6.2 4.8 2.8 1.4
2 * 30.0 35.7 34.0 36.4 33.5 35.1 30.1 30.2 21.5 25.2 13.3 9.2 8.5 6.0 8.1
7.8 6.9 5.4 3.1 1.6
3 * 0.0 0.0 0.0 0.0 0.0 40.4 34.1 34.1 23.9 27.8 14.8 10.0 8.9 6.3 8.6

```

Appendix C

8.2 7.3 5.7 3.3 1.8

4 * 0.0 0.0 0.0 0.0 0.0 0.0 0.0 0.0 0.0 0.0 0.0 0.0 0.0 10.0 7.0 9.6 8.6
7.7 6.4 3.7 0.0

5 * 0.0 0.0 0.0 0.0 0.0 0.0 0.0 0.0 0.0 0.0 0.0 0.0 0.0 0.0 0.0 0.0 10.0
9.1 0.0 0.0 0.0

TRANSECT

LAYER	22	23	24	25	26	27	28	29	30	31	32	33	34	35	36
-------	----	----	----	----	----	----	----	----	----	----	----	----	----	----	----

1 *	2.3	0.2	9.8	4.8	3.9	2.5	1.4	1.2	1.9	1.0	0.6	0.6	0.4	0.3	0.1
2 *	2.5	0.3	11.9	6.3	5.2	4.2	1.5	2.2	2.8	1.0	1.3	0.8	0.5	0.4	0.1
3 *	2.8	1.0	40.1	75.1	11.0	4.9	-0.6	3.8	3.5	0.8	1.7	0.8	0.5	0.4	0.1
4 *	0.0	0.0	55.9	146.4	-28.7	42.5	-4.3	5.0	4.1	0.6	2.1	0.8	0.6	0.4	0.1
5 *	0.0	0.0	0.0	0.0	0.0	46.2	29.0	-2.8	6.0	0.1	2.6	0.3	0.6	0.4	0.1
6 *	0.0	0.0	0.0	0.0	0.0	0.0	0.0	-2.8	10.6	-0.5	3.2	0.0	0.7	0.3	0.0
7 *	0.0	0.0	0.0	0.0	0.0	0.0	0.0	3.7	13.1	-9.2	5.3	-0.2	0.7	0.3	0.0
8 *	0.0	0.0	0.0	0.0	0.0	0.0	0.0	0.0	0.0	0.0	5.4	-0.8	0.9	0.3	0.0
9 *	0.0	0.0	0.0	0.0	0.0	0.0	0.0	0.0	0.0	0.0	5.3	-0.6	1.6	0.2	0.0
10 *	0.0	0.0	0.0	0.0	0.0	0.0	0.0	0.0	0.0	0.0	7.9	-0.1	2.1	0.1	0.0

AVERAGE WATER SURFACE ELEVATION FOR THE 20TH TIDAL CYCLE

TRANSECT

AYER	2	3	4	5	6	7	8	9	10	11	12	13	14	15	16	17	18
------	---	---	---	---	---	---	---	---	----	----	----	----	----	----	----	----	----

19 20 21

45.0	43.8	42.4	40.8	39.4	38.1	37.1	36.2	35.3	34.6	33.7	32.7	32.1	31.9	31.5
31.1	30.8	30.5	30.1	29.6										

Appendix C

TRANSECT

LAYER	22	23	24	25	26	27	28	29	30	31	32	33	34	35	36

	28.9	28.3	27.6	27.2	26.7	26.2	25.7	25.4	25.1	24.7	24.5	24.2	23.9	23.6	22.7

AVERAGE HORIZONTAL VELOCITIES FOR THE 20TH TIDAL CYCLE

TRANSECT

LAYER	2	3	4	5	6	7	8	9	10	11	12	13	14	15	16	17	18
19	20	21	*****														
1	*	20.4	20.8	18.8	17.0	14.8	14.0	11.9	10.2	9.5	8.6	8.1	7.3	6.7	6.2	5.3	
4.8	4.1	4.4	4.7	4.6													
2	*	20.4	15.6	14.3	13.2	11.7	12.0	10.5	9.0	8.3	7.9	7.7	6.8	6.4	5.7	4.6	
4.8	4.4	4.6	4.5	4.5													
3	*	0.0	0.0	0.0	0.0	0.0	0.0	8.0	6.6	6.1	6.2	5.9	4.8	6.0	5.0	4.0	4.7
4.5	4.4	4.1	4.0														
4	*	0.0	0.0	0.0	0.0	0.0	0.0	0.0	0.0	0.0	0.0	0.0	0.0	0.0	3.4	3.3	5.0
4.3	3.6	3.2	0.0														
5	*	0.0	0.0	0.0	0.0	0.0	0.0	0.0	0.0	0.0	0.0	0.0	0.0	0.0	0.0	0.0	0.0
3.3	0.0	0.0	0.0														
6	*	0.0	0.0	0.0	0.0	0.0	0.0	0.0	0.0	0.0	0.0	0.0	0.0	0.0	0.0	0.0	0.0
0.0	0.0	0.0	0.0														
7	*	0.0	0.0	0.0	0.0	0.0	0.0	0.0	0.0	0.0	0.0	0.0	0.0	0.0	0.0	0.0	0.0
0.0	0.0	0.0	0.0														
8	*	0.0	0.0	0.0	0.0	0.0	0.0	0.0	0.0	0.0	0.0	0.0	0.0	0.0	0.0	0.0	0.0
0.0	0.0	0.0	0.0														
9	*	0.0	0.0	0.0	0.0	0.0	0.0	0.0	0.0	0.0	0.0	0.0	0.0	0.0	0.0	0.0	0.0
0.0	0.0	0.0	0.0														
10	*	0.0	0.0	0.0	0.0	0.0	0.0	0.0	0.0	0.0	0.0	0.0	0.0	0.0	0.0	0.0	0.0
0.0	0.0	0.0	0.0														

Appendix C

		TRANSECT														
LAYER		22	23	24	25	26	27	28	29	30	31	32	33	34	35	36

1	*	4.7	4.7	4.6	4.1	3.7	4.0	4.4	5.2	5.4	7.6	7.7	8.1	8.7	8.1	9.8
2	*	4.2	4.3	3.5	3.3	1.9	1.8	1.4	1.2	1.5	2.1	4.1	3.2	3.8	4.7	3.6
3	*	3.5	3.8	2.8	1.2	0.3	-0.9	-1.0	-2.0	-0.7	-1.1	1.0	0.6	0.7	2.0	-0.4
4	*	0.0	0.0	0.0	-2.9	-2.2	-2.7	-1.5	-5.2	-2.3	-3.6	-1.9	-1.3	-1.8	-0.5	-3.7
5	*	0.0	0.0	0.0	0.0	0.0	0.0	-3.6	-2.4	-3.4	-5.0	-4.7	-2.9	-3.6	-2.9	-6.6
6	*	0.0	0.0	0.0	0.0	0.0	0.0	0.0	0.0	-3.5	-3.6	-6.2	-4.8	-5.5	-5.1	-9.8
7	*	0.0	0.0	0.0	0.0	0.0	0.0	0.0	0.0	-1.4	-3.6	-4.0	-6.2	-7.4	-7.1	-14.3
8	*	0.0	0.0	0.0	0.0	0.0	0.0	0.0	0.0	0.0	0.0	0.0	-6.2	-9.3	-8.8	0.0
9	*	0.0	0.0	0.0	0.0	0.0	0.0	0.0	0.0	0.0	0.0	0.0	-4.4	-9.1	-9.3	0.0
10	*	0.0	0.0	0.0	0.0	0.0	0.0	0.0	0.0	0.0	0.0	0.0	-1.2	-7.2	-7.0	0.0

AVERAGE VERTICAL VELOCITIES FOR THE 20TH TIDAL CYCLE

TRANSECT																	
LAYER	2	3	4	5	6	7	8	9	10	11	12	13	14	15	16	17	18
19	20	21															

1	*	1.7	0.4	0.0	-0.2	-0.4	-1.5	-0.2	-0.3	-0.2	0.0	0.1	-0.6	-1.0	0.4	-0.5	-0.8
0.8	0.1	0.0	0.1	0.1													
2	*	0.0	0.0	0.0	0.0	0.0	-2.5	0.3	-0.2	-0.1	0.4	0.4	-1.2	-1.1	0.5	-0.9	-1.1
0.6	0.2	0.5	0.4														
3	*	0.0	0.0	0.0	0.0	0.0	0.0	0.0	0.0	0.0	0.0	0.0	0.0	-0.9	0.4	-1.4	-1.1
1.1	0.4	0.8	0.0														
4	*	0.0	0.0	0.0	0.0	0.0	0.0	0.0	0.0	0.0	0.0	0.0	0.0	0.0	0.0	0.0	-1.0
1.1	0.0	0.0	0.0														
5	*	0.0	0.0	0.0	0.0	0.0	0.0	0.0	0.0	0.0	0.0	0.0	0.0	0.0	0.0	0.0	0.0
0.0	0.0	0.0	0.0														
6	*	0.0	0.0	0.0	0.0	0.0	0.0	0.0	0.0	0.0	0.0	0.0	0.0	0.0	0.0	0.0	0.0

Appendix C

```

0.0 0.0 0.0 0.0
 7 * 0.0 0.0 0.0 0.0 0.0 0.0 0.0 0.0 0.0 0.0 0.0 0.0 0.0 0.0 0.0 0.0 0.0
0.0 0.0 0.0 0.0
 8 * 0.0 0.0 0.0 0.0 0.0 0.0 0.0 0.0 0.0 0.0 0.0 0.0 0.0 0.0 0.0 0.0 0.0
0.0 0.0 0.0 0.0
 9 * 0.0 0.0 0.0 0.0 0.0 0.0 0.0 0.0 0.0 0.0 0.0 0.0 0.0 0.0 0.0 0.0 0.0
0.0 0.0 0.0 0.0
10 * 0.0 0.0 0.0 0.0 0.0 0.0 0.0 0.0 0.0 0.0 0.0 0.0 0.0 0.0 0.0 0.0 0.0
0.0 0.0 0.0 0.0

```

TRANSECT

LAYER	22	23	24	25	26	27	28	29	30	31	32	33	34	35	36
-------	----	----	----	----	----	----	----	----	----	----	----	----	----	----	----

1 *	-0.1	0.0	0.1	0.2	0.2	0.1	0.5	0.1	0.7	-0.9	0.3	0.8	-0.4	0.7	0.1
2 *	-0.1	0.0	0.7	0.2	0.5	0.4	1.3	0.4	1.3	-0.5	0.1	1.3	-0.2	0.3	-0.6
3 *	0.0	0.0	1.3	0.2	0.4	0.5	1.8	1.1	1.9	0.2	0.0	1.7	0.4	-0.6	-1.8
4 *	0.0	0.0	0.0	0.0	0.0	1.4	0.3	2.2	1.7	0.8	0.2	2.3	1.0	-2.0	-3.8
5 *	0.0	0.0	0.0	0.0	0.0	0.0	0.0	1.7	0.8	1.2	1.4	3.9	1.5	-3.4	-8.2
6 *	0.0	0.0	0.0	0.0	0.0	0.0	0.0	0.5	0.9	0.5	2.6	6.1	1.5	-4.7	-15.0
7 *	0.0	0.0	0.0	0.0	0.0	0.0	0.0	0.0	0.0	0.0	2.7	5.8	1.2	-6.2	0.0
8 *	0.0	0.0	0.0	0.0	0.0	0.0	0.0	0.0	0.0	0.0	1.4	4.3	0.7	-4.1	0.0
9 *	0.0	0.0	0.0	0.0	0.0	0.0	0.0	0.0	0.0	0.0	0.4	2.3	0.0	-1.9	0.0
10 *	0.0	0.0	0.0	0.0	0.0	0.0	0.0	0.0	0.0	0.0	0.0	0.0	0.0	0.0	0.0

ACCUMULATED BOTTOM SEDIMENT IN MILIGM./CM**2

TRANSECT

LAYER	2	3	4	5	6	7	8	9	10	11	12	13	14	15	16	17	18
-------	---	---	---	---	---	---	---	---	----	----	----	----	----	----	----	----	----

19 20 21

1 *	0.0	0.0	0.0	0.0	0.0	0.0	0.0	0.0	0.0	0.0	0.0	0.0	0.0	0.0	0.0	0.0	0.0
-----	-----	-----	-----	-----	-----	-----	-----	-----	-----	-----	-----	-----	-----	-----	-----	-----	-----

Appendix C

```

0.0 0.0 0.0 0.0
 2 * 0.0 0.0 0.0 0.0 0.0 0.0 0.0 0.0 0.0 0.0 0.0 0.0 0.0 0.0 0.0 0.0 0.0 0.0
0.0 0.0 0.0 0.0
 3 * 0.0 0.0 0.0 0.0 0.0 0.0 0.6 0.0 0.0 0.0 0.0 0.0 0.0 0.0 0.0 0.0 0.0 0.0
0.0 0.0 0.0 0.0
 4 * 0.0 0.0 0.0 0.0 0.0 0.0 0.0 0.0 0.0 0.0 0.0 0.0 0.0 0.0 0.1 0.0 0.0 0.0
0.0 0.0 1.1 0.0
 5 * 0.0 0.0 0.0 0.0 0.0 0.0 0.0 0.0 0.0 0.0 0.0 0.0 0.0 0.0 0.0 0.0 0.0 0.2
0.2 0.0 0.0 0.0
 6 * 0.0 0.0 0.0 0.0 0.0 0.0 0.0 0.0 0.0 0.0 0.0 0.0 0.0 0.0 0.0 0.0 0.0 0.0
0.0 0.0 0.0 0.0
 7 * 0.0 0.0 0.0 0.0 0.0 0.0 0.0 0.0 0.0 0.0 0.0 0.0 0.0 0.0 0.0 0.0 0.0 0.0
0.0 0.0 0.0 0.0
 8 * 0.0 0.0 0.0 0.0 0.0 0.0 0.0 0.0 0.0 0.0 0.0 0.0 0.0 0.0 0.0 0.0 0.0 0.0
0.0 0.0 0.0 0.0
 9 * 0.0 0.0 0.0 0.0 0.0 0.0 0.0 0.0 0.0 0.0 0.0 0.0 0.0 0.0 0.0 0.0 0.0 0.0
0.0 0.0 0.0 0.0
10 * 0.0 0.0 0.0 0.0 0.0 0.0 0.0 0.0 0.0 0.0 0.0 0.0 0.0 0.0 0.0 0.0 0.0 0.0
0.0 0.0 0.0 0.0

```

TRANSECT

LAYER	22	23	24	25	26	27	28	29	30	31	32	33	34	35	36

1 *	0.0	0.0	0.0	0.0	0.0	0.0	0.0	0.0	0.0	0.0	0.0	0.0	0.0	0.0	0.0
2 *	0.0	0.0	0.0	0.0	0.0	0.0	0.0	0.0	0.0	0.0	0.0	0.0	0.0	0.0	0.0
3 *	0.0	0.0	0.0	0.0	0.0	0.0	0.0	0.1	0.1	0.0	0.0	0.0	0.0	0.0	0.0
4 *	0.0	0.0	7.1	0.6	0.0	0.1	0.0	0.1	0.1	0.0	0.0	0.0	0.0	0.0	0.0
5 *	0.0	0.0	0.0	0.0	0.0	16.5	0.6	0.0	0.2	0.0	0.1	0.0	0.0	0.0	0.0
6 *	0.0	0.0	0.0	0.0	0.0	0.0	0.0	-2.1	0.4	0.0	0.1	0.0	0.0	0.0	0.0
7 *	0.0	0.0	0.0	0.0	0.0	0.0	0.0	19.3	3.4	-0.4	0.2	0.0	0.0	0.0	0.0
8 *	0.0	0.0	0.0	0.0	0.0	0.0	0.0	0.0	0.0	0.0	0.3	0.0	0.0	0.0	0.0

Appendix C

9	*	0.0	0.0	0.0	0.0	0.0	0.0	0.0	0.0	0.0	0.0	0.2	0.0	0.0	0.0	0.0
10	*	0.0	0.0	0.0	0.0	0.0	0.0	0.0	0.0	0.0	0.0	5.7	0.0	0.1	-0.1	0.0

MAXIMUM WATER SFC ELEVATION

MINIMUM WATER SFC ELEVATION

2	77.33	9.20
3	75.52	8.47
4	74.81	7.88
5	72.98	7.35
6	71.63	7.08
7	70.08	6.91
8	67.15	7.16
9	65.72	7.76
10	61.18	8.62
11	54.49	9.68
12	52.54	10.79
13	50.89	12.02
14	49.68	12.58
15	48.65	13.40
16	48.43	13.71
17	48.43	14.12
18	47.32	14.71
19	47.26	14.85
20	48.14	14.82
21	48.18	13.22

Appendix C

22	48.07	9.62
23	48.74	5.71
24	49.24	3.13
25	49.35	2.29
26	48.88	2.10
27	48.13	2.17
28	47.20	2.44
29	46.12	2.94
30	45.16	3.50
31	44.01	4.09
32	42.76	5.03
33	41.47	5.74
34	40.23	6.37
35	38.97	7.08
36	37.16	7.37

VITA

The author was born in October, 1964 in Reykjavik, Iceland. After graduating from junior college in 1984, he was enrolled at the Florida Institute of Technology and majored in civil engineering. In March, 1988, he graduated with a Bachelor of Science degree. From April 1988 to August 1989 he worked for a civil engineering consulting firm in Reykjavik, Iceland. In August, 1989, he began graduate studies at Virginia Polytechnic Institute and State University. His area of concentration was water resources engineering.